論文 / 著書情報
Article / Book Information

題目(和文)	溶液プロセスによる酸化亜鉛マイクロ/ナノ構造体の作製と光機能材料への応用
Title(English)	Solution-Processed Zinc Oxide Micro/Nanostructures and Their Application as Photoresponsive Material
著者(和文)	井原大貴
Author(English)	Taiki Ihara
出典(和文)	学位:博士（工学）, 学位授与機関:東京工業大学, 報告番号:甲第9831号, 授与年月日:2015年3月26日, 学位の種別:課程博士, 審査員:松下　伸広,川路　均,大坂　武男,冨田　育義,野村　淳子
Citation(English)	Degree:, Conferring organization: Tokyo Institute of Technology, Report number:甲第9831号, Conferred date:2015/3/26, Degree Type:Course doctor, Examiner:,,,,
学位種別(和文)	博士論文
Type(English)	Doctoral Thesis

Solution-Processed Zinc Oxide Micro/Nanostructures and Their Application as Photoresponsive Material

Thesis Submitted to
Tokyo Institute of Technology

By

Taiki Ihara

In Partial Fulfillment of the Requirements

for the Degree of

Doctor of Engineering

Supervisor: Prof. Nobuhiro Matsushita

Department of Electronic Chemistry
Tokyo Institute of Technology
Japan

March 2015

CONTENTS

Chapter-1

Background and Objective of This Study

1.1 Introduction

Modern human society has been sustained by standout development of advanced artificial materials and by huge consumption of energies and resources. Since we are not able to stop using them now and in the near future, the wastes of materials, chemicals, energies, and heats would increase noticeably and they cause environmental problems on the earth. We must seek for environmentally friendly processing to fabricate those materials.

Functional ceramics or inorganic materials are generally fabricated by novel processing using a gaseous phase, like CVD, MOCVD, etc., or vacuum systems such as sputtering, MBE, etc., which requires even more energy than standard high temperature processing. Generally speaking, all these techniques have resulted in environmental problems because the consumed energies are emitted as exhaust gases or exhaust heat except for the part involved in the product.

Soft solution processing of the inorganic materials proposed by Prof. Yoshimura and his co-worker has become common among material scientists. Advantages of the soft solution processing are low energy consumption, minimized environmental load, no sophisticated instruments and no complicated multi-step process. Soft solution processes can be defined as

environmentally friendly processing using solutions. It can consume less total energy in solution system for various kind of material processing. It is, however, still unclear whether the processes can provide similar quality of products compared with the other processes including vapor phase and high-temperature heat-treatment or not.[1,2]

Recently, there are growing interest for solution processes to achieve functional metal oxide materials because of low-temperature, low-cost and low-environmental load. Solution syntheses including solvothermal, hydrothermal, electrochemical, electroless deposition, and chemical bath deposition (CBD) are promising methods to fabricate micro/nanostructures due to their low manipulating temperatures. These methods have provided opportunities to exploit excellent properties due to the unique micro/nanostructures and explore possible novel phenomena arising from the structures. In particular, various inorganic semiconductor micro/nanostructures have been investigated for their potential usage to the industry. Zinc oxide (ZnO) is one of semiconductor materials and is expected to offer various practical uses such as ultraviolet lasing,[3] field emission device,[4] gas sensors,[5] photocatalysts,[6] hydrophilic-hydrophobic converting surface,[7] transparent conducting electrode,[8] piezoelectric devices[9] and thin film transistors.[10] Preparation of ZnO films by using solution chemistry have been researched intentionally because anisotropic crystal growth of ZnO in solution and controllability of the growth rate using structure-directing agent have enabled us to make unique and special

architectures.

1.2 Solvothermal / Hydrothermal method

A solvothermal process can be defined as "a chemical reaction in a closed system in the presence of a solvent (aqueous and non aqueous solution) at a temperature higher than that of the boiling point of such a solvent". Therefore a solvothermal process involves high pressures. In the case of aqueous solutions as solvent, it is so-called "hydrothermal process". The hydrothermal process have been studied and developed a long time ago with different objectives such as mineral extraction ores[11], investigation of the synthesis of geological materials,[12,13] synthesis of novel materials,[14-16] crystal growth in particular the elaboration of α-quartz single crystals due to its piezoelectric properties,[17] the deposition of thin films,[18] the development of sintering processes in mild conditions,[19] and the synthesis of fine particles well defined in size and morphology.[20]

1.3 Zinc Oxide (ZnO)

1.3.1 General Aspects

There has been a great deal of interest in zinc oxide (ZnO) semiconductor materials recently, as seen from a surge of a relevant number of publications. The interest in ZnO is fueled by its prospects in optoelectronics applications owing to its direct wide band gap (E_g~3.3 eV at 300

K). Some optoelectronic applications of ZnO overlap with that of GaN, another wide-gap semiconductor (E_g ~3.4 eV at 300 K) which is widely used for production of green, blue-ultraviolet, and white light-emitting devices. However, ZnO has some advantages over GaN among which are the availability of fairly high-quality ZnO bulk single crystals and a large exciton binding energy (60 meV). ZnO also has much simpler crystal-growth technology, resulting in a potentially lower cost for ZnO-based devices. ZnO is not really a newly discovered material. Interest in this material is again at a high point at present. In terms of its characterization, reports go back to 1935 or even earlier. For example, lattice parameters of ZnO were investigated for many decades.[21–25] Likewise, optical properties and processes in ZnO as well as its refractive index were extensively studied many decades ago.[26–40] Vibrational properties by techniques such as Raman scattering were also determined early on.[41–47] Growth methods not much different from what is employed lately have been explored, among which are chemical-vapor transport,[48] vapor-phase growth,[49] hydrothermal growth[50] which also had the additional motivation of doping with Li in an effort to obtain p-type material and so on.[51]

The ZnO bulk crystals have been grown by a number of methods, as has been reviewed recently,[52] and large-size ZnO substrates are available.[53,54] High-quality ZnO films can be grown at relatively low temperatures less than 700 °C. The large exciton binding energy of 60 meV paves the way for an intense near-band-edge excitonic emission at room and higher

temperatures, because this value is 2.4 times that of the room-temperature thermal energy (k_BT=25 meV). There have also been a number of reports on laser emission from ZnO-based structures at room temperature and beyond. It should be noted that besides the above-mentioned properties of ZnO, there are additional properties which make it preferable over other wide-band-gap materials: its high energy radiation stability and amenability to wet chemical etching.[52] Several experiments confirmed that ZnO is very resistive to high-energy radiation,[55–57] making it a very suitable candidate for space applications. ZnO is easily etched in all acids and alkalis, and this provides an opportunity for fabrication of small-size devices. In addition, ZnO has the same crystal structure and close lattice parameters to that of GaN and as a result can be used as a substrate for epitaxial growth of high-quality GaN films.[58,59]

1.3.2 General Property

Table 1-1 lists basic physical parameters for a ZnO single crystal and bulk.[60] It should be noted that there still exists uncertainty in some of these values. For example, the values for thermal conductivity show some spreading in the reported values and this may be a result of the influence of defects such as dislocations. The values for carrier mobility will undoubtedly increase if more effective control over compensation and defects in the material is gained. Among various semiconductors with tetrahedrally coordinated structures, ZnO has the highest

piezoelectric tensor, which is attributed to spontaneous polarization along *c*-axis of wurtzite structure originating from relative displacement of Zn and O ion, and at least one comparable to those of gallium nitride and aluminum nitride. This property makes it a large electromechanical coupling. ZnO has n-type conductivity, even in the absence of intentional doping of other metal ions, which is attributed to the nonstoichiometry of ZnO by forming interstitial Zn atoms (Zn_i) or oxygen vacancies (V_o).[61,62] An alternative explanation is substitutional hydrogen impurities.[63] As Zn belongs to the group 12, the two valence electrons form closed-shell structure of 4*s* orbital. For controlling the conductivity, n-type doping is easily achieved by substituting Zn with group 13 such as B, Al, Ga, In, which have one valence electron at outermost shell (4*p*) and lower first ionization energy than Zn.

Table 1-1. Basic properties of wurtzite ZnO single crystal and bulk.

Property	
Lattice parameter at 300 K	
a_0	0.32495 nm
c_0	0.52069 nm
a_0/c_0	1.602 (1.633 in ideal crystal)
u	0.345 (0.375 in ideal crystal)
Density	5.606
Stable phase at 300 K	Wurtzite
Melting point (°C)	1973
Sublimation point (°C)	1100
Thermal conductivity (W/cm·K)	0.46-1.67 (Bulk)
Linear expansion coefficient (/°C)	a_0: 4.75×10^{-6} c_0: 2.92×10^{-6}
Static dielectric constant	E‖*c*: 8.50-8.91
Refractive index	E‖*c*: 1.97 (760 nm) – 2.19 (420 nm)
Intrinsic carrier concentration	$<10^6$ cm^{-3} (n-type doping > 10^{20} cm^{-3})
Electron effective mass	0.24
Electron Hall mobility at 300 K for low n-type conductivity	200 $cm^2/V \cdot s$

1.3.3 Crystal Structure

Most of the group-II-VI binary compound semiconductors crystallize in either cubic zinc-blende or hexagonal wurtzite structure where each anion is surrounded by four cations at the corners of a tetrahedron, and vice versa. This tetrahedral coordination is typical of sp^3 covalent bonding, but these materials also have a substantial ionic character. ZnO is a II-VI compound semiconductor whose ionicity resides at the borderline between covalent and ionic semiconductor. The crystal structures shared by ZnO are wurtzite (B4), zinc blende (B3), and rocksalt (B1), as schematically shown in Figure 1-1.[64] At ambient conditions, the thermodynamically stable phase is wurtzite. The zinc-blende ZnO structure can be stabilized only by growth on cubic substrates, and the rocksalt (NaCl) structure may be obtained at relatively high pressures.

The wurtzite structure has a hexagonal unit cell with two lattice parameters, *a* and *c*, in the ratio of $c/a = \sqrt{8/3} = 1.633$ and belongs to the space group of C^4_{6v} or $P6_3mc$. A schematic representation of the wurtzitic ZnO structure is shown in Figure 1-2.[64] The structure is composed of two interpenetrating hexagonal-close-packed (hcp) sublattices, each of which consists of one type of atom displaced with respect to each other along the threefold *c*-axis by the amount of $u = 3/8 = 0.375$ (in an ideal wurtzite structure. in fractional coordinates the *u* parameter is defined as the length of the bond parallel to the *c* axis, in units of *c*). Each

sublattice includes four atoms per unit cell and every atom of one kind (group-II atom) is surrounded by four atoms of the other kind (group VI), or vice versa, which are coordinated at the edges of a tetrahedron. In a real ZnO crystal, the wurtzite structure deviates from the ideal arrangement, by changing the *c*/*a* ratio or the *u* value. It should be pointed out that a strong correlation exists between the *c*/*a* ratio and the u parameter in that when the *c*/*a* ratio decreases, the *u* parameter increases in such a way that those four tetrahedral distances remain nearly constant through a distortion of tetrahedral angles due to long-range polar interactions.

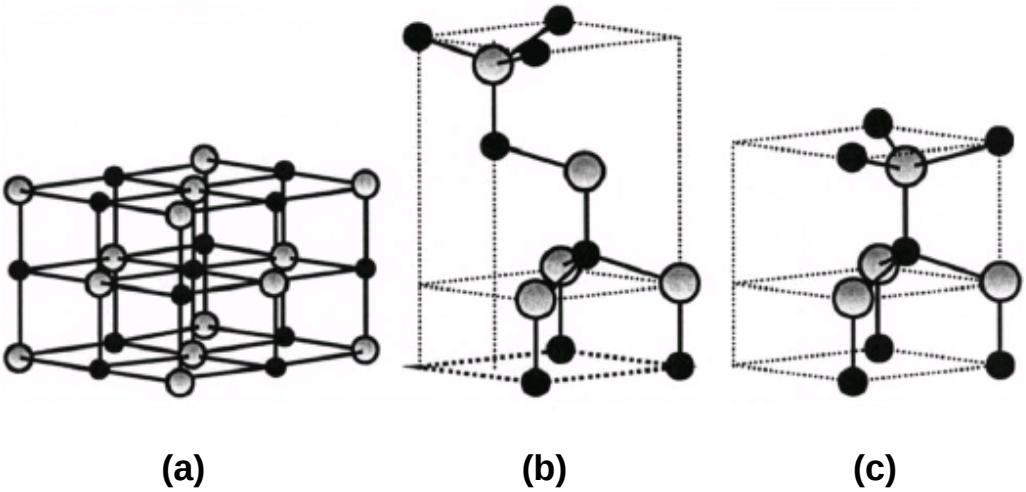

Figure 1-1. Stick and ball representation of ZnO crystal structures: (a) cubic rocksalt (B1), (b) cubic zinc blende (B3), and (c) hexagonal wurtzite (B4). The shaded gray and black spheres denote Zn and O atoms, respectively.[64]

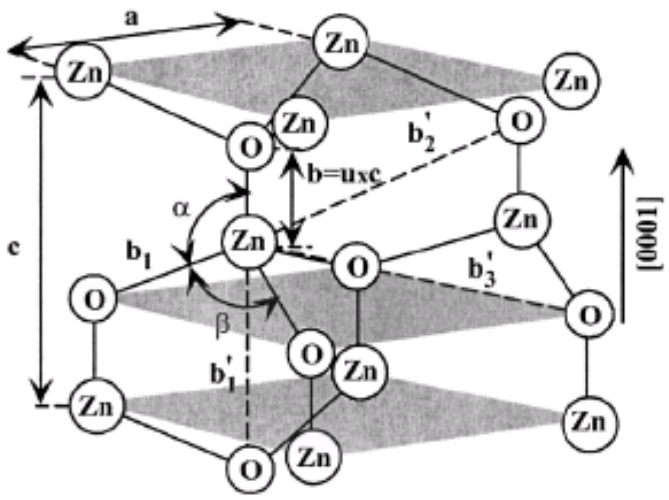

Figure 1-2. Schematic representation of a wurtzite ZnO structure having lattice constants *a* in the basal plane and *c* in the basal direction; *u* parameter is expressed as the bond length or the nearest-neighbor distance *b* divided by *c* (0.375 in ideal crystal), and *α* and *β* (109.47° in ideal crystal) are the bond angles.[64]

1.3.4 Potential Applications

Because of its diverse properties, both chemical and physical, zinc oxide is widely used in many areas. It plays an important role in a very wide range of applications, ranging from tires to ceramics, from pharmaceuticals to agriculture, and from paints to chemicals.

The most common potential application of ZnO is blue/ultraviolet laser diode (LD) and light emitting diode (LED) because its direct wide bandgap of 3.37 eV is comparable to GaN and excitation binding energy (~60 meV) is higher than room temperature thermal energy. However, it is difficult to produce a p-type ZnO semiconductor due to a strong selfcompensation effect arising from the presence of native defects or hydrogen impurities. Kawasaki et al. developed the preparation of p-i-n junction only consisting of ZnO and achieved violet electroluminescence.[65]

ZnO has also attracted much attention as a potential candidate to replace tin-doped In_2O_3 (ITO) transparent electrodes due to low cost, nontoxicity, and good electrical and optical properties. ZnO is an n-type semiconductor and its conductivity can be controlled by thermal treatment or by adequate doping. The doping of ZnO films with the group III elements can increase the conductivity of the films. In comparison with other elements, Al and Ga are the best dopants because their ionic radii are similar to that of Zn.

Due to its moderately high (very high for a semiconductor) electromechanical coupling coefficients, ZnO has been successfully used in thin film piezoelectric devices such as bulk acoustic wave and SAW resonators, filters, sensors, and microelectromechanical systems (MEMS), the most common application being the SAW filter, which has been an important component in mass consumer items such as TV filters and wireless communications systems. Successful development of sputtering of high-quality ZnO thin films on Si has been a breakthrough in the SAW device field as it allowed integration of ultrasonics with Si electronics for the first time, liberating device design from bulk piezoelectric substrates. For implementing acousticwave devices piezoelectric ZnO thin films grown on nonpiezoelectric substrates having high acoustic velocity and low propagation loss (diamond, sapphire), weakly piezoelectric materials such as quartz, amorphous substrates such as glass, and other semiconductors (Si, GaAs, InP, etc.) have been used.[67,68]

ZnO also has a potential to be applied for the efficient photocatalyst. When the ZnO is illuminated with a light having appropriate energy, electron/hole pairs with free electrons in the conduction band and positive holes in the valence band are generated. These electron/hole pairs have a high reduction/oxidation power and are capable of initiating a series of chemical reactions that eventually decompose the organic compounds. Although titanium dioxide (TiO_2) is well-known photocatalyst and widely used for various applications such as water and air purification,[68] anti-fogging[69] and self-cleaning surface,[70] ZnO have not been used like TiO_2. The main reason is the photolysis of ZnO crystal in aqueous solution under UV illumination,[71] which probably cause instability and less catalytic activity in the solution. However, in recent studies, ZnO has exhibited a better efficiency than TiO_2 in photocatalytic degradation of some dyes, even in aqueous solution.[72-74] Thus, ZnO can be a potential candidate for the future photocatalyst because of its strong photochemical reaction.

1.3.5 Synthesis of ZnO Micro/Nanostructures

Currently, there are many methods to fabricate ZnO micro/nanostructures. Oxidation of zinc vapor[75] involves placing metal zinc powder into a crucible and heating it in a furnace; at 419.53°C, the powder melts into liquid state before evaporating into zinc vapor. Oxygen is introduced to react with the zinc vapor and form needle-shaped crystal whiskers of ZnO.

Chemical vapor deposition (CVD)[76] is another approach that utilizes energy sources such as heat, plasma discharge, or UV irradiation to enable chemical reactions of vapor substances on the heated surface of a solid, where the stable solid products of the reaction are deposited. The vapor-liquid-solid method (VLS)[77,78] is the most common process for the fabrication of ZnO nanostructures. High temperatures are required to vaporize or decompose ZnO growth sources; a catalyst and the resulting zinc vapor then produce an alloy with a low melting point. Zinc precipitates from the supersaturated alloy before merging with atmospheric oxygen to form ZnO nanowires. The ZnO nanowires synthesized via the VLS method are generally monocrystalline, the diameter of which is determined by the particle size of the catalyst. Finally, the template-based method[79] employs methods such as electroplating, CVD, and the sol-gel method to grow the desired substance in the holes of a porous alumina substrate, the growth template. The ZnO nanostructures obtained from this method are polycrystalline. However these approaches generally require high temperatures. A low-temperature, large-scale, and versatile synthetic process is required before ZnO micro/nano structures find realistic applications in solar energy conversion, light emission, and other promising areas.

Solution processes to fabricate ZnO nanowires are attractive because of their low growth temperatures and good potential for scale-up. This thesis is aimed at developing the solution processes for the fabrication of ZnO micro/nanostructures.

1.4 Thesis Objective & Overview

The main focuses of the thesis are as follows:

(1) To prepare ZnO micro/nanostructure in powder and film form by solution process.

(2) To control the micro/nanostructures for widening the application of solution processed ZnO.

(3) To investigate and analyze the growth mechanisms.

(4) To propose future applications.

This thesis is composed of 6 chapters.

Chapter-1 includes the background and the objective of the thesis. The general properties, applications and synthesis method of ZnO micro/nanostructures are described in this chapter.

In Chapter-2, the direct preparation of ZnO hollow microspheres by solvothermal method is demonstrated. The effect of experimental conditions such as reaction temperature, additive or Zn source concentration and reaction time are investigated. The formation mechanism of ZnO hollow microspheres is also proposed.

In Chapter 3, the heat treatment for ZnO hollow microspheres and their application for visible light responsible photocatalyst and dye sensitized solar cells are demonstrated. Effect of heat treatment for ZnO hollow microspheres is discussed.

Chapter-4 describes the synthesis of nitrogen-doped ZnO rods by hydrothermal method. Using ammine-hydroxo zinc complex as a precursor solution enabled N-doping in ZnO crystal which is usually difficult without post heat treatment in N_2 or NH_3 atmosphere. Detail

characterization of prepared samples by UV-vis, Raman spectroscopy and XPS is shown in this chapter.

In Chapter 5, the fabrication of N-doped ZnO nanowire arrays by hydrothermal method using ZnO seeded substrate is demonstrated. Fundamental experiment for fabrication of N-doped ZnO nanowire arrays and detail characterization are shown in this chapter.

In Chapter 6, the thesis has been summarized and the future work and possible application are also highlighted.

The flowchart of the thesis is shown below;

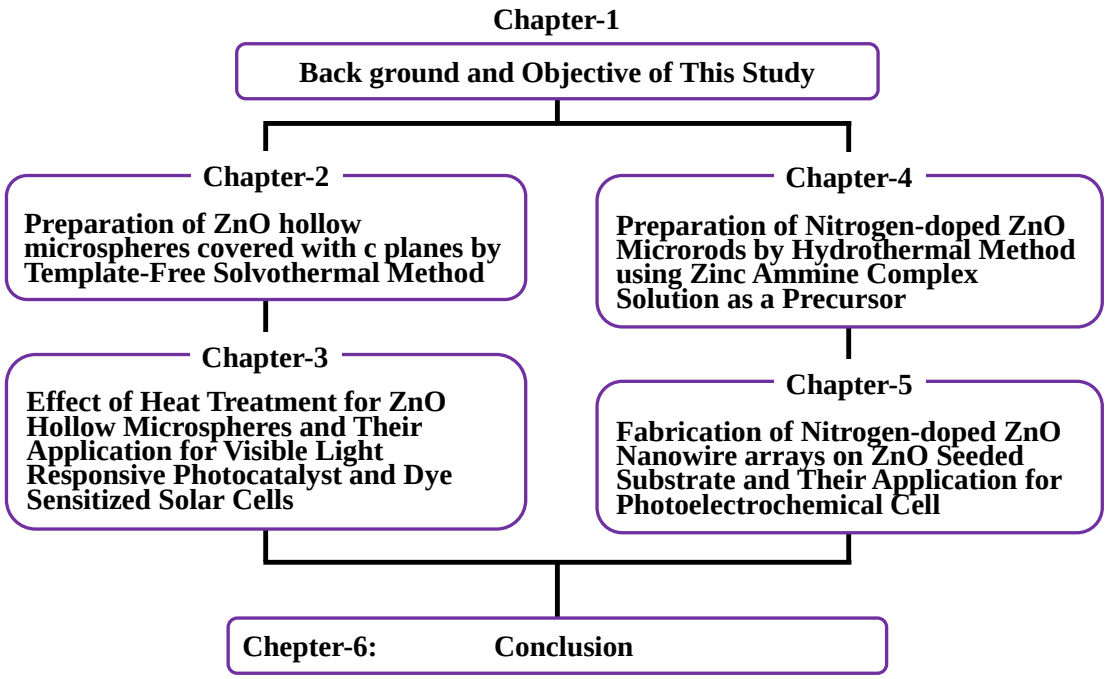

Figure 1-3. Flow chart of this thesis.

References

1. M. Yoshimura, *J. Mater. Res.*, 1998, **13**, 796-802.

2. M. Yoshimura, *J. Mater. Sci*., 2006, **41**, 1299-1306

3. J. H. Choy, E. S. Jang, J. H. Chung, D. J. Jang, Y. W. Kim, *Adv Mater.*, 2003, **15**, 1911-1914.

4. J. Liu, J. C. She, S. Z. Deng, J. Chen, N. S. Xu, *J. Phys. Chem. C*, 2008, **112**, 11685-11690.

5. T. J. Hsueh, C. L. Hsu, S. J. Chang, I. C. Chen, *Sensor. Actuat. B-Chem.*, 2007, **126**, 473-477.

6. Y. Liu, Z. H. Kang, Z. H. Chen, I. Shafiq, J. A. Zapien, I. Bello, W. J. Zhang, S. T. Lee, *Cryst. Growth Des.*, 2009, **9**, 3222-3227.

7. X. J. Feng, L. Feng, M. H. Jin, J. Zhai, L. Jiang, D. B. Zhu, *J. Am. Chem. Soc.*, 2004, **126**, 62-63.

8. T. Minami, *Semicond. Sci. Tech.*, 2005, **20**, S35-S44.

9. M. Y. Choi, D. Choi, M. J. Jin, I. Kim, S. H. Kim, J. Y. Choi, S. Y. Lee, J. M. Kim, S. W. Kim, *Adv. Mater.*, 2009, **21**, 2185-2189.

10. J. J. Schneider, R. C. Hoffmann, J. Engstler, O. Soffke, W. Jaegermann, A. Issanin, A. Klyszcz, *Adv. Mater.*, 2008, **20**, 3383-3387.

11. F. Habashi, *Hydrometallurgy*, 2005, **79**, 15.

12. R.W. Goranson, *Am. J. Sci*. 1931, **22**, 481.

13. M. Hosaka, *Prog. Cryst. Growth Charact. Mater.*, 1991, **21**, 71.

14. G. Demazeau, *J. Mater. Chem*. 1999, **9**, 15.

15. S. Feng and R. Xu Acc. *Chem. Res*, 2001, **34**, 239.

16. L.N. Demianets, *Prog. Cryst. Growth Charact. Mater.*, 1990, **21**, 299.

17. A. Rabenau, H. Rau, *Philips Tech. Rev*., 1969, **30**, 89.

18. Y.G. Gogotsi, M. Yoshimura, *Nature*, 1994, **367**, 628.

19. N. Yamasaki, K. Yanagisawa, M. Nishioka, S. Nakahara, *J. Mater. Sci. Lett.*, 1986, **5**, 355.

20. M. Rajamathi, R. Seshadri, *Curr. Opin. Solid State Mater. Sci.*, 2002, **6**, 337.

21. C. W. Bunn, *Proc. Phys. Soc. London*, 1935, **47**, 835.

22. R. B. Heller, J. McGannon, A. H. Weber, *J. Appl. Phys.*, 1950, **21**, 1283.

23. T. J. Gray, *J. Am. Ceram. Soc.*, 1954, **37**, 534.

24. G. P. Mohatny, L. V. Azaroff, *J. Chem. Phys.*, 1961, **35**, 1268.

25. R. R. Reeber, *J. Appl. Phys.*, 1970, **41**, 5063.

26. D. C. Reynolds, T. C. Collins, *Phys. Rev.*, 1969, **185**, 1099.

27. D. G. Thomas, *J. Phys. Chem. Solids*, 1960, **15**, 86.

28. Y. S. Park, C. W. Litton, T. C. Collins, D. C. Reynolds, *Phys. Rev.*, 1965, **143**, 512.

29. R. J. Collins, D. A. Kleinman, *J. Phys. Chem. Solids*, 1959, **11**, 190.

30. R. L. Weiher, *Phys. Rev.*, 1966, **152**, 736.

31. W. S. Bear, *Phys. Rev.*, 1967, **154**, 785.

32. E. Mollwo, *Z. Angew. Phys.*, 1954, **6**, 257.

33. W. L. Bond, *J. Appl. Phys.*, 1965, **36**, 1674.

34. W. Y. Liang, A. D. Yoffe, *Phys. Rev. Lett.*, 1968, **20**, 59.

35. A. R. Hutson, *J. Appl. Phys.*, 1961, **32**, 2287.

36. J. L. Freeouf, *Phys. Rev. B*, 1973, **7**, 3810.

37. O. F. Schirmer, D. Zwingel, *Solid State Commun.*, 1970, **8**, 1559.

38. J. J. Hopfield, D. G. Thomas, *Phys. Rev. Lett.*, 1965, **15**, 22.

39. Y. S. Park, J. R. Schneider, *J. Appl. Phys.*, 1968, **39**, 3049.

40. G. Heiland, E. Mollwo, and F. Stöckmann, *Solid State Phys.*, 1959, **8**, 191.

41. T. C. Damen, S. P. S. Porto, B. Tell, *Phys. Rev.*, 1966, **142**, 570.

42. C. A. Arguello, D. L. Rousseau, S. P. S. Porto, *Phys. Rev.*, 1969, **181**, 1351.

43. R. H. Callender, S. S. Sussman, M. Selders, R. K. Chang, *Phys. Rev. B*, 1973, **7**, 3788.

44. J. M. Calleja, M. Cardona, *Phys. Rev. B*, 1977, **16**, 3753.

45. M. Tsuboi, A. Wada, *J. Chem. Phys.*, 1968, **48**, 2615.

46. S. P. S. Porto, R. S. Krishnan, *J. Chem. Phys.*, 1967, **47**, 1009.

47. S. S. Mitra, O. Brafman, W. B. Daniels, R. K. Crawford, *Phys. Rev.*, 1969, **186**, 942.

48. G. Galli, J. E. Coker, *Appl. Phys. Lett.*, 1970, **16**, 439.

49. M. Shiloh, J. Gutman, *J. Cryst. Growth*, 1971, **11**, 105.

50. D. F. Croxall, R. C. C. Ward, C. A. Wallace, R. C. Kell, *J. Cryst. Growth*, 1974, **22**, 117.

51. W. Kern, R. C. Heim, *J. Electrochem. Soc.*, 1970, **117**, 562.

52. D. C. Look, *Mater. Sci. Eng. B*, 2001, **80**, 381.

53. E. Ohshima, H. Ogino, I. Niikura, K. Maeda, M. Sato, M. Ito, T. Fukuda, *J. Cryst. Growth*, 2004, **260**, 166.

54. J.-M. Ntep, S. S. Hassani, A. Lusson, A. Tromson-Carli, D. Ballutaud, G. Didier, R. Triboulet, *J. Cryst. Growth*, 1999, **207**, 30.

55. D. C. Look, D. C. Reynolds, J. W. Hemski, R. L. Jones, J. R. Sizelove, *Appl. Phys. Lett.*, 1999, **75**, 811.

56. A. Y. Polyakov et al., *J. Appl. Phys.*, 2003, **94**, 2895.

57. S. O. Kucheyev, J. S. Williams, C. Jagadish, J. Zou, C. Evans, A. J. Nelson, A. V. Hamza, *Phys. Rev. B*, 2003, **67**, 094115.

58. X. Gu, M. A. Reshchikov, A. Teke, D. Johnstone, H. Morkoc, B. Nemeth, J. Nause, *Appl. Phys. Lett.*, 2004, **84**, 2268.

59. F. Hamdani et al., *J. Appl. Phys.*, 1998, **83**, 983.

60. S. J. Pearton, D. P. Norton, K. Ip, Y. W. Heo, T. Steiner, *Prog. Mater. Sci.*, 2005, **50**,

293-340.

61. K. Vanheusden, C. H. Seager, W. L. Warren, D. R. Tallant, J. A. Voigt, *Appl. Phys. Lett.*, 1996, **68**, 403-405.

62. D. C. Look, J. W. Hemsky, J. R. Sizelove, *Phys. Rev. Lett.*, 1999, **82**, 2552-2555.

63. A. Janotti, C. G. Van de Walle, *Nat. Mater.*, 2007, **6**, 44-47.

64. Ü. Özgür, Ya. I. Alivov, C. Liu, A. Teke, M. A. Reshchikov, S. Doğan, V. Avrutin, S.-J. Cho, H. Morkoç, *J. Appl. Phys.*, 2005, **98**, 041301.

65. A. Tsukazaki, A. Ohtomo, T. Onuma, M. Ohtani, T. Makino, M. Sumiya, K. Ohtani, S. F. Chichibu, S. Fuke, Y. Segawa, H. Ohno, H. Koinuma, M. Kawasaki, *Nat. Mater.*, 2005, **4**, 42-46.

66. Y. Lu, N. W. Emanetoglu, Y. Chen, ZnO piezoelectric devices, Zinc Oxide Bulk, Thin Films and Nanostructures: Processing, Properties and Applications, C. Jagadish and S. J. Pearton, Eds. Amsterdam, The Netherlands: Elsevier, 2006, pp. 443–489.

67. N. W. Emanetoglu, S. Muthukumar, P. Wu, R. Wittstruck, Y. Chen, Y. Lu, *IEEE Trans. Ultrason. Ferroelectr. Freq. Control*, 2003, **50 (5)**, 537–543.

68. D. F. Ollis, *Comptes Rendus De L Academie Des Science Serie Ii Fascicule C-Chimie*, 2000, **3**, 405-411.

69. A. Tricoli, M. Righettoni, S. E. Pratsinis, *Langmuir*, 2009, **25**, 12578-12584.

70. A. Nakajima, K. Hashimoto, T. Watanabe, K. Takai, G. Yamaguchi, A. Fujishima, *Langmuir*, 2000, **16**, 7044-7047.

71. A. van Dijken, A. H. Jassen, M. H. P. Smitsmans, D. Vanmaekelbergh, A. Meijerink, *Chem. Mater.*, 1998, **10**, 3513-3522.

72. C. Hariharan, *Appl. Catal. a-General*, 2006, **304**, 55-61.

73. Y. J. Jang, C. Simer, T. Ohm, *Mater. Res. Bull.*, 2006, **41**, 67-77.

74. S. Sakthivel, B. Neppolian, M. V. Shankar, B. Arabindoo, M. Palanichamy, V. Murugesan, *Sol. Energy Mater. Sol. Cells*, 2003, **77**, 65-82.

75. W. Lee, M. C. Jeong, J. M. Myoung, *Acta Mater.*, 2004, **52 (13)**, 3949–3957.

76. B. P. Zhang, N. T. Binh, K. Wakatsuki et al., *J. Phys. Chem. B*, 2004, **108 (30)**, 10899–10902.

77. Y. W. Wang, L. D. Zhang, G. Z. Wang, X. S. Peng, Z. Q. Chu, C. H. Liang, *J. Cryst. Growth*, 2002, **234 (1)**, 171–175.

78. M. H. Huang, Y. Wu, H. Feick, N. Tran, E. Weber, P. Yang, *Adv. Mater.*, 2001, **13 (2)**, 113–116.

79. C. H. Liu, W. C. Yiu, F. C. K. Au, J. X. Ding, C. S. Lee, S. T. Lee, *Appl. Phys. Lett.*, 2003, **83 (15)**, 3168–3170.

Chapter-2

Preparation of ZnO hollow microspheres covered with *c* planes by Template-Free Solvothermal Method and Their Application for Photocatalyst and Dye Sensitized Solar Cells

Chapter-2 demonstrates the preparation of ZnO hollow microspheres by template-free solvothermal method. Reaction at 150 °C yielded highly crystalline ZnO particles, whose shape could be controlled from solid to hollow spheres, by varying the reaction time. The ZnO hollow spheres were covered with c planes. Low-temperature, template-free preparation of highly crystalline ZnO hollow microspheres with controllable surface morphology and orientation would be invaluable. The detailed formation mechanism of ZnO hollow microspheres by solvothermal method is also discussed.

2.1 Introduction

In this chapter, template-free synthesis of ZnO hollow microspheres using solvothermal method is presented. Preparing ZnO hollow spheres has received much attention, because of their low density, high surface area and good surface permeability.[1,2] ZnO hollow spheres have potential in gas sensing, drug delivery, microcapsule reactors and photoelectric devices.[3-5] ZnO hollow spheres exhibit large light-harvesting efficiencies, so are also applicable in photocatalysts and dye sensitized solar cells (DSSCs). We believe that ZnO hollow spheres with the surface exposing the c planes will exhibit better performance than ZnO solid microspheres, in various applications. However, preparing well-crystallized ZnO hollow microspheres with controllable surface morphology and crystal orientation remains a challenge.[6,7]

The thermal evaporation[8-10] and template hydrothermal processess[11,12] have been the two common processes to prepare ZnO hollow microspheres. The thermal evaporation process generally involves the vaporization of Zn powder, solidification of liquid Zn droplets, oxidation of spherical Zn particle surfaces, and sublimation of Zn within particles. Its disadvantages include requirements of specialized equipments, high temperatures (typically >500 °C) and vacuum conditions. The hydrothermal synthesis of ZnO hollow spheres is usually template-assisted using hard[11] and soft templates.[12] The usage of such templates complicates the synthesis process, and often requires further steps to remove the templates. Accordingly, Development of a facile, low temperature and template-free preparation method is desirable. Zhu *et al*.[13] recently developed a template-free method to prepare ZnO hollow spheres, in aqueous solution at low temperature. Li *et al*.[14] also developed a template-free solvothermal route to prepare ZnO hollow spheres, with the assistance of polyoxometalate. However, these reports have not clarified the crystal orientation in the prepared hollow spheres. There have been few reports of ZnO spherical hollow powders whose surface is covered with the *c* planes.[15,16] Hu *et al*.[15] prepared ZnO hollow microspheres consisting of ZnO nanorods which expose their *c* planes to the surface, using a water/glycerol solvent. Qui *et al*.[16] prepared hierarchical $Zn_{1-x}Co_xO$ nanodiscs into hollow spheres whose surface is covered with the *c* planes, using a water/ethylene glycol solvent. However, further investigation is required to reveal the formation

mechanism.

Here, ZnO hollow microspheres were synthesized by the template-free solvothermal method using ethylene glycol (EG) and hexamethylenetetramine (HMT) as a main solvent and pH buffer respectively. The synthetic process is simple, and does not require specialized equipment or templates. Microspheres with high crystallinity and a unique morphology have been obtained at a relatively low temperature (150 °C). The shape of the ZnO particles can be controlled from solid to hollow spheres, by varying the reaction time. The outer surfaces of ZnO hollow spheres are covered with the c planes. Their formation mechanism is proposed, considering the Zn^{2+} solubility and inner structure of the microspheres.

2.2 Experimental

2.2.1 Preparation of ZnO Hollow microspheres

Zinc acetate dihydrate [$Zn(CH_3COO)_2 \cdot 2H_2O$] (>99%, Wako Pure Chemical Industries, Japan), HMT [$C_6H_{12}N_4$] (>99%, Wako Pure Chemical Industries, Japan) and EG [$C_2H_4(OH)_2$] (>99.5%, Wako Pure Chemical Industries, Japan), were used as chemical reagent without further purification. For the solvothermal synthesis of ZnO hollow microspheres, a closed cylindrical Teflon-lined stainless steel autoclave with 35 ml capacity was used. In a typical synthesis, 3 mmol of $Zn(CH_3COO)_2 \cdot 2H_2O$ and 12 mmol of HMT were dissolved in a 30 ml solution of EG (95 vol.%) and distilled water (5 vol.%). The resulting solution was transferred to the autoclave

and heated at 150 °C for 1-12 h. The precipitate was collected, thoroughly washed with ethanol, and dried at 60 °C.

2.2.2 Characterization

X-Ray diffraction (XRD) was used to determine crystal phases, with a RINT2000 diffractometer (Rigaku, Japan) and Cu-Kα radiation. The morphology was observed using a scanning electron microscope (SEM) with a field-emission electron gun (S4500, Hitachi, Japan) and the microstructure was further analyzed using a transmission electron microscope (TEM) (JEM-2010UHR, JEOL, Japan) operated at 200 kV. Specimens for TEM were prepared by a focused ion beam (FIB) instrument (FB-2100, Hitachi, Japan). The Zn^{2+} concentration of the supernatant after reaction was measured by inductively coupled plasma-atomic emission spectroscopy (ICP-AES) (ICPS-8100, SHIMADZU, Japan). Photoluminescence (PL) measurements were recorded at room temperature using a luminescence spectrometer (LS55, PerkinElmer Inc., USA), at an excitation wavelength of 325 nm.

2.3 Result and Discussion

2.3.1 Formation Mechanism of ZnO Hollow Mcrospheres

The dried products were characterized by XRD to determine the crystal structure of the products. Figure 2-1 shows the XRD pattern of the samples obtained after different reaction times, when the reaction temperature was fixed at 150 °C. All the diffraction peaks were in

good agreement with that of the hexagonal wurtzite structure of ZnO (JCPDS No. 36-1451) even for the sample prepared only for 1 h. No other peaks were detected, indicating the high purity of the samples.

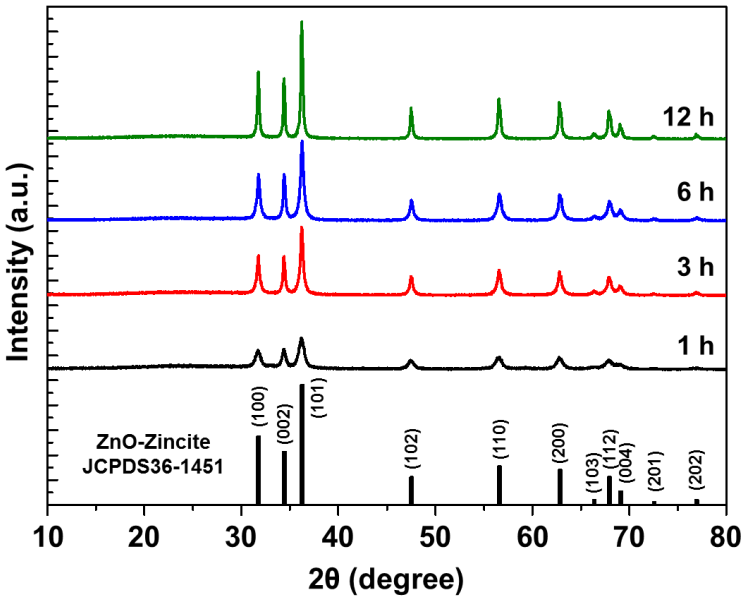

Figure 2-1. XRD patterns of ZnO particles prepared at 150 °C for different reaction times.

The morphologies of products prepared by solvothermal treatment at 150 °C for different reaction times were observed by SEM, as shown in Figure 2-2. Figure 2-2a shows an SEM image of ZnO sample obtained after 1 h, in which uniform solid microspheres of 1-2 μm in diameter were observed. The high-magnification image in Figure 2-2b implied that the ZnO spheres were composed of nanoparticles of ~20 nm in diameter. Uniform microspheres were also obtained after reaction for 3 h (Figure 2-2c). In this case, particles on the sphere surfaces had exhibited plate-like hexagonal crystals, which were ~200 nm in diameter (Figure 2-2d).

Isolated hollow spheres were observed in the sample prepared for 6 h, as shown by the red arrows in Figure 2-2e. Figure 2-2f indicated that the shell thickness was 200-300 nm, and that the surface particles appeared to be dissolved and roughened, compared with the sample prepared for 3 h (Figure 2-2c and 2-2d). The number of hollow spheres increased with increasing reaction time, as shown in Figure 2-2g.

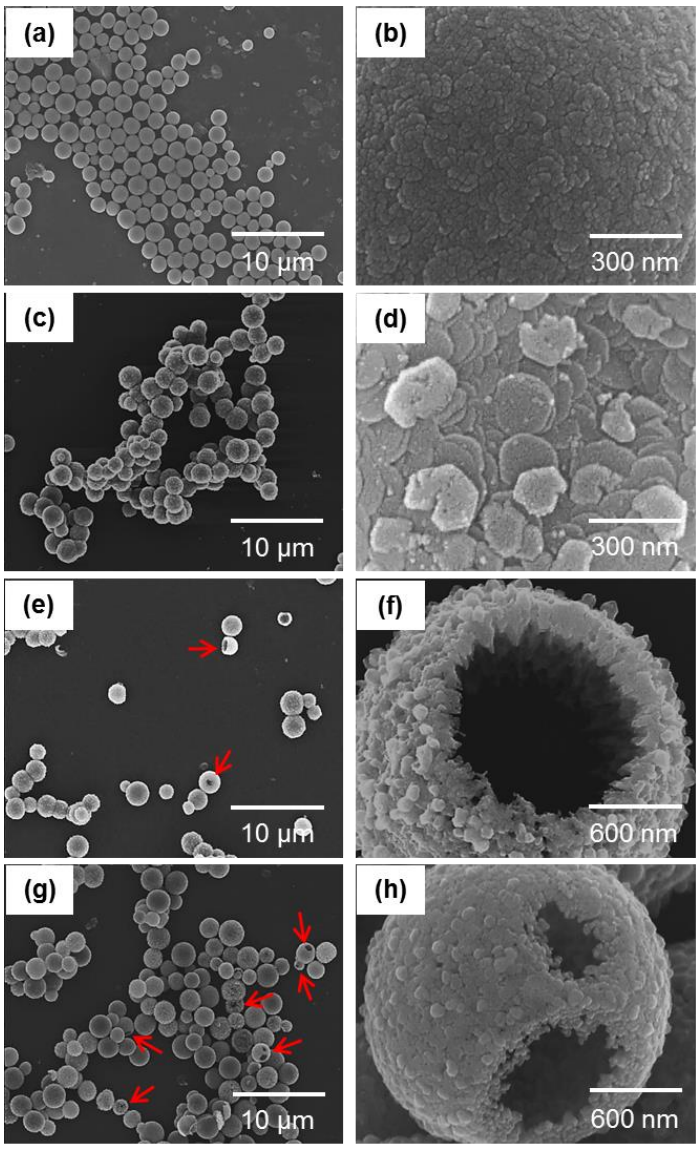

Figure 2-2. SEM images of ZnO particles prepared at 150 °C for (a) 1, (c) 3, (e) 6 and (g) 12 h, and their higher magnification views in (b), (d), (f) and (h), respectively.

Figure 2-3 shows the particle size distribution of the spheres prepared at 150 °C for different reaction time. They were extracted from 500 spheres in total which were observed in a scanning electron microscopy (SEM) photographs. The mean particle size and the standard deviation were 2.3 and 0.5 μm for the sample prepared for 1 h, 3.1 and 0.6 μm for 3 h and 2.8 and 0.6 μm for 12 h, respectively. The mean sphere size became larger with the increase of the reaction time from 1 to 3 h due to proceeding of crystal growth, while the particle size of the sample prepared for 12 h was slightly decreased due to the dissolution of the nanoparticles into the solution.

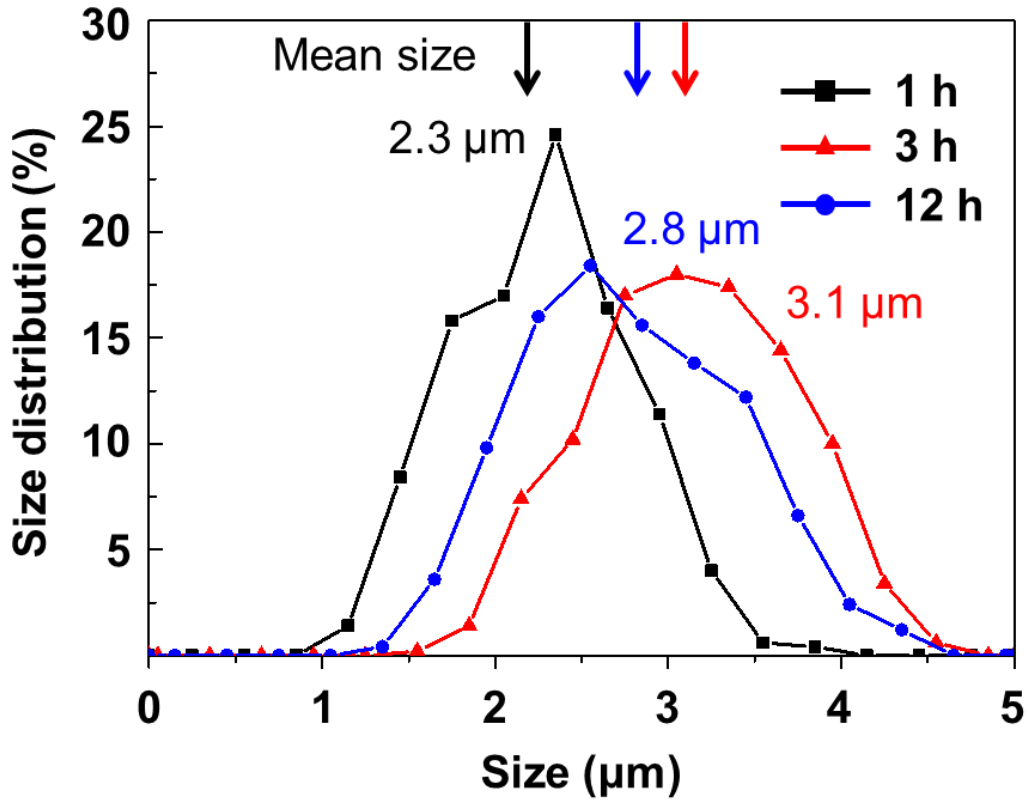

Figure 2-3. Particle size distribution of the spheres prepared at 150 °C for different reaction time.

The size, shape and surface morphology of the solid and hollow microspheres were characterized by TEM. TEM images of the products prepared for 3, 6 and 12 h, dispersed on carbon films are shown in Figure 2-4. For the sample prepared by reaction for 3 h, difference of the contrasts between the sphere edges and centers could not be observed, indicating that the microspheres were solid, not hollow (Figure 2-4a). On the other hand, the difference of the contrast became apparent for some spheres prepared by reaction for 6 h (Figure 2-4b). When the reaction time was 12 h, the shell appeared porous, and difference of the contrast between the shell and core was apparent for all spheres, indicating transformation to a hollow structure (Figure 2-4c).

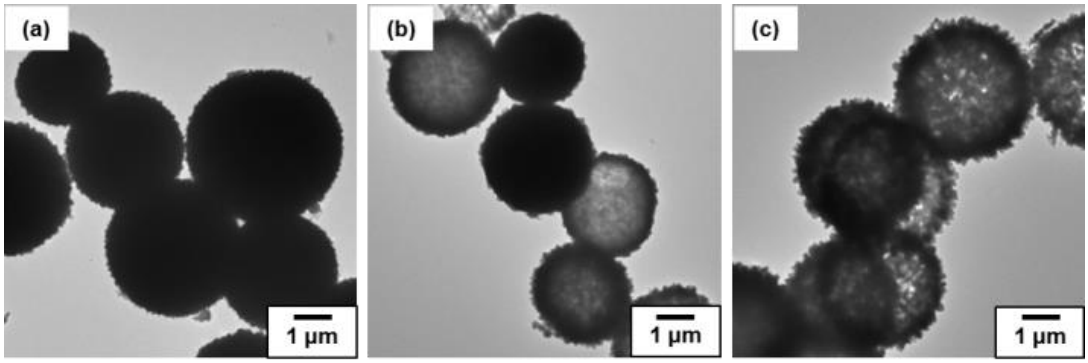

Figure 2-4. TEM images of top views of ZnO microspheres prepared at 150 °C for (a) 3, (b) 6 and (c) 12 h.

The Zn concentration in the supernatants of reacted solutions was measured to investigate the formation mechanism of the ZnO hollow microspheres. Figure 2-5 shows the variation of supernatant Zn concentration, measured by ICP-AES after each reaction duration at 150 °C. The Zn concentration at 3 h was lower than that at the beginning of the reaction, because Zn^{2+} was

consumed for the formation of ZnO spheres. The concentration increased after 3 h, and had become saturated by 9 h. This increase was attributed to the dissolution of particles at the centers of spheres.

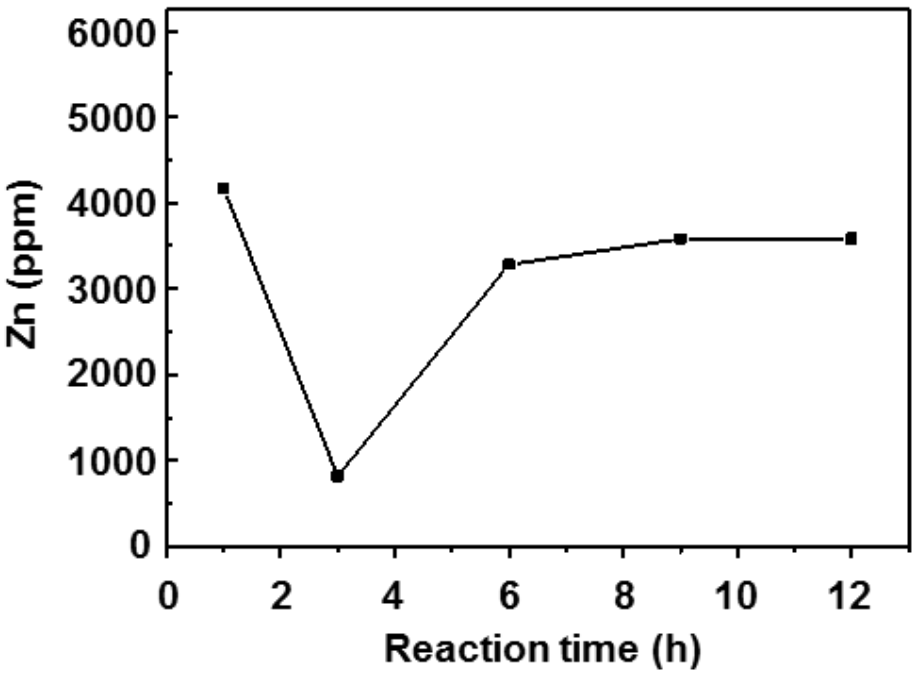

Figure 2-5. ICP-AES analysis of the variation of Zn concentration in the supernatant after various reaction times.

The variation of supernatant Zn concentration in the case of the reaction temperature at 100 and 200 °C was also measured (Figure 2-6). For reaction after 1 h at 100 °C, no precipitate was obtained, and the Zn concentration was comparable to the initial Zn concentration (~6000 ppm). For reaction at 100 °C, the supernatant Zn concentration gradually decreased with increasing reaction time, because of the formation of ZnO. An increase in Zn concentration was not observed until a reaction time of 12 h. The supernatant Zn concentration exhibited an unstable

change, upon reaction at 200 °C. For reaction after 1 h, the Zn concentration was much lower than the initial concentration (~6000 ppm), and the concentration fluctuated with increasing reaction time. These results indicated that 150 °C was the optimal temperature for preparing ZnO hollow microspheres. This was because dissolution did not occur at lower reaction temperatures (100 °C), and the reaction was too fast to readily control at higher temperatures (200 °C).

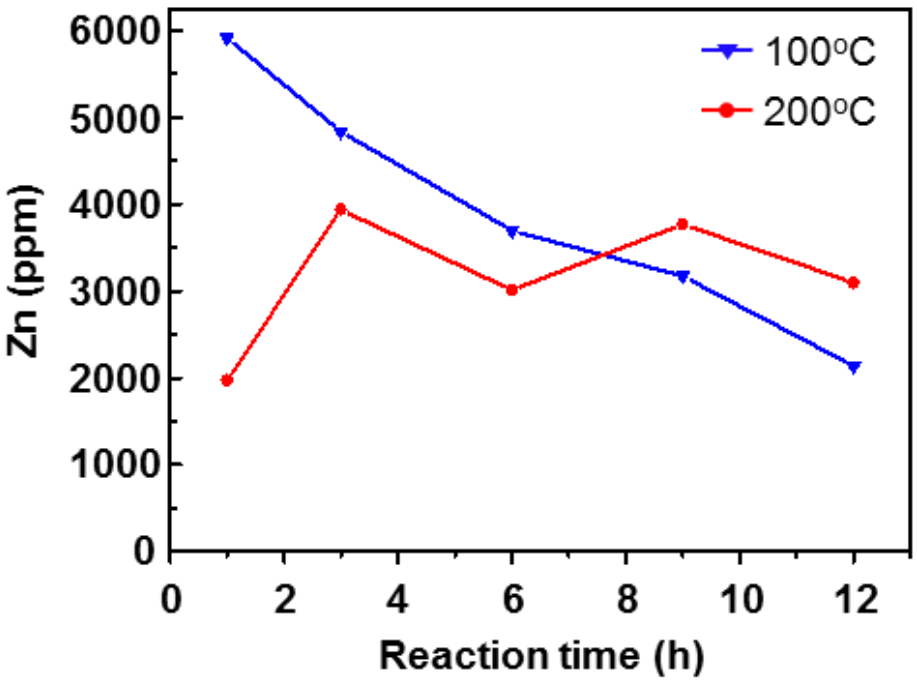

Figure 2-6. ICP-AES analyses of the variation of supernatant Zn concentration, after reaction at 100 and 200 °C for different reaction times.

From the SEM, TEM, XRD and ICP-AES results, a formation mechanism for the ZnO hollow microspheres was proposed, and shown in Figure 2-7. The following reactions are thought to have occurred in the first step of the formation of solid ZnO microspheres:

$$C_6H_{12}N_4 + 6H_2O \rightarrow 6HCHO + 4NH_3 \quad (1)$$

$$NH_3 + H_2O \rightarrow NH_4^+ + OH^- \quad (2)$$

$$Zn^{2+} + 2OH^- \rightarrow Zn(OH)_2 \quad (3)$$

$$Zn(OH)_2 \rightarrow ZnO + H_2O \quad (4)$$

The role of HMT ($C_6H_{12}N_4$) in the growth of the solid microspheres could be regarded as a pH buffer, which slowly released OH^- during thermal decomposition (Eqs. 1 and 2).[28] OH^- reacted with Zn^{2+} to form $Zn(OH)_2$ nanoclusters in solution (Eq. 3), which subsequently transformed into an initial ZnO crystal (Eq. 4). After nucleation, the initial crystals agglomerated to form ZnO solid microspheres, to minimize the surface energy. When the reaction time was extended, particles on or near the surface grew into hexagonal crystals. After the degree of supersaturation decreased, the following reaction occurred:

$$ZnO + NH_3 + 2H^+ \rightarrow Zn(NH_3)^{2+} + H_2O \quad (5)$$

Particles at the sphere center possessing low crystallinity preferentially dissolved according to Eq. 5, and hollow spheres were formed through Ostwald ripening process.

Room-temperature PL measurements were recorded to investigate the quality of the ZnO hollow microspheres. Figure 2-8 shows the PL spectrum of the ZnO hollow microspheres, which exhibits strong UV emission at ~392 nm. Weak blue emission at around ~420 nm was observed and the visible wavelength emission was almost negligible.[15,17,18] Since the UV

emission originated from the recombination of free excitons in the ZnO near band edge,[19] the intensity of room-temperature UV emission is an indicator of the ZnO quality. Visible emission is associated with interstitial Zn ions,[20] oxygen vacancies,[21] cationic impurities[22] and damaged crystals.[23] Visible emission indicates the existence of deep centers within the ZnO. Therefore, strong band-edge emission accompanied by insignificant visible emission might be evidence of the high crystal quality of the ZnO hollow spheres. The effect of non-radiative recombination centers were not considered in the current study. Thus, it should not be concluded that the ZnO hollow spheres had a lower defect concentration than reported studies.[15,17,18] Further investigation about the total defect concentration of the ZnO hollow spheres is required.

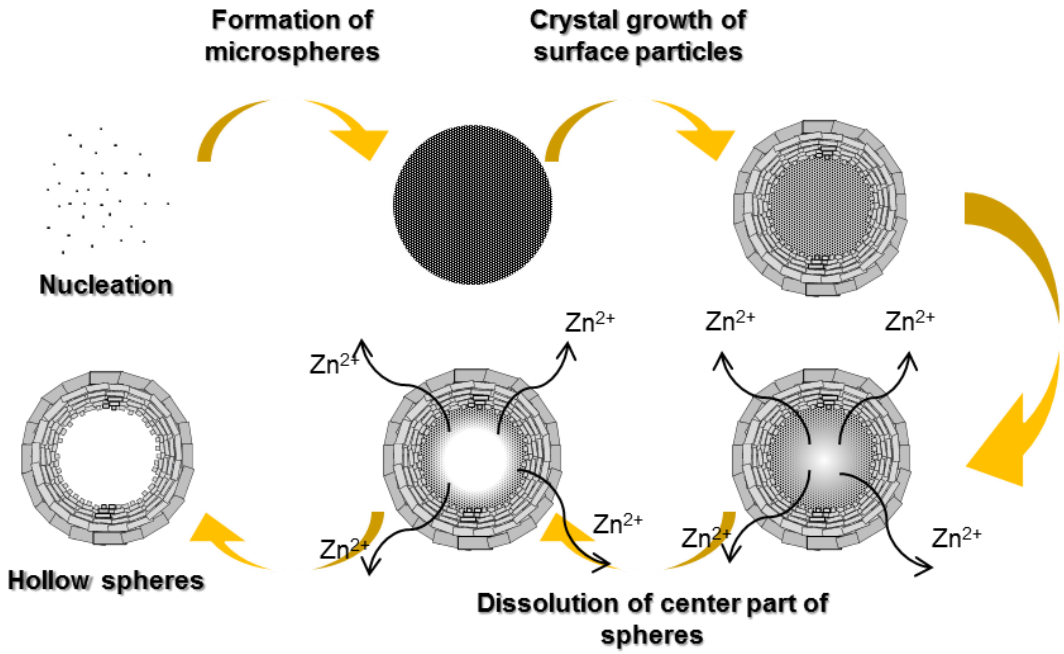

Figure 2-7. Schematic showing the proposed formation mechanism of the ZnO hollow spheres.

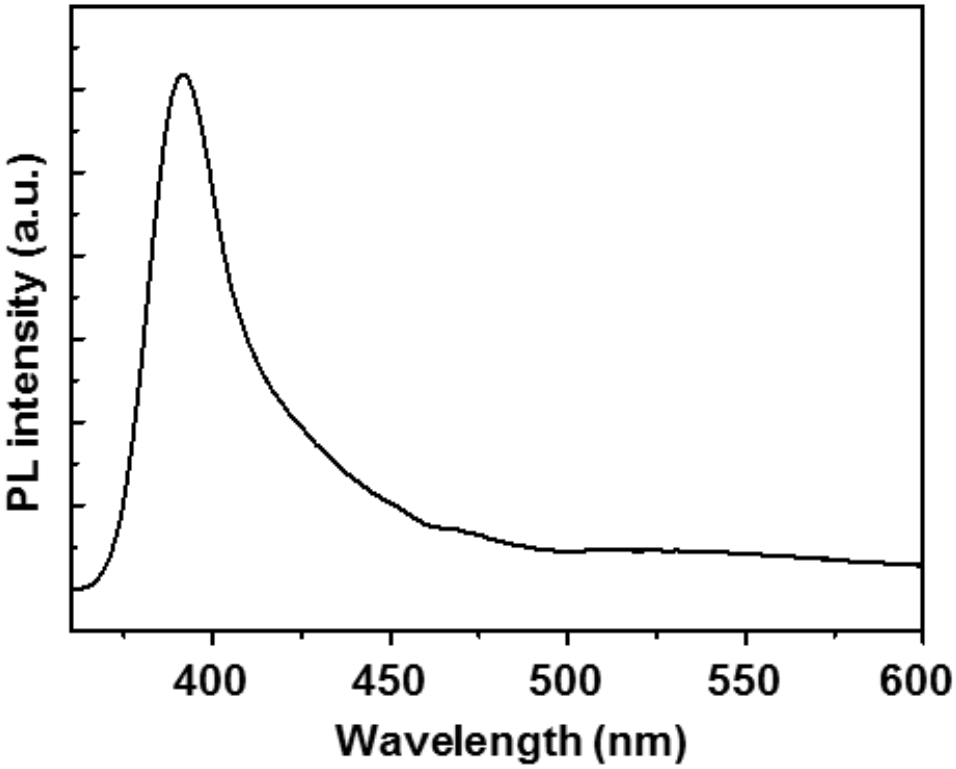

Figure 2-8. PL spectrum of ZnO hollow microspheres prepared at 150 °C for 12 h.

2.3.2 Structure Analysis of ZnO Solid and Hollow Microspheres

Figure 4 shows SEM and corresponding cross-sectional TEM images, of solid and hollow spheres prepared at 150 ℃ for 3 (Figures 2-9a-c) and 12 h (Figures 2-9d, e), respectively.

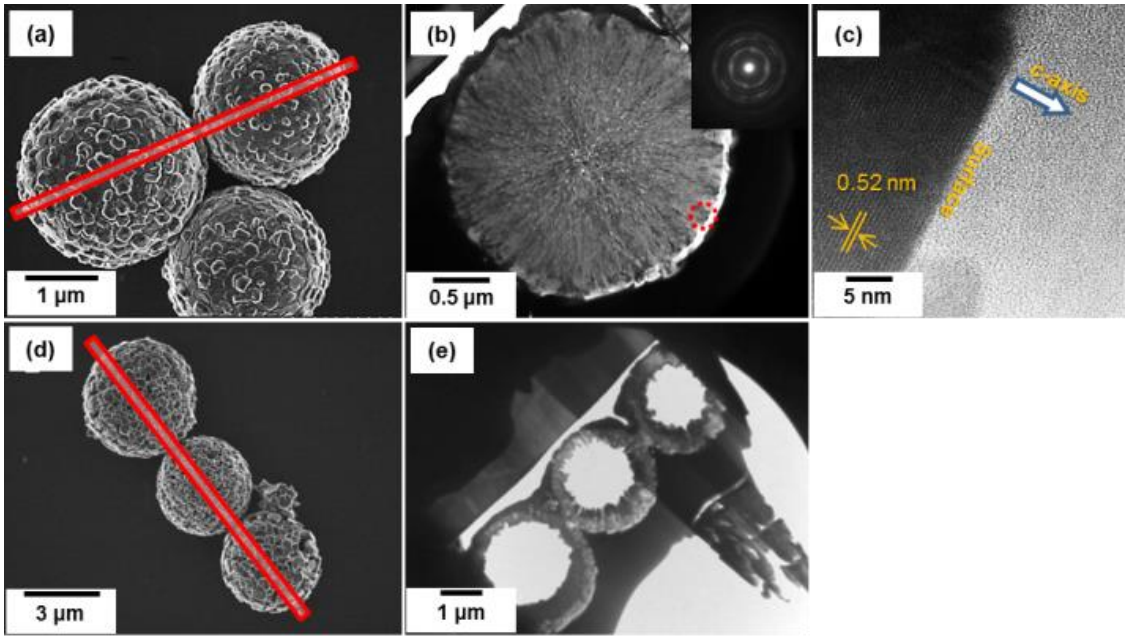

Figure 2-9. SEM images of ZnO prepared from reaction times of (a) 3 and (d) 12 h at 150°C, and their corresponding cross-sectional TEM images in (b) and (e), respectively. (c) HR-TEM image of the circled area (b).

The solid sphere was dense, and a radial contrast was observed inside the sphere (Figure 2-9b). The region around the center of the sphere appeared porous, while that near (~ 500 nm) the surface appeared dense. Different crystal sizes at the surface and core were also confirmed. The selected-area electron diffraction (SAED) pattern around the center of the sphere exhibited a ring-like pattern, as shown in the inset in Figure 2-9b. This indicated the center was composed of polycrystalline ZnO, rather than being amorphous. The high-resolution TEM (HRTEM)

image at the sphere surface (Figure 2-9c) shows clear and continuous lattice fringes with the spacing of 0.52 nm which corresponded to the 0001, indicating that the spheres were covered with the *c* planes. Figure 2-9e shows that the sample prepared for 12 h is actually hollow microspheres, whose shells were composed of needle-like ZnO crystals.

The effect of reaction temperature on the formation of ZnO hollow microspheres was also investigated. For the sample prepared at 100 °C for 12 h, solid microspheres were clearly obtained, as shown in Figure 2-10. Their surfaces consisted of hexagonal crystals of hundreds of nm in diameter, and were similar to the surfaces of the sample prepared at 150 °C for 3 h (Figure 2-2d). The SEM image of a broken sphere revealed its solid hierarchal structure, with pyramid-like crystals (Figure 2-10b). Microspheres prepared at 200 °C were composed of larger particles (Figure 2-10c), and the SEM image of a broken sphere revealed a hollow structure (Figure 2-10d). The shell was much thicker, compared with that of the sample prepared at 150 °C.

Figure 2-11 shows SEM images and corresponding cross-sectional TEM images of ZnO microspheres prepared at 200 °C for 1 and 4 h. The cross-sectional TEM image of the microspheres prepared at 200 °C revealed a clear difference between the sphere surfaces and centers. The cross-sectional TEM image for the sample prepared for 1 h in Figure 2-11b, was similar to that of the sample prepared at 150 °C for 3 h (Figure 2-9b). The center of the sphere

was porous, and the surface appeared dense to a depth of ~200 nm. The high magnification TEM image of the sphere surface shown inset in Figure 7b indicated the sphere surfaces consisted of pyramid-like crystals. The HR-TEM image in Figure 2-11c shows that surface particles were single crystals with lattice fringes of 0.52 nm, which corresponded to the [0001] ZnO growth direction. This indicated that the spheres were covered with ZnO *c* planes. Figure 2-11d shows that the centers of spheres prepared by reaction for 4 h had begun to hollow. A difference in the particle shape was clearly observed from the center to surface of spheres, as they changed from granular, needle-like to pyramid-like crystals (Figure 2-11e). The surface of this sphere was surrounded by highly crystalline pyramid-like crystals, of 300-600 nm in diameter. Some surface crystals had side facets, appearing as brilliant-cut diamonds, seen inset in Figure 2-11e. The well-resolved lattice fringes also indicated the surface was highly crystalline with flat planes, as shown in Figure 2-11f.

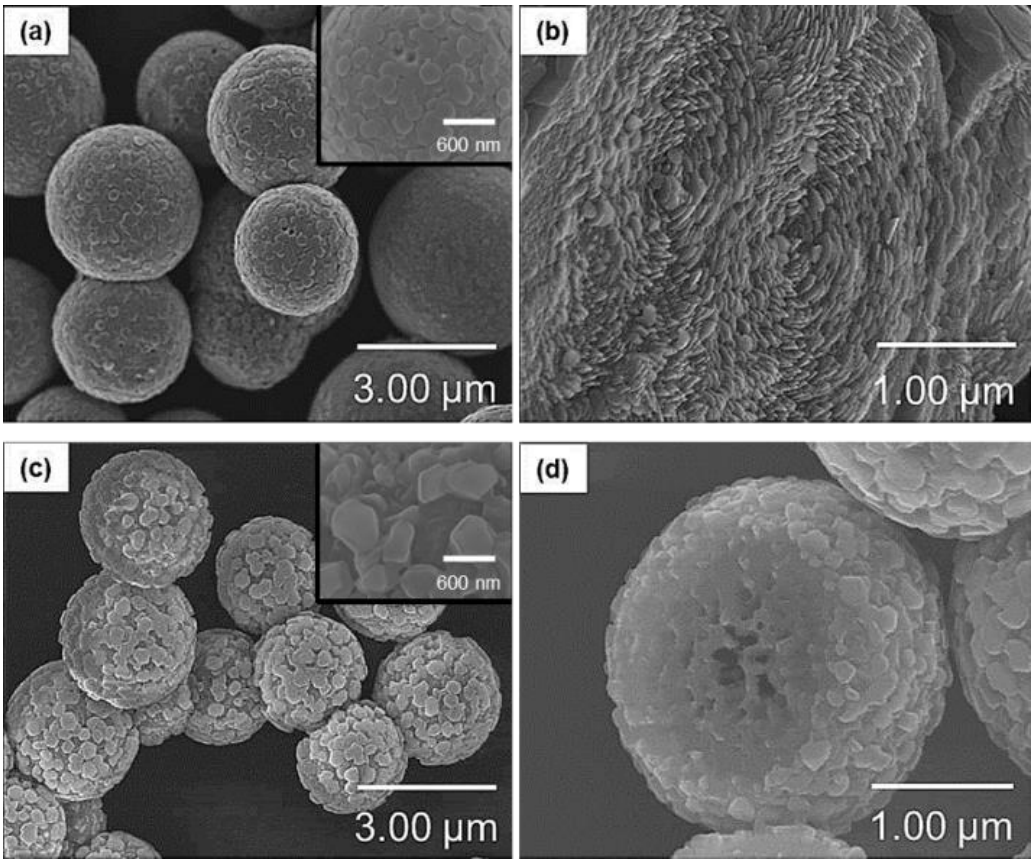

Figure 2-10. SEM images of ZnO microspheres prepared at (a) 100 and (c) 200 °C for 12 h, and their corresponding high magnification images in (b) and (d), respectively.

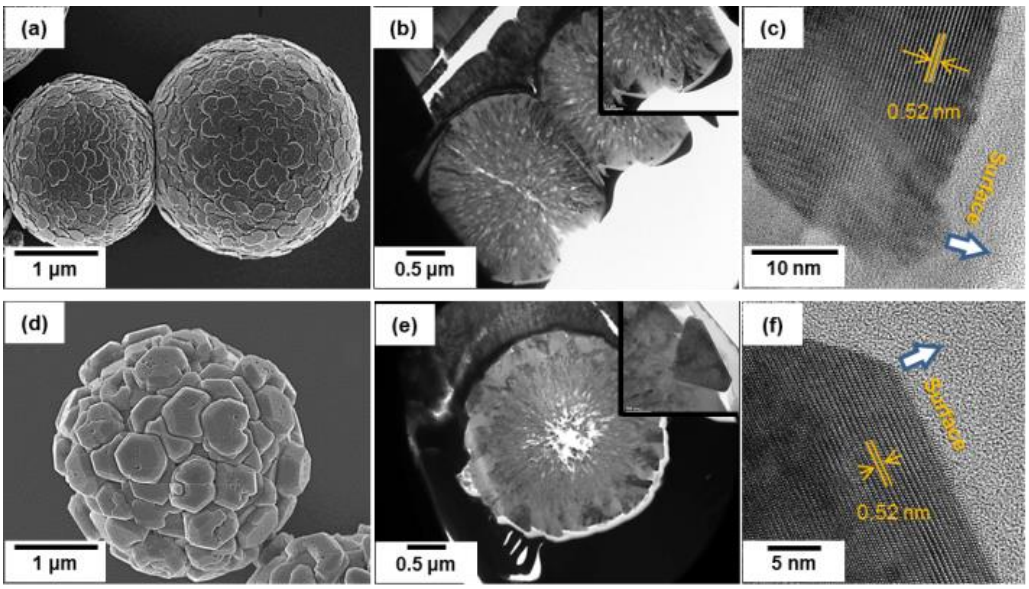

Figure 2-11. SEM images of ZnO microspheres prepared at 200 °C for (a) 1 and (d) 4 h, and their corresponding cross-sectional TEM images in (b) and (e), respectively. (c) and (f) HR-TEM images of the surface particles shown in the insets in (b) and (e), respectively.

2.3.3 Effect of Experimental Conditions on Morphology of ZnO Particles

Figure 2-12 shows the SEM images and size distribution of the ZnO spheres prepared using different HMT amount while the $Zn(CH_3COO)_2 \cdot 2H_2O$ amount was fixed at 3 mmol. The size distribution of ZnO spheres slightly shifted to smaller size and became narrower in the case of higher HMT amount. There is almost no change in the mean size and distribution between 24 and 36 mmol of HMT. Figure 2-13 shows the SEM images and size distribution of the ZnO spheres prepared from different $Zn(CH_3COO)_2 \cdot 2H_2O$ amount while the HMT amount was fixed at 12 mmol. The size distribution of ZnO spheres dominantly became narrower and shifted to smaller size as decreasing the Zn source amount. The mean size of ZnO spheres could be controlled from 3.1 μm down to 0.8 μm. From these results, it is revealed that the amount of Zn source plays a critical role in controlling the size of ZnO spheres

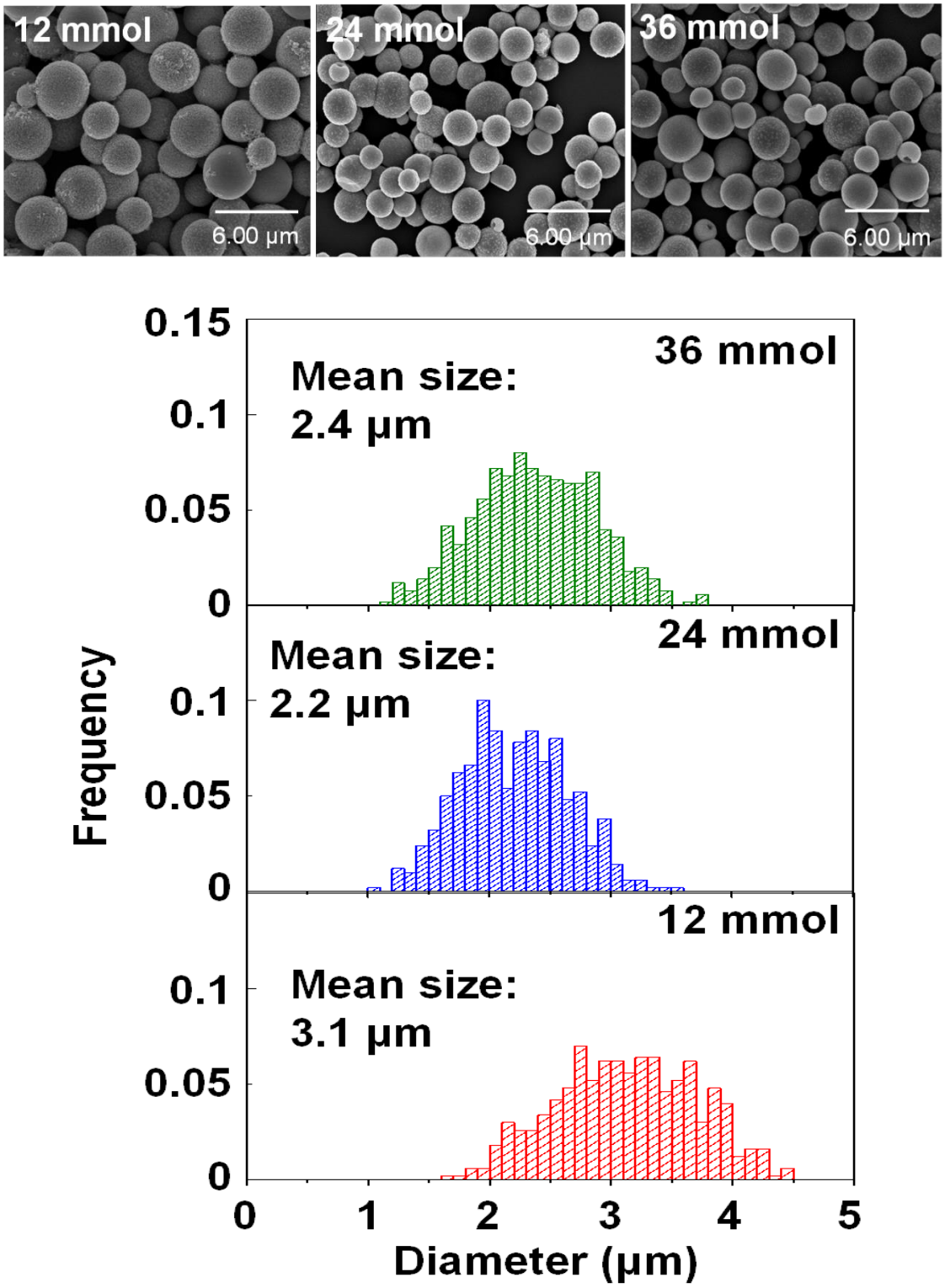

Figure 2-12. SEM images and their size distribution of ZnO microspheres prepared from different HMT amount of 12, 24, 36 mmol while the $Zn(CH_3COO)_2 \cdot 2H_2O$ amount was fixed at 3 mmol.

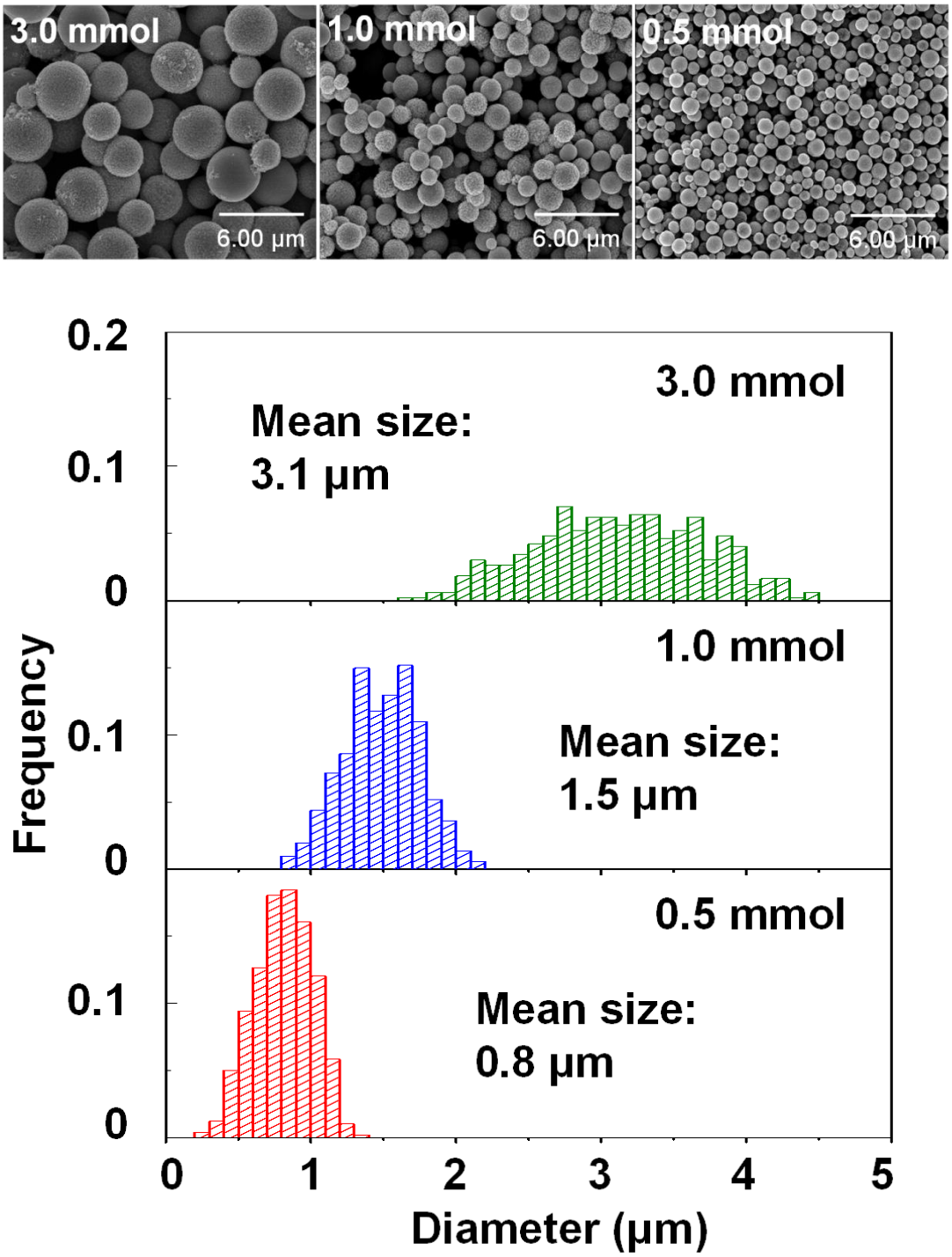

Figure 2-13. SEM images and their size distribution of ZnO microspheres prepared from different Zn source amount of 0.5, 1.0, 3.0 mmol while the HMT amount was fixed at 12 mmol.

2.4 Summary

A template-free solvothermal preparation of ZnO hollow microspheres was invistigated. The mean size of ZnO hollow microspheres were 2.8 μm in diameter. A formation mechanism of the ZnO hollow microspheres was proposed, based on the morphological evolution observed by SEM, TEM and ICP-AES analyses during microspheres growth. Solid microspheres initially consisting of ten nm particles were formed, by the agglomeration of primary particles after nucleation. Surface particles on the solid microspheres then grew into hexagonal crystals. When the degree of saturation decreased, the low crystallinity sphere centers preferentially dissolved, and hollow microspheres were formed through Ostwald ripening process. HR-TEM indicated that the microspheres were covered with ZnO *c* planes. These ZnO hollow microspheres may have applications in photocatalysis, dye sensitized solar cells, photonic crystals and advanced optoelectronic devices. The preparation described in this chapter may provide a new strategy for designing generic hollow materials.

References

1 X. Wang, P. Hu, F. L. Yuan, L. J. Yu, *J. Phys. Chem. C*, 2007, **111**, 6706-6712.

2 J. X. Duan, X. T. Huang, E. K. Wang, H. H. Ai, *Nanotechnology*, 2006, **17**, 1786-1790.

3 X.W. Lou, L.A. Archer, Z. Yang, *Adv. Mater*., 2008, **20**, 3987-4019.

4 K. An, T. Hyeon, *NanoToday*, 2009, **4**, 359-373.

5 J. Zhang, S. Wang, Y. Wang, M. Xu, H. Xia, S. Zhang, W. Huang, X. Guo, S. Wu, *Sens. Actuators B: Chem*., 2009, **139**, 411-417.

6 H. Zhou, T. X. Fan, D. Zhang, *Microporous Mesoporous Mater*., 2007, **100**, 322-327.

7 H. Qian, G. Lin, Y. Zhang, P. Guanwan, R. Xu, *Nanotechnology*, 2007, **18**, 355602.

8 P. X. Gao, Z. L. Wang, *J. Am. Chem. Soc*., 2003, **125**, 11299-11305.

9 G. Shen, Y. Bando, C.-J. Lee, *J. Phys. Chem. B*, 2005, **109**, 10578-10583.

10 H. Lu, L. Liao, J. Li, D. Wang, H. He, Q. Fu, L. Xu, Y. Tian, *J. Phys. Chem. B*, 2006, **110**, 23211-23214.

11 Y. Yang, Y. Chu, Y. Zhang, F. Yang, J. Liu, *J. Solid State Chem*., 2006, **179**, 470-475.

12 S. Cheng, D. Yan, J. T. Chen, R. F. Zhuo, J. J. Feng, H. J. Li, H. T. Feng, P. X. Yan, *J. Phys. Chem. C*, 2009, **113**, 13630–13635.

13 Y. F. Zhu, D. H. Fan, W. Z. Shen, *J. Phys. Chem. C*, 2007, **111**, 18629-18635.

14 Q. Li, E. Wang, S. Li, C. Wang, C. Tian, G. Sun, J. Gu, R. Xua, *J. Solid State Chem*., 2009,

182, 1149-1155.

15 P. Hu, X. Zhang, N. Han, W. Xiang, Y. Cao, F. Yuan, *Cryst. Growth Des.*, 2011, **11**, 1520-1526.

16 Y. Qiu, W. Chen, S. Yang, B. Zhang, X. X. Zhang, Y. C. Zhong, K. S. Wong, *Cryst. Growth Des*., 2010, **10**, 177-183.

17 T. Ghoshal, S. Kar, S. Chaudhuri, *Cryst. Growth Des*., 2007, **7**, 136-141.

18 S. Cheng, D. Yan, J. T. Chen, R. F. Zhuo, J. J. Feng, H. J. Li, H. T. Feng, P. X. Yan, *J. Phys. Chem. C*, 2009, **113**, 13630-13635.

19 M. K. Lee, H. F. Tu, *J. Appl. Phys*., 2007, **101**, 126103.

20 H. Zeng, G. Duan, Y. Li, S. Yang, X. Xu, W. Cai, *Adv. Funct. Mater*., 2010, **20**, 561–572.

21 H.-M. Cheng, H.-C. Hsu, Y.-K. Tseng, L.-J. Lin, W.-F. Hsieh, *J. Phys. Chem. B*, 2005, **109**, 8749-8754.

22 N. Y. Garces, L. Wang, L. Bai, N. C. Giles, L. E. Halliburton, *Appl. Phys. Lett*., 2002, **81**, 622-624.

23 A. B. Djurisic, Y. H. Leung, K. H. Tam, Y. F. Hsu, L. Ding, W. K. Ge, Y. C. Zhong, K. S. Wong, W. K. Chan, H. L. Tam, K. W. Cheah, W. M. Kwok, D. L. Phillips, *Nanotechnology*, 2007, **18**, 095702.

Chapter-3

Effect of Heat Treatment for ZnO Hollow Microspheres and Their Application for Visible Light Responsive Photocatalyst and Dye Sensitized Solar Cells

Chapter-3 demonstrates the effect of heat treatment for ZnO hollow microspheres and their application for visible light responsive photocatalyst and dye sensitized solar cells. The subsequent heat treatment for as-prepared ZnO hollow microspheres effected on optical property. The absorption edge showed red shift compared with commercial ZnO powder and as-prepared ZnO hollow microspheres caused by carbon-doping from impurity in the as-prepared sample. The hollow structure could be kept even after heat treated at 700^{o}C. The photocatalytic activity of heat treated ZnO hollow microspheres were evaluated under the visible light. ZnO hollow microspheres were also applied for dye sensitized solar cells.

4.1 Introduction

In chapter-2, the template-free preparation of ZnO hollow microspheres and their formation mechanism was demonstrated. In this chapter, the effect of heat treatment for ZnO hollow microspheres was investigated and they were applied for visible light responsive photocatalyst and dye sensitized solar cells (DSSCs).

Among various oxide semiconductor photocatalysts, TiO_2 and ZnO are recognized as most excellent materials for photocatalytic processes.[1–10] In addition to TiO_2, ZnO has been intensively studied due to their high photosensitivity, nontoxic nature, wide bandgap and low cost.[7–10] Moreover, the ZnO photocatalyst can be easily manipulated with desirable microstructures, which are proved to be important factors affecting the photocatalytic

activities.[7,10] Usually, most ZnO photocatalysts are only active under UV light (3–5% of the total sunlight), and it is highly desirable to develop highly active ZnO photocatalysts under visible light. Here, the C-doping will extend optical absorption of ZnO to the visible-light region (400–700 nm) and it enables to fabricate the visible-light responsive ZnO-based photocatalysts. Therefore, the combined features of hollow structure and C-doping prepared by this route have great potential for visible-light associated photocatalytic applications, which is, however, has been less considered.

Recently, dye-sensitized solar cells (DSSCs) have been attracted tremendous scientific and industrial interest owing to their low cost and respectable photovoltaic performance.[11] ZnO is an important photo-anode material in the applications of DSSCs because of its wide band gap (3.37 eV) and high electron mobility (115–155 $cm^2V^{-1}s^{-1}$). Hierarchical hollow spheres consisting of nanoparticles possess both dye adsorption properties and light scattering effects, which might be an ideal structure for the enhancement of the photovoltaic performance in DSSCs. Therefore, herein the photovoltaic performance in DSSCs fabricated using the ZnO hollow microspheres, demonstrated in chapter-2, was also investigated.

2.2 Experimental

3.2.1 Preparation of Carbon-Doped ZnO Hollow Microspheres

All the chemicals in this study, $Zn(CH_3COO)_2 \cdot 2H_2O$(>98%, Wako), hexamethylenetetramine (HMT) (Wako), ethylene glycol (EG) (Wako), were used as chemical reagent without further purification. ZnO hollow microspheres were synthesized by template-free solvothermal method which has been demonstrated in Chapter-2. In a typical synthesis, 3 mmol of $Zn(CH_3COO)_2 \cdot 2H_2O$ and 12 mmol of HMT were dissolved in 30 ml of mixed solution of EG(95 vol%) and distilled water (5 vol%). It was transferred into a 35 ml Teflon-lined stainless steel autoclave, followed by heating in an oven at 150^{o}C for 12 h. After the reaction, the precipitates were collected, washed with ethanol several times, and dried in an oven at 60^{o}C. The obtained powders were subsequently heat treated in the electronic furnace at 300, 500, and 700^{o}C.

3.2.2 Analysis of hydroxyl radicals (·OH) under visible light irradiation

The formation of hydroxyl radicals (·OH) on the surface of photo-illuminated ZnO was detected by the photoluminescence (PL) technique using terephthalic acid (TA) as a probe molecule, which readily reacted with ·OH to produce the highly fluorescent product, 2-hydroxyterephthalic acid (TAOH). The method relied on the PL signal at 425 nm of TAOH. The PL intensity of TAOH was proportional to the amount of ·OH radicals produced on the surface of ZnO.[12,13] Experimental procedures were as follows. 0.1 g of ZnO powder sample was

dispersed in 20 mL of a 5×10^{-4} M TA aqueous solution with a concentration of 2×10^{-3} M NaOH at ambient temperature. A fluorescent light (6000 lx) with a 420 nm cutoff filter was used as a light source. PL spectra of generated TAOH were measured by a luminescence spectrometer (LS55, PerkinElmer Inc., USA). After visible-light irradiation for a certain time, the reaction solution was filtered to measure the increase in the PL intensity at 425 nm of TAOH excited by 315 nm light.

3.2.3 Fabrication of Dye Sensitized Solar Cells

For the photoanode, ZnO hollow microspheres powder was screen-printed on FTO glass substrate through a 34T mesh size screen. The films were sintered at 300-600°C for 1 h before solar cell construction. After sintering, the films were soaked in a 0.3 mM N719 (B2, Dyesol) dye solution (1:1 acetonitrile and tertbutanol) at room temperature for 1 h. The resulting ZnO working electrodes were assembled and sealed using a 25 μm thick Surlyn gasket, melted by heating with the counter electrodes made by thermal deposition of H_2PtCl_6 on FTO glass at 400°C for 15 min under air to produce a sandwich cell. The electrolyte, 0.6 M 1-butyl-3-methylimidazolium iodide (BMII), 0.1 M guanidinium thiocyanate (GuSCN), 0.03 M I_2, and 0.5 M 4-tertbutylpyridine (Aldrich) in acetonitrile/valeronitrile (85:15, vol%), was introduced into the cell via a vacuum backfilling method. Device fabrication process and the structure of device are shown in figure 3-1.

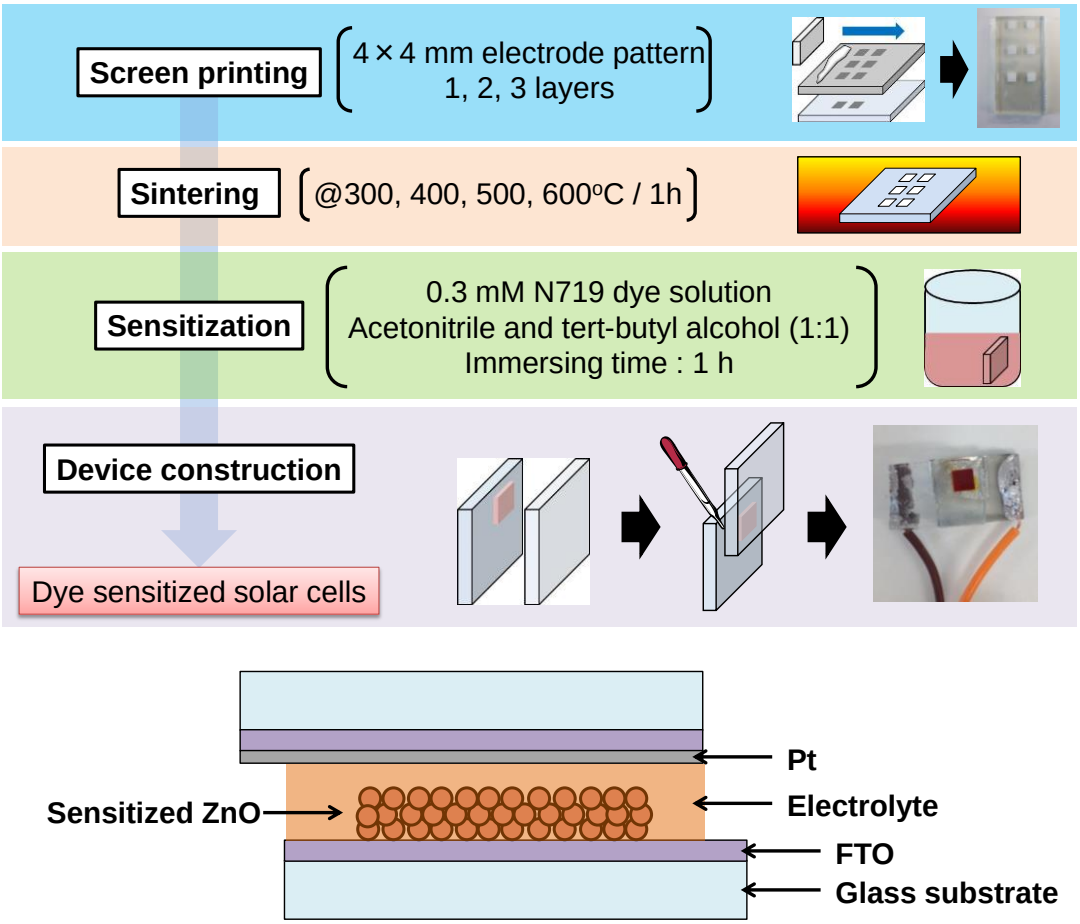

Figure 3-1. Device fabrication process and the structure of device.

3.2.4 Photovoltaic Measurement

A 450Wxenon light source (Oriel, USA) was used to provide an incident irradiance of 100 mW/cm^2 at the surface of the solar cells. The spectral output of the lamp was filtered using Schott K113 Tempax sunlight filter (Pra¨zisions Glas & Optik GmbH, Germany) that enables light from 350 to 750 nm to pass through and hence to reduce light mismatch between real solar illumination and the simulated illumination to less than 2%. Light intensities were regulated

with wire mesh attenuators. The (JV) measurements were performed using a Keithley model 2400 digital source meter (Keithley, USA) by independently applying external voltage to the cell and by measuring the photogenerated current out from the cell. Incident photon-to-current conversion measurements were realized using a 300 W xenon light source (ILC Technology, USA).

3.2.5 Sample Characterization

X-Ray diffraction (XRD) patterns were obtained by a RINT2100 diffractometer (Rigaku, Japan) using Cu-Ka radiation and were used to determine the phase structures of the samples. The morphology and structure of the samples were observed using a scanning electron microscope (SEM) (S4500, Hitachi, Japan) and a high resolution transmission electron microscope (JEM-2010UHR). X-Ray photoelectron spectroscopy (XPS) measurements were performed on the ESCALAB-210 spectrometer (Thermo VG Scientific, UK) with an Mg-Ka source. All the binding energies were referenced to the C 1s peak at 285 eV of the surface adventitious carbon. The UV–vis diffuse reflectance spectra were obtained on a UV-2550 UV-visible spectrophotometer (Shimadzu, Japan). $BaSO_4$ was used as a reflectance standard in the UV-visible diffuse reflectance experiment. Fourier transform infrared spectroscopy (FT-IR) was performed using a JIR-7000, JEOL, Japan.

3.3 Result and Discussion

3.3.1 Effect of Heat Treatment for ZnO Hollow Microspheres

The heat treated products were characterized by XRD to determine the crystal structure of the products. Figure 3-2 shows the XRD pattern of the ZnO hollow microspheres obtained after different heat treatment temperature. All the diffraction peaks were in good agreement with that of the hexagonal wurtzite structure of ZnO (JCPDS No. 36-1451). No other peaks were detected, indicating the high purity of the samples. There was no major change in XRD patterns by the increase of heat treatment temperature up to 700°C.

The morphologies of products prepared after heat treatment at 300, 500, 700°C were observed by SEM, as shown in Figure 3-3. The hollow structure was sustained even after high heat treatment temperature at 700°C. The particles which consist of the shell of hollow spheres seemed to be sintered and the shell became denser as increasing the heat treatment temperature.

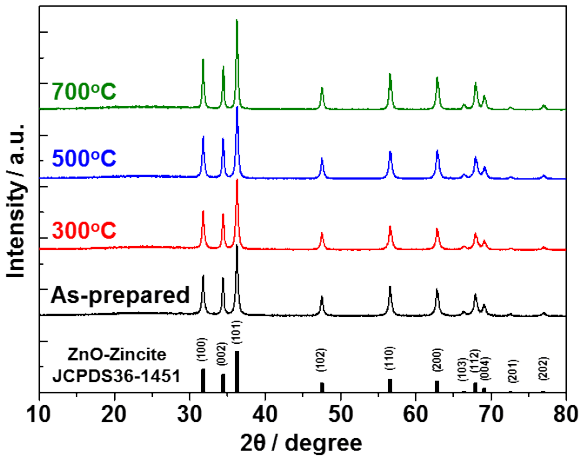

Figure 3-2. XRD patterns of as-prepared ZnO hollow microspheres and heat treated samples at 300, 500, 700°C.

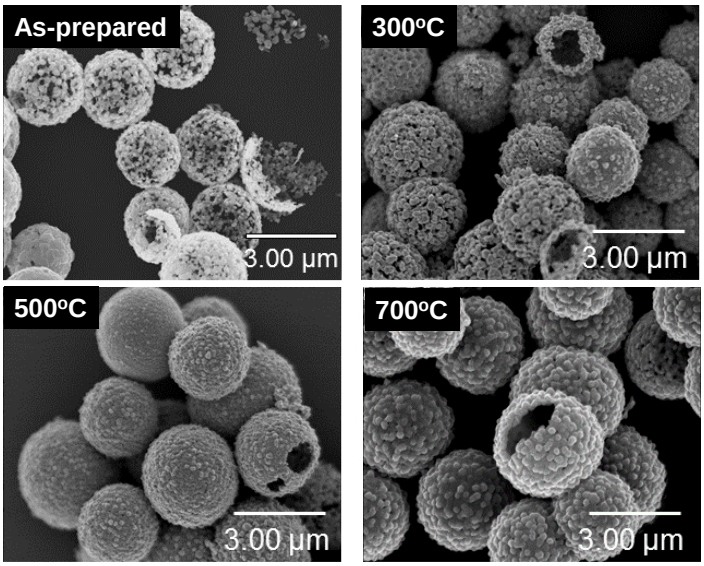

Figure 3-3. SEM images of as-prepared ZnO hollow microspheres and heat treated samples at 300, 500, 700°C.

Fig. 3-4a shows the UV-vis diffuse reflectance spectra for the ZnO hollow microspheres obtained at varying heat treatment temperatures. An obvious increase in the absorption at wavelengths less than 400 nm can be assigned to the intrinsic band gap absorption of ZnO due to the electronic transitions from the valence to the conduction band ($O_{2p} \rightarrow Zn_{3d}$).[7] Interestingly, all the obtained ZnO hollow microspheres exhibit significantly enhanced absorption in the visible-light region, relative to commercial ZnO. The hollow structure itself are advantageous for enhanced light absorption due to multi-reflection of trapped incident light within the samples.[14,15] Such an enhanced absorption capacity is beneficial for photocatalytic applications, which will be further discussed below. On the other hand, with increasing heat treatment temperature from 300 to 500°C, an obvious red-shift occurs in the absorption edge. Such a red shift expands the light response range of ZnO hollow microspheres to the visible region and will

increase the number of photogenerated electrons and holes able to participate in the photocatalytic reaction. However, a significant blue-shift in the absorption edge occurs with further increasing the calcination temperature at 700°C. Fig. 3-4b shows the direct bandgap energies estimated from a plot of $(ahν)^2$ vs. photo energy (hν) according to the K-M model.[7,16] The estimated band gap energies are 3.22, 3.07, 3.02, 3.05 eV for the commercial ZnO powder and ZnO hollow microspheres heat treated at 300, 500 and 700°C, respectively. It is apparent that the variation in the bandgap of ZnO hollow microspheres is consistent with the change in the corresponding absorption edge.

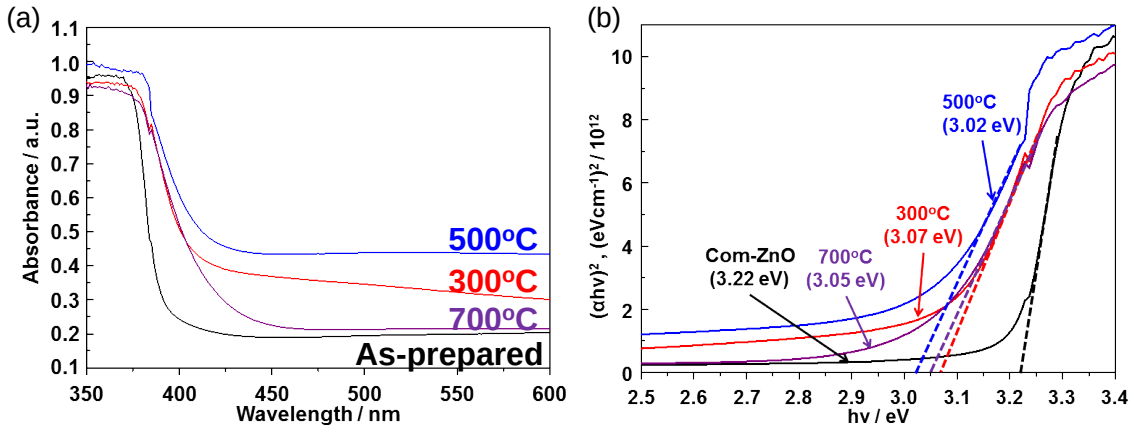

Figure 3-4. UV-vis absorption spectra (a) and the corresponding plots of $(ahν)^2$ vs. hν (b) for as-prepared ZnO hollow microspheres and heat treated samples at 300, 500, 700°C.

In order to clarify the origin for the changes in optical response mentioned above, XPS analysis was carried out to reveal the surface chemical compositions for the ZnO hollow microspheres. Fig. 3-5 shows the high-resolution XPS spectra of the C 1s region for the ZnO hollow microspheres heat treated at 500°C. The C 1s spectra of the product obtained at 500°C

was attributed to four contributions. The first minor peak at ca. 283.5 eV is assigned to the presence of carbon atoms in carbide form, indicating carbon substitution for oxygen and formation of Zn–C bonds in the carbon-doped ZnO.[17-19] The second main peak at 284.6 eV is ascribed to the residual carbon and the adventitious hydrocarbon from the XPS instrument itself. The third peak at 286.0 eV is related to Zn–O–C bonds and the further peak at 288.4 eV is related to adsorbed carbonate or carbon dioxide on the surface.[17-19]

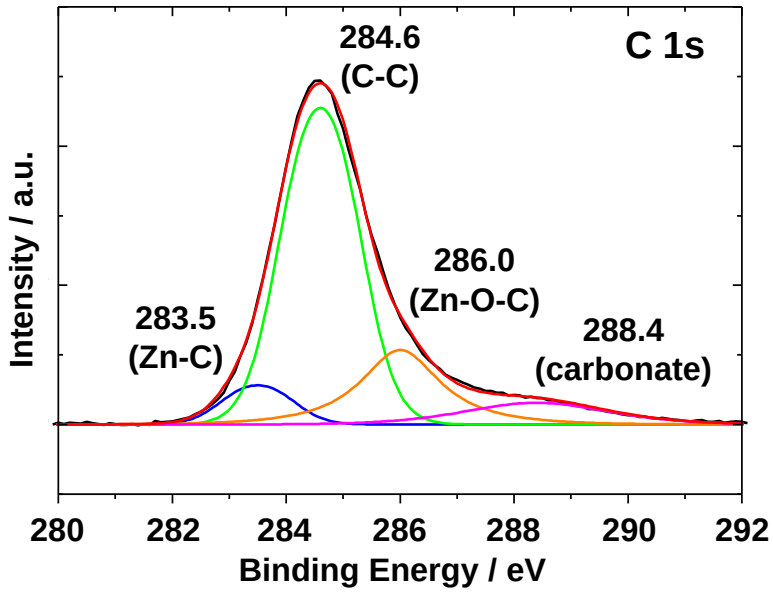

Figure 3-5. C 1s XPS spectra for ZnO hollow microspheres heat treated at 500°C.

IR spectroscopy was performed to investigate the residual organic compounds in as-prepared ZnO hollow spheres. Figure 3-6 shows an FT-IR spectrum of as-prepared ZnO hollow microspheres. A series of sharp bands in the region 2700-3100 cm^{-1} are attributable to the symmetric and asymmetric stretching of CH_2 groups and the terminal CH_3 group.[20] The

broadband around 3500 cm^{-1} corresponds to the OH group of adsorbed water on metal centers. The absorption band around 500 cm^{-1} corresponds to the Zn-O stretching band in the ZnO structure.[21] The bands in the region 1300-1800 cm-1 corresponding to the stretching frequency of the carboxylate group.[20] This reveals that organic compounds still remained in as-prepared ZnO hollow microspheres even they were rinsed with ethanol several times. Carbon-doping would occur by thermal decomposition of residual organic compounds when they were heat treated.

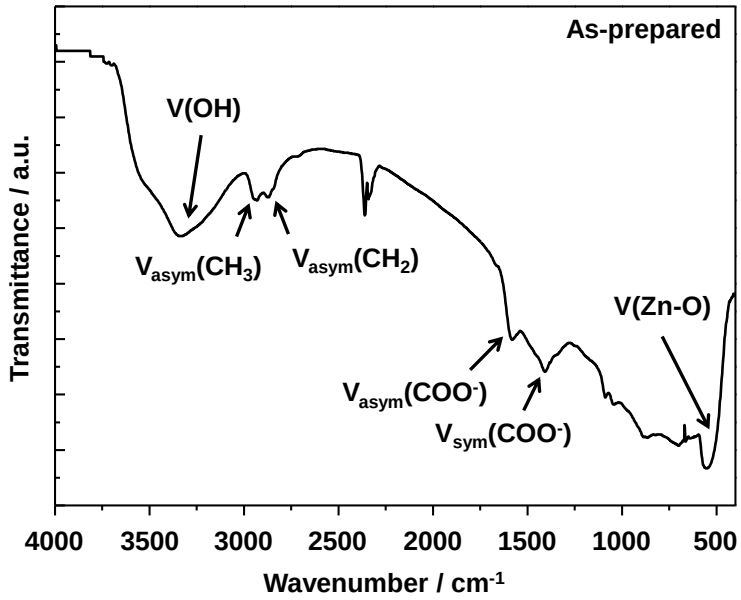

Figure 3-6. FT-IR spectrum for as-prepared ZnO hollow microspheres.

Subsequent to photoexcitation, holes with sufficient oxidation power in the VB, or in localized states within the band gap, can either be directly involved in the photocatalytic degradation reactions or, alternatively, generate active species, such as ·OH, by reacting with surface adsorbed water and hydroxyl groups. It is known that ·OH can readily react with TA in

aqueous solution and generates TAOH, which emits a unique PL signal with the peak centered at ca. 425 nm.[12,13,19] As shown in Figure 3-7a, obvious PL signals associated with TAOH are generated upon visible light irradiation in the suspension of ZnO hollow microspheres heat treated at 700^{o}C mixed with TA aqueous solution. Moreover, a gradual increase in PL intensity occurs with increasing irradiation time. However, no PL signal is observed in the absence of light illumination or ZnO samples. Figure 3-7b shows the plots of PL intensity at 425 nm against irradiation time for ZnO samples heat treated at various temperatures. For each sample, the PL intensity increased linearly vs. irradiation time. The formation rate of ·OH could be compared via the slope of these lines. Obviously, the formation rate of ·OH for 700^{o}C is much larger than that for the another temperatures. Such a result is largely correlated with the optical absorption properties. More photo-generated holes and ·OH are produced for 700^{o}C because more visible light are harvested.

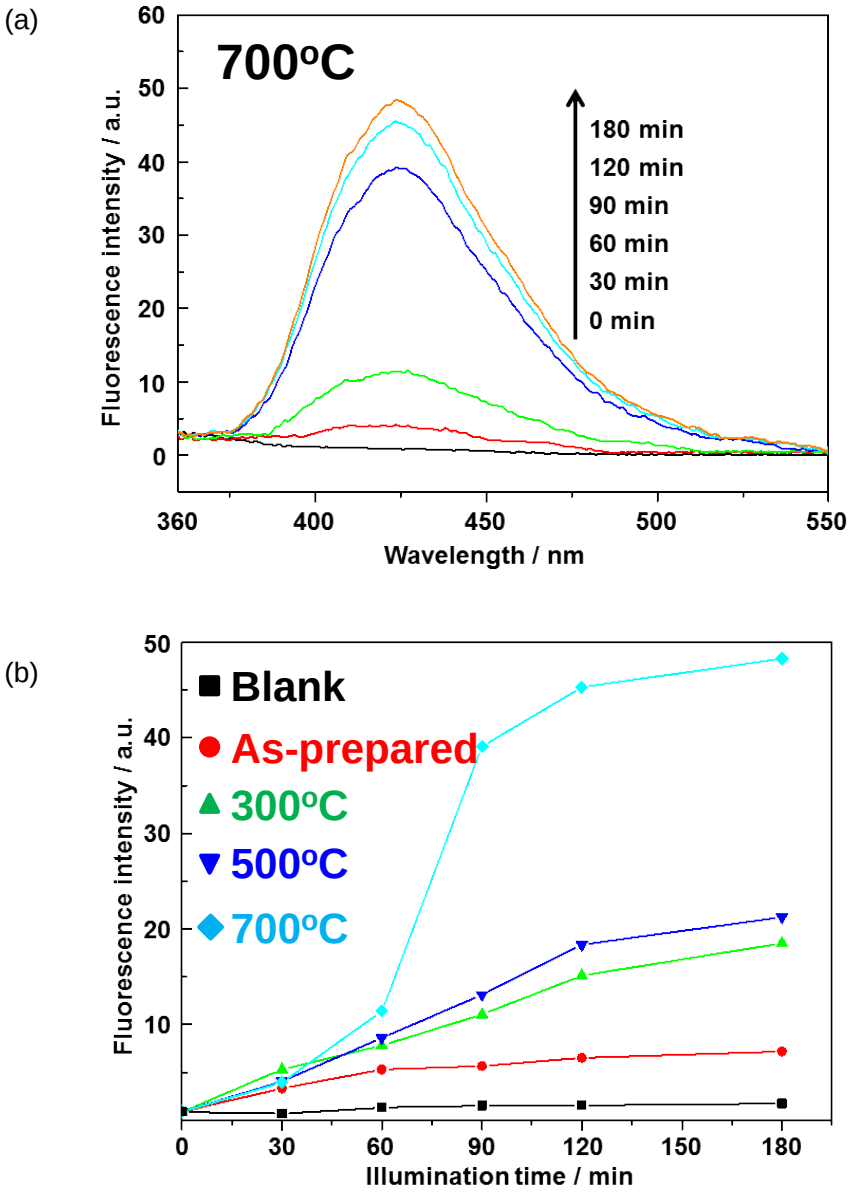

Figure 3-7. (a) PL spectra associated with TAOH generated in the presence of 700°C-heat treated ZnO hollow microspheres under visible-light irradiation. (b) Plots of PL intensity at 425 nm against irradiation time for ZnO hollow microspheres heat treated at various temperatures.

3.3.3 Performance of Dye Sensitized Solar Cells using ZnO Hollow Microspheres

SEM images of ZnO hollow spheres layer fabricated by screen printing repeated 1-3 times were shown in figure3-8. Here, each films are named as 1, 2, 3 layer, respectively. The thickness of each film was 10, 19, 22 μm for 1, 2, 3 layers respectively. Top view and high magnification cross sectional image of ZnO hollow microspheres layer are shown in figure 3-8d and e. The hollow structure was clearly observed in both images.

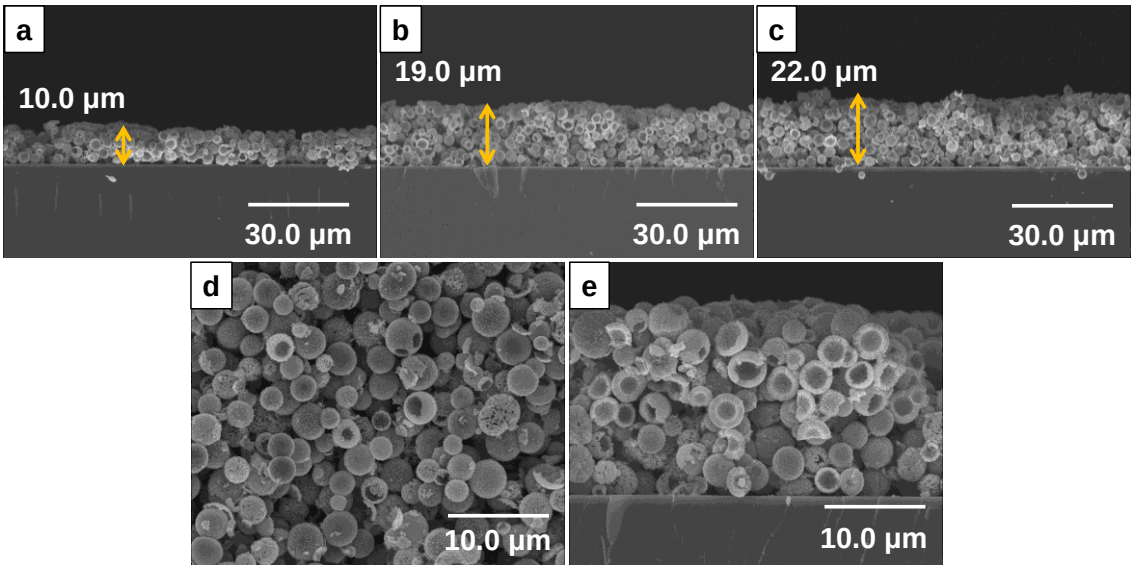

Figure 3-8. SEM images of ZnO hollow spheres layer fabricated by screen printing repeated (a) 1, (b) 2 and (c) 3 times and (d) the top and (e) high magnification cross-sectional view of 3 layers.

Figure 3-9 shows J-V curves of DSSCs fabricated with various thickness of ZnO hollow microspheres layer. The short circuit current density became larger as increasing the thickness. The open voltage for 3 layers became smaller slightly compared with 2 layers. This is attributed to the electron transfer pathway become longer as increasing thickness. From these results, the

optimal thickness for DSSC using ZnO hollow microspheres was 3 layer.

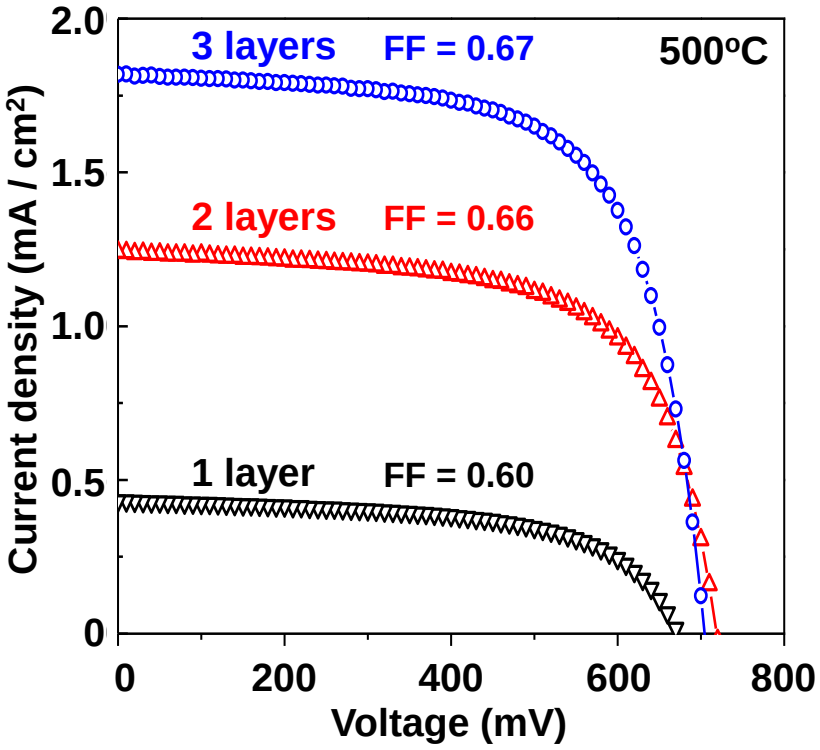

Figure 3-9. J-V curves of DSSCs fabricated with various thickness of ZnO hollow microspheres layer.

Figure 3-10a shows J-V curves for the device fabricated by various sintering temperature while the thickness was fixed 3 layers. The short circuit current density become larger as increasing the sintering temperature up to 500°C and then decreased at 600°C. The open voltage became larger as increasing the sintering temperature. The crystallinity should be higher as increasing the sintering temperature so that is why the open voltage became larger as increasing the sintering temperature. However, if the sintering temperature is too high, the sintering occurs prominently and it results in decreasing the surface area so the amount of dye adsorption is

decreased. That is why the short circuit current density is decreased at 600°C. The Power conversion efficiency of the device fabricated by various sintering temperature was shown in figure 3-10b. The best efficiency was 0.86% for the sample sintered at 500°C.

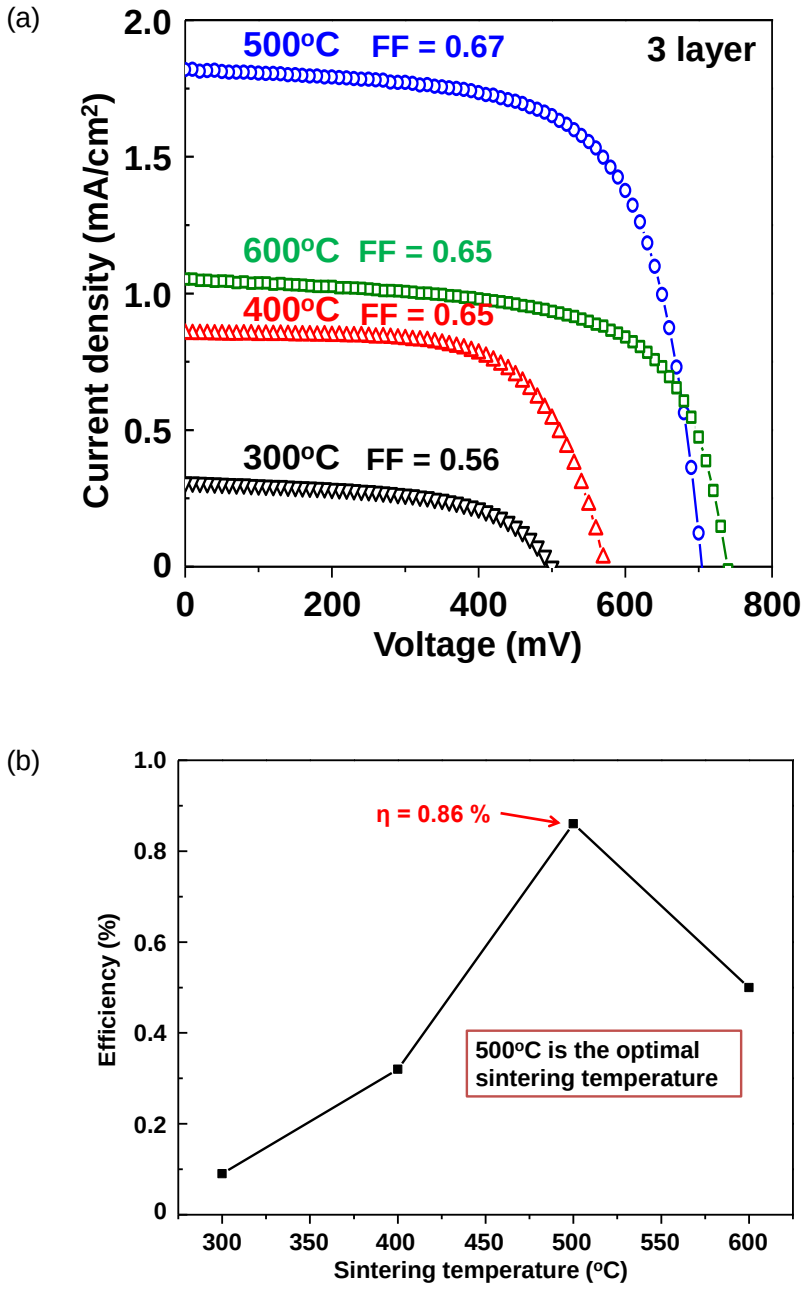

Figure 3-10. (a) J-V curves of DSSCs fabricated with various sintering temperature and (b) their power conversion efficiency.

To obtain the higher efficiency, pre-UV treatment for ZnO hollow microspheres before preparing the paste was employed. This was because that the organic compounds remain on the surface and inside of the as-prepared ZnO hollow microspheres as indicated in the previous section and they still remain even heat treated at 500°C. These impurity would trap the electrons and be affected to the device performance. Therefore, pre-UV treatment was employed to eliminate the residual organic compounds. FT-IR spectra for ZnO hollow microspheres before and after UV treatment for 24 h were shown in figure 3-11. The residual organic compounds were successfully eliminated by UV treatment as shown in figure 3-11.

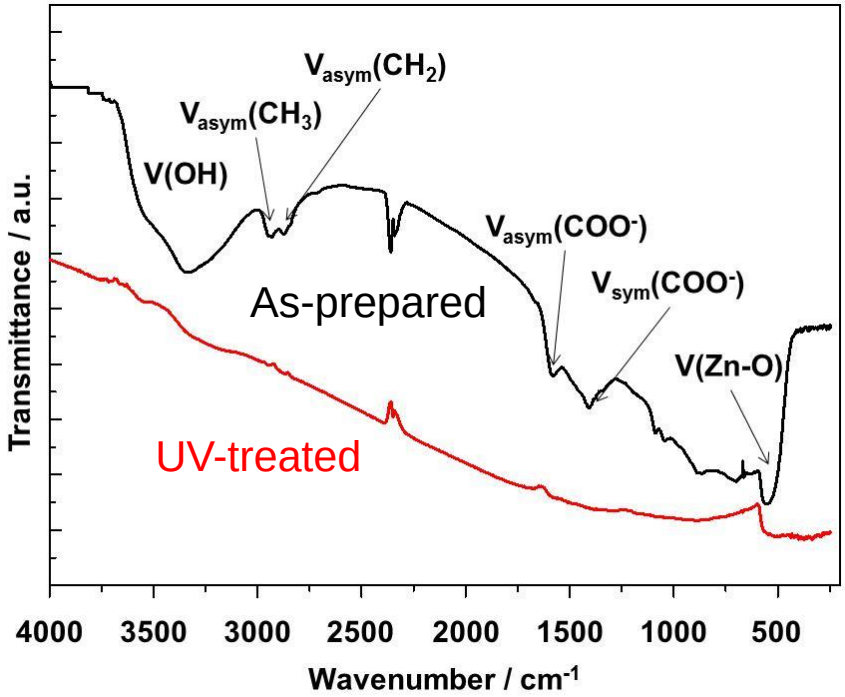

Figure 3-11. FT-IR spectra of ZnO hollow microspheres with and without pre-UV treatment.

Figure 3-12 shows the J-V curves of with and without UV treated sample. The device performance was improved by pre-UV treatment for ZnO hollow microspheres as shown in figure 3- and the efficiency was increased up to 1.05%.

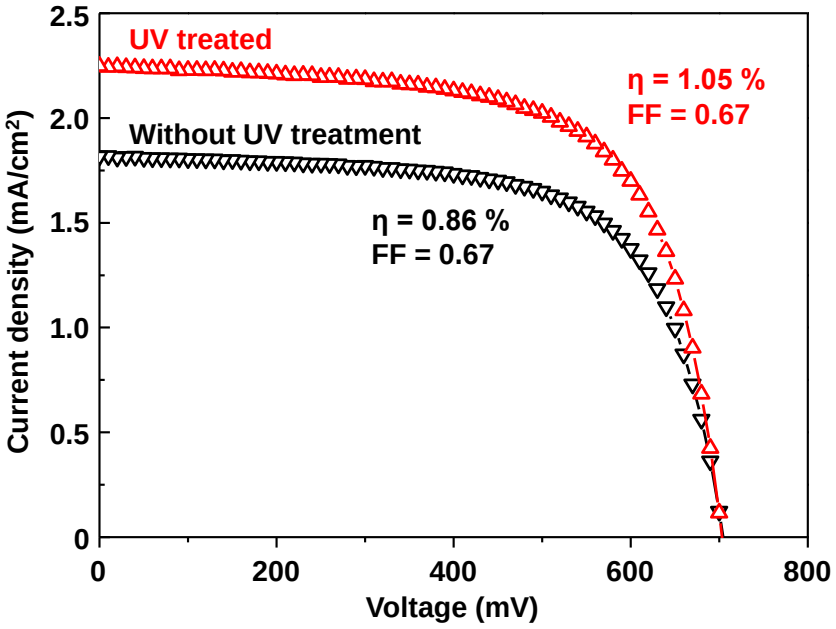

Figure 3-12. J-V curves of DSSCs fabricated using ZnO hollow microspheres with and without pre-UV treatment.

Figure 3-13 shows the comparison of J-V curves with DSSCs fabricated using commercial ZnO powder and ZnO hollow microspheres. The performance of DSSC fabricated using ZnO hollow microspheres was slightly low compared with commercial ZnO. This was because that the specific surface area would be higher for commercial ZnO powder, therefore, the amount of dye adsorption would be higher than hollow microspheres. However, ZnO hollow microspheres could show similar performance with commercial ZnO even though it has micron size and these results indicate the hollow structure would be useful for DSSCs and this ZnO hollow

microspheres would be useful as scattering layer of DSSC as shown in figure 3-14.

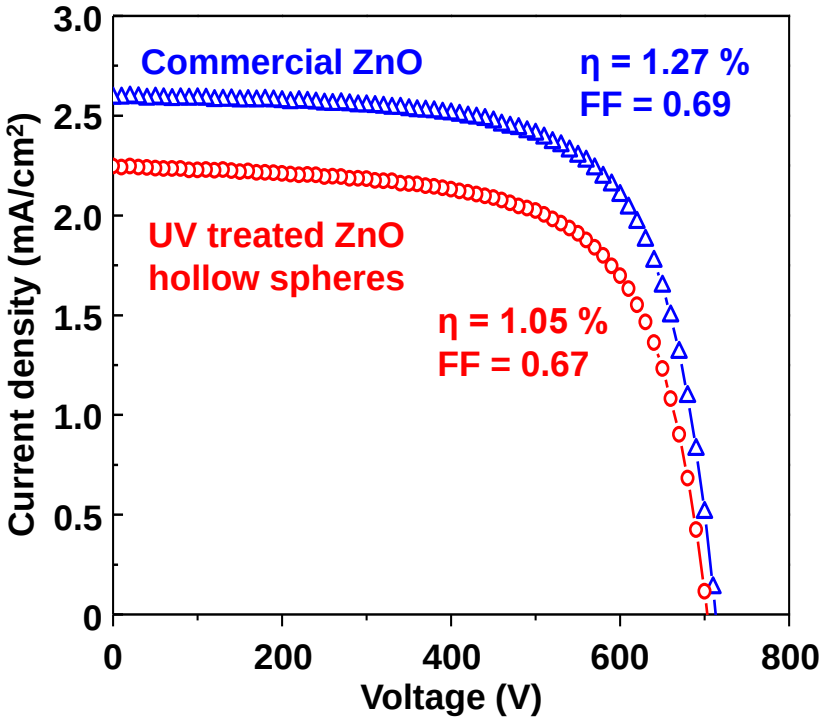

Figure 3-13. Comparison of J-V curves with DSSCs fabricated using commercial ZnO powder and ZnO hollow microspheres.

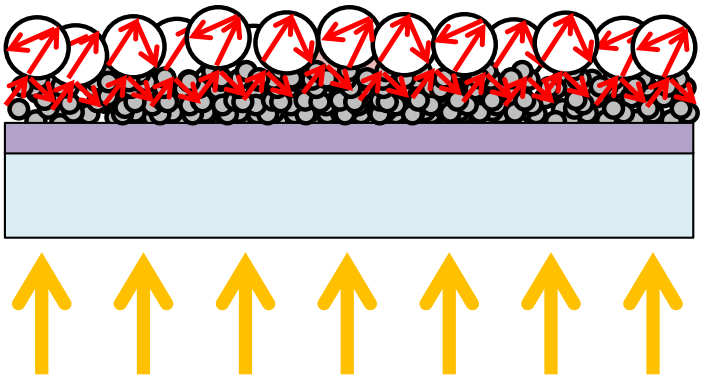

Figure 3-14. Schematic illustration of the structure of device using ZnO hollow microspheres as a scattering layer.

3.4 Summary

In this chapter, the effect of heat treatment for ZnO hollow microspheres was investigated and they were applied for visible light responsive photocatalyst and dye sensitized solar cells (DSSCs). The hollow structure could be kept even heat treated at 700^{o}C. C-doping occurred when the ZnO hollow microspheres were heat treated by decomposition of residual organic compound in the as-prepared sample. Heat treated samples showed a red shift of absorption edge in the UV-vis spectra. Such a red shift expands the light response range of ZnO hollow microspheres to the visible region. The sample heat treated at 700^{o}C showed the best formation rate of ·OH under visible light irradiation.

The DSSCs were successfully fabricated using ZnO hollow microspheres. The conditions such as the thickness of film and sintering temperature were optimized. The best power conversion efficiency was 0.86 %. The device performance was improved by pre-UV treatment for as-prepared ZnO hollow microspheres to eliminate the residual organic compounds up to 1.05 % of power conversion efficiency. These ZnO hollow microspheres would be useful for DSSCs as scattering layer.

References

1 G. Liu, L. Z. Wang, H. G. Yang, H. M. Cheng, G. Q. Lu, *J. Mater. Chem.*, 2010, **20**, 831.

2 J. G. Yu, Y. R. Su, B. Cheng, *Adv. Funct. Mater.*, 2007, **17**, 1984.

3 T. Y. Leung, C. Y. Chan, C. Hu, J. C. Yu, P. K. Wong, *Water Res.*, 2008, **42**, 4827.

4 C. Trapalis, M. Gartner, M. Modreanu, G. Kordas, M. Anastasescu, R. Scurtu, M. Zaharescu, *Appl. Surf. Sci.*, 2006, **253**, 367.

5 C. Trapalis, N. Todorova, M. Anastasescu, C. Anastasescu, M. Stoica, M. Gartner, M. Zaharescu, T. Stoica, *Thin Solid Films*, 2009, **517**, 6243.

6 J. G. Yu, S. W. Liu, H. G. Yu, *J. Catal.*, 2007, **249**, 59.

7 J. G. Yu, X. X. Yu, *Environ. Sci. Technol.*, 2008, **42**, 4902.

8 S. Sakthivel, B. Neppolian, M. V. Shankar, B. Arabindoo, M. Palanichamy, V. Murugesan, *Sol. Energy Mater. Sol. Cells*, 2003, **77**, 65.

9 N. Daneshvar, D. Salari, A. R. Khataee, *J. Photochem. Photobiol., A*, 2001, **141**, 231.

10 J. L. Yang, S. J. An, W. I. Park, G. C. Yi, W. Choi, *Adv. Mater.*, 2004, **16**, 1661.

11 B. O'Regan, M. Gratzel, *Nature*, 1991, **353**, 737.

12 K. Ishibashi, A. Fujishima, T. Watanabe, K. Hashimoto, *Electrochem. Commun.*, 2000, **2**, 207.

13 J. G. Yu, W. G. Wang, B. Cheng, B. L. Su, *J. Phys. Chem. C*, 2009, **113**, 6743.

14 S. W. Liu, J. G. Yu, *J. Solid State Chem.*, 2008, **181**, 1048.

15 W. Q. Han, L. J. Wu, R. F. Klie, Y. M. Zhu, *Adv. Mater.*, 2007, **19**, 2525.

16 X. X. Yu, J. G. Yu, B. Cheng, B. B. Huang, *Chem.–Eur. J.*, 2009, **15**, 6731.

17 L. Ramqvist, K. Hamrin, G. Johansson, A. Fahlman, C. Nordling, *J. Phys. Chem. Solids*, 1969, **30**, 1835.

18 H. Pan, J. B. Yi, L. Shen, R. Q. Wu, J. H. Yang, J. Y. Lin, Y. P. Feng, J. Ding, L. H. Van, J. H. Yin, *Phys. Rev. Lett.*, 2007, **99**, 127201.

19 S. Liu, C. Li, J. Yu, Q. Xiang, *CrystEngComm*, 2011, **13**, 2533–2541.

20 N. Q. Wu, L. Fu, M. Su, M. Aslam, K. C. Wong, V. P. Dravid, *Nano Lett.*, 2004, **4**, 383.

21 C. M. Ho, J. C. Yu, T. Kwong, A. C. Mak, S. Y. Lai, *Chem. Mater.*, 2005, **17**, 4514.

Chapter-4

Preparation of Nitrogen-doped ZnO Microrods by Hydrothermal Method using Zinc Ammine Complex Solution as a Precursor

Chapter-4 demonstrates the preparation of Nitrogen-doped ZnO (N-doped ZnO) micro rods by hydrothermal method using zinc ammine complex solution as a precursor. Reaction at 100 °C yielded highly crystalline rod like ZnO powder, whose size could be controlled by varying the reaction time. Low-temperature and facile preparation of highly crystalline N-doped ZnO would be invaluable. The detailed analyses for prepared samples are investigated.

4.1 Introduction

In this chapter, hydrothermal synthesis of N-doped ZnO rods using zinc ammine complex solution is presented. The optical properties of ZnO can be tuned by controlling the size and shape of the nanocrystals, and also the type and concentration of dopants.[1–4] Several methods have been developed for controlling the size and shape of ZnO nanocrystals.[5]

Doping heteroatoms at Zn or O sites in ZnO can be used to tune the band gap. N is a common heteroatom dopant, due to its compatible size to O and small ionization energy. N-doping in ZnO is a promising technique for obtaining p-type oxide semiconductors and controlling their electrical states. However, doping N in the ZnO lattice remains difficult, so developing methods which give high dopant yields and carrier densities is highly required.

N-doped ZnO films and powders have been fabricated by molecular beam epitaxy,[6] pulsed laser ablation,[7] chemical vapor deposition,[8] and combustion methods.[9] Keszler *et al*. reported the

green fabrication of ZnO thin film transistors (TFTs) at low temperatures (<150 °C), by spin-coating aqueous solutions of the ammine-hydroxo zinc complex, $Zn(OH)_x(NH_3)_y^{(2-x)+}$.[10] This approach has several advantages for fabricating ZnO semiconductors, such as its low temperature and resulting high electrical performance. The latter is due to the rapid kinetics and low activation energy of the metal-ammine dissociation and hydroxide condensation/dehydration reactions. We consider the aqueous ammine-hydroxo zinc complex to be well-suited for hydrothermally synthesizing N-doped ZnO powder. Although there are several reports of ZnO semiconductor films fabricated using the zinc ammine complex, there are none for N-doped ZnO powder. This therefore is the focus of the current study.

4.2 Experimental

4.2.1 Preparation of Nitrogen-doped ZnO Microrods

$Zn(NO_3)_2 \cdot 6H_2O$ (>99%, Wako Pure Chemical Industries, Japan), NaOH (>97%, Wako Pure Chemical Industries, Japan) and NH_3 aqueous solution (28%, Wako Pure Chemical Industries, Japan) were used as chemical reagent without further purification. N-doped ZnO rods were hydrothermally synthesized using an ammine-hydroxo zinc complex, which was prepared according to Keszler *et al.*[10] In brief, 10 ml of aqueous 2.5 M NaOH was added dropwise to 15 ml of aqueous 0.5 M $Zn(NO_3)_2 \cdot 6H_2O$ under vigorous stirring. The resulting hydroxide slurry was centrifuged, and the supernatant was removed. Rinsing and separation was carried out three

further times to remove Na^+ and NO_3^-. The resulting hydrated precipitate was dissolved in 50 ml of aqueous 6.6 M NH_3, 30 ml of which was transferred to a 35 ml polytetrafluoroethylene-lined stainless steel autoclave, and heated in an oven at 100 °C for 6 h. After reaction, the precipitate was separated by centrifugation and thoroughly washed with water.

4.2.2 Characterization

Crystal phases were determined by X-Ray diffraction (XRD), using a RINT2000 diffractometer (Rigaku, Japan) with Cu K_α radiation (λ = 1.542 Å). The observed interplanar d-spacing was corrected with respect to silicon. Sample morphologies were observed by field-emission scanning electron microscopy (SEM) (S4500, Hitachi, Japan). Microstructures were analyzed by transmission electron microscopy (TEM) (H-8100, Hitachi, Japan) at 200 kV. Diffuse reflectance UV-vis spectra were recorded on a spectrophotometer (V-550, JASCO, Japan), with $BaSO_4$ as the reference material. Raman spectra were recorded at room temperature on a Jobin Yvon T64000 spectrometer, with an Ar laser (λ=514.5 nm) excitation source. X-ray photoelectron spectroscopy (XPS) spectra were recorded on a Perkin-Elmer model 5500 MT XPS system, using monochromatic Al K_α radiation (1486.6 eV) with a pass energy of 23.5 eV. Binding energies were calibrated with respect to the C 1s core level at 285 eV. Commercial ZnO powder (>99%, Wako Pure Chemical Industries, Japan) was used for all measurements as

a reference.

4.3 Result and Discussion

N-doped ZnO rods were hydrothermally prepared at 100 °C for different reaction times. Figure 4-1 shows powder XRD patterns for commercial ZnO and samples prepared at 100 °C for 6 and 24 h. The observed diffraction peaks were in good agreement with those of hexagonal wurtzite ZnO (JCPDS No. 36-1451). The absence of other peaks indicated the high purity of the samples. The relative intensity of the peaks corresponding to the (101)/(002) and (100)/(002) planes significantly differed from literature values (JCPDS card 36-1451) and those of commercial ZnO. The preferred orientation of the prepared samples along the [100] direction was explained by the crystallography and morphology of the ZnO crystals. The growth of the one-dimensional ZnO crystals was predominantly in the longitudinal direction, *i.e.* [002]. The side facets of the ZnO hexagonal rods/whiskers were composed of (100) planes. There was a small shift of the (100) and (101) peaks to lower diffraction angles, compared with commercial ZnO. This shift increased with increasing reaction time, as shown in Fig. 4-1b. This indicated that the lattice expansion may have been caused by N doping, because the covalent radii of O and N are 0.73 and 0.75 Å, respectively or OH group in the lattice. The SEM image in Fig. 4-2 shows that the samples consisted of ZnO microcrystalline hexagonal rods. The XRD beam irradiation area of the side facets was much larger than that of *c*-axis, so a stronger (100) peak

was observed in XRD pattern in Fig. 4-1a. The length and diameter of the ZnO rods prepared at 100 °C for 6 h were approximately 20 and 1.5 μm, respectively. When the reaction time was 24 h, these increased to approximately 30 and 3 μm, respectively.

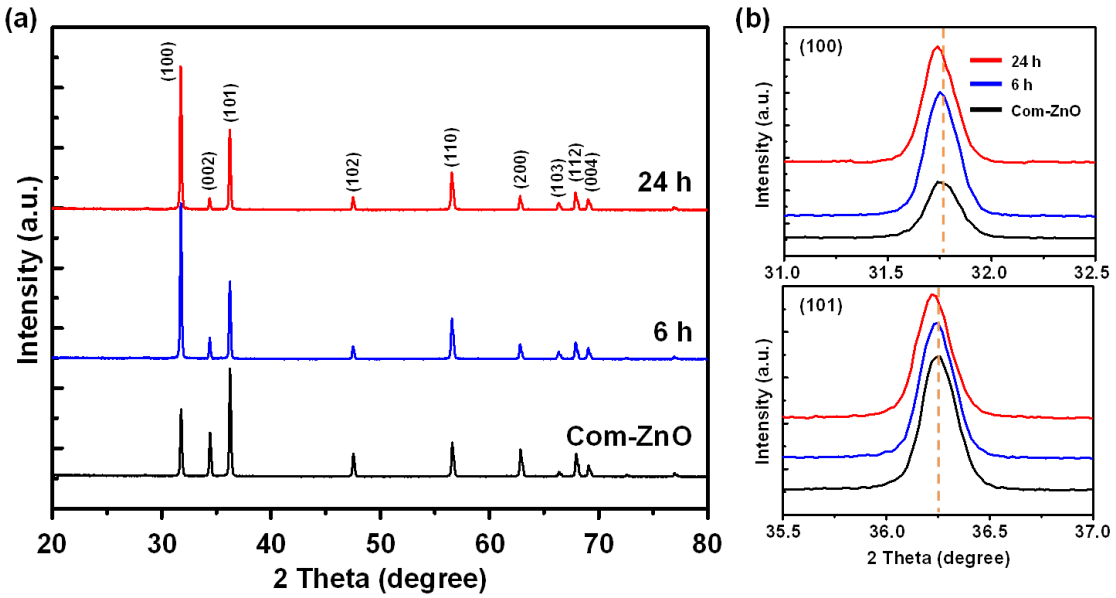

Figure 4-1. (a) XRD patterns of ZnO rods prepared at 100 °C for 6 and 24 h. Expanded (b) (100) and (101) regions showing peak shifts compared with those of commercial ZnO.

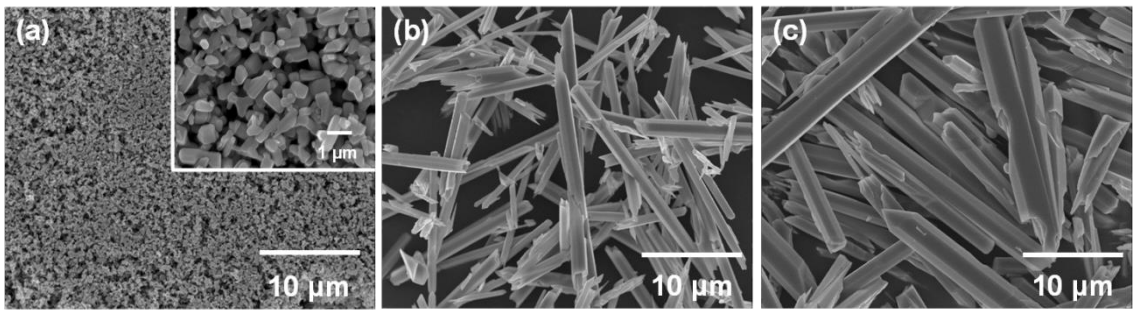

Figure 4-2. SEM images of (a) commercial ZnO, and ZnO rods prepared at 100 °C for (b) 6 and (c) 24 h.

Figure 4-3 shows a representative high-resolution TEM (HRTEM) image of a N-doped ZnO rod prepared at 100 °C for 6 h, and corresponding fast Fourier transform (FFT) pattern of the real-space HRTEM image. The periodicity of the lattice fringes along the growth direction was 0.26 nm, and the FFT analysis suggested that the ZnO rods were predominantly single crystals with this *d*-spacing. Thus, the ZnO rods were single crystalline, and grew along the *c*-axis without any intergrowth.

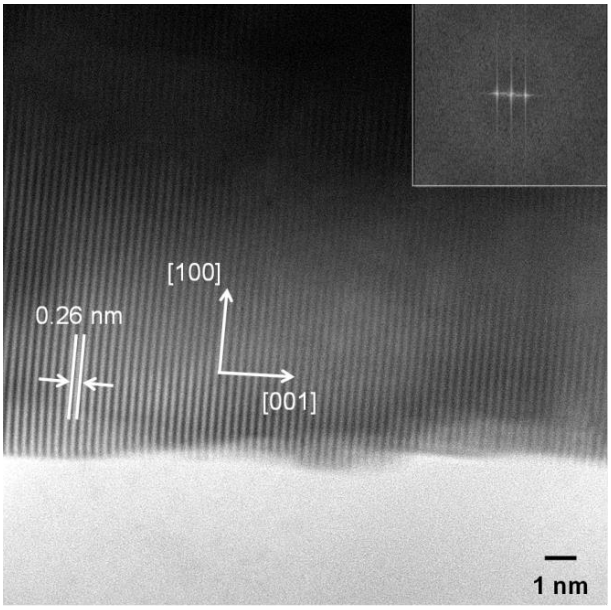

Figure 4-3. HRTEM image of a N-doped ZnO rod prepared at 100 °C for 6 h, and corresponding FFT pattern (inset).

Diffuse reflectance absorption spectra of the N-doped ZnO rods are shown in Fig. 4-4. The absorption edge shifted to longer wavelength with increasing reaction time, and occurred at longer wavelength than that of commercial ZnO. This may have reflected the presence of N in the ZnO rods, which can shift absorption edge toward the visible region via band gap

narrowing.[11, 12] The red shift in the absorption spectra were consistent with the change in color of the powder samples from white (pure ZnO) to pale-yellow (N-doped ZnO).

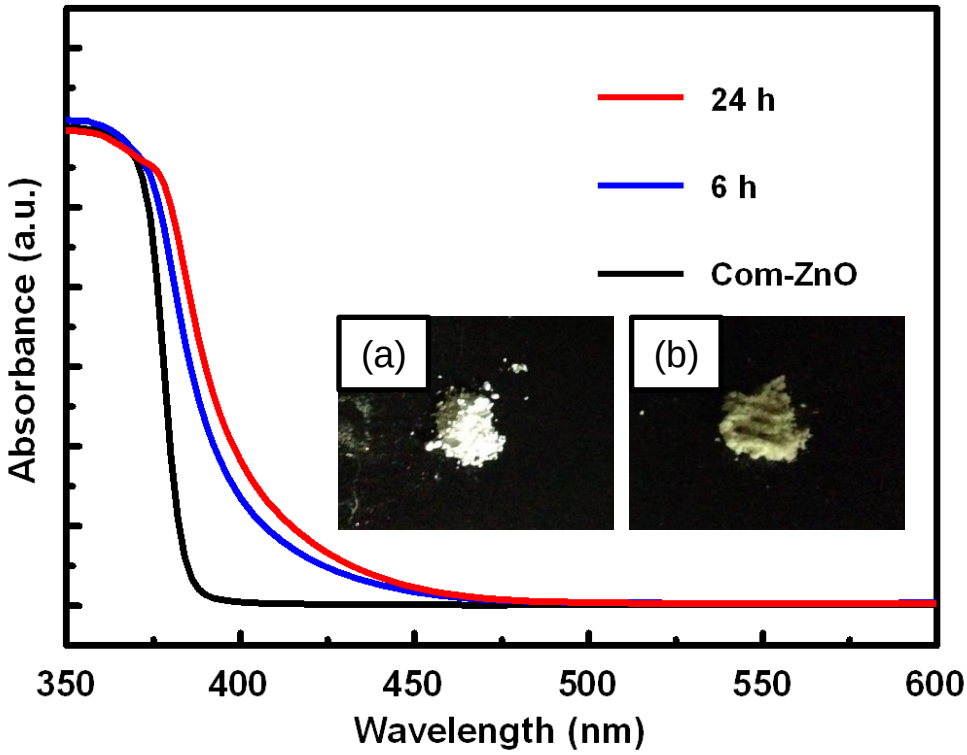

Figure 4-4. Diffuse reflectance UV-vis spectra of commercial ZnO and ZnO rods prepared at 100 °C for 6 and 24 h. (inset) The pictures of (a) commercial ZnO powder and (b) N-doped ZnO rods prepared at 100oC for 24 h.

Raman and X-ray photoelectron (XPS) spectra of the samples were recorded at room temperature, to elucidate their chemical species. Figure 4-5 shows Raman spectra of the N-doped ZnO samples prepared at 100 °C for 6 and 24 h, and commercial ZnO as a reference. To aid analysis, all spectra were normalized with respect to the highest intensity ZnO peak at 437 cm^{-1}. This peak was observed for all samples, and was attributed to vibration of the high frequency E_2 mode, characteristic of the wurtzite phase. Weak peaks at 330 and 380 cm^{-1} arose

from the second-order Raman scattering by zone-boundary phonons, E_2 (M),[13] and first-order phonons of A_1 (TO), respectively. A new peak at 582 cm^{-1} attributed to the E_2 mode (Zn–N) for N-doped ZnO was not observed for commercial ZnO.[9] Other absorption bands classically ascribed to N-related local vibrational modes (*i.e.* near 275, 507 and 635 cm^{-1}) were not observed in the samples.[14-16]

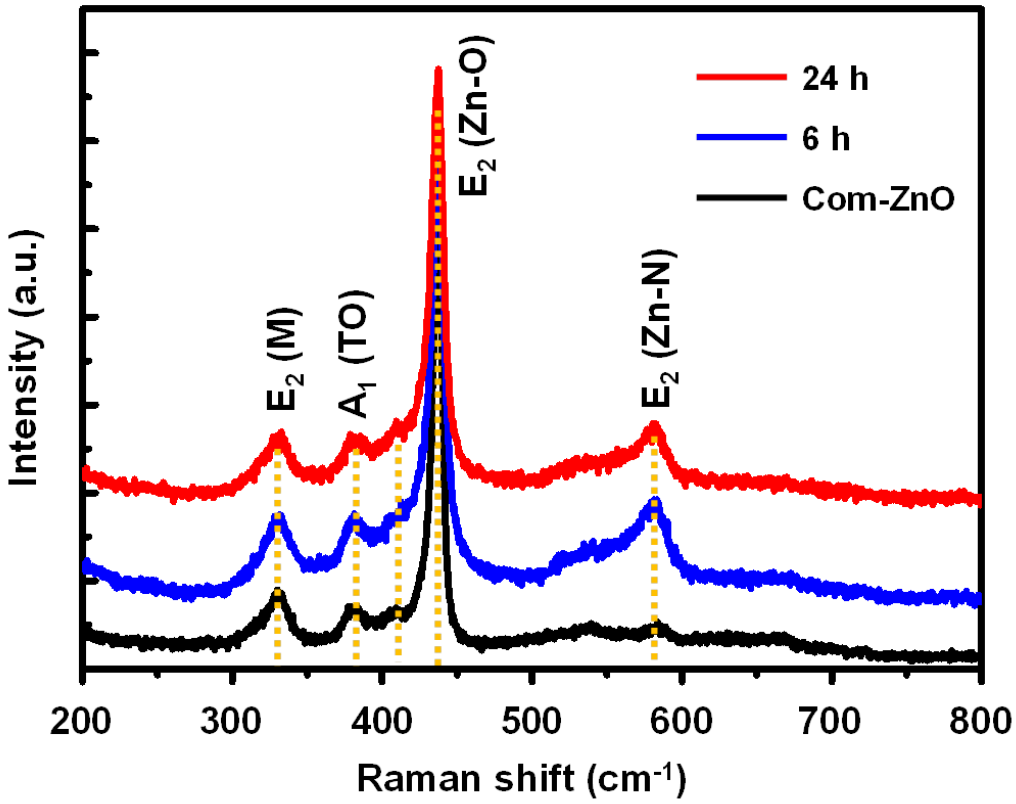

Figure 4-5. Raman spectra of commercial ZnO and ZnO rods prepared at 100 °C for 6 and 24 h.

XPS spectra of the N 1s and Zn $2p_{3/2}$ core levels for commercial ZnO and the samples prepared at 100 °C for 6 and 24 h are shown in Figs. 4-6 and 4-7, respectively. The core level spectrum of the N 1s region for the sample prepared at 100 °C for 6 h exhibited an asymmetric

broad peak. This was deconvoluted into two peaks centered at 399.8 and 398.5 eV as shown in Fig. 4-6a. No such peak was observed in the spectrum of commercial ZnO shown in Fig. 6b. The peak centered at 398.5 eV was attributed to Zn–N bonds,[17] and that at 399.8 eV to the N 1s binding energy of amines.[18] These results suggested that N was doped at the O sites of crystalline ZnO. N might be incorporated into ZnO rods during the crystal growth process rather than through the thermal diffusion process. Figure 6b shows that the surface N content also increased with increasing reaction time. The N concentration refers to the percentage of atomic ratio of N to Zn in ZnO rods was 1.0 % and 2.2 % for 6 h and 24 h respectively.

XPS spectra of the Zn $2p_{3/2}$ region are shown in Fig. 4-7. The $2p_{3/2}$ peak occurred at 1021.5 eV in the spectrum of commercial ZnO. The Zn $2p_{3/2}$ peaks of the samples prepared at 100 °C for 6 and 24 h occurred at lower binding energy than that of commercial ZnO, with a longer reaction time giving a greater shift. This indicated that the Zn 2p binding energy in the N-doped ZnO was lower than that in the commercial ZnO. Similar Zn 2p XPS spectra were reported by Chavillon *et al.* for N-doped ZnO nanoparticles prepared by the ammonolysis of ZnO_2.[16]

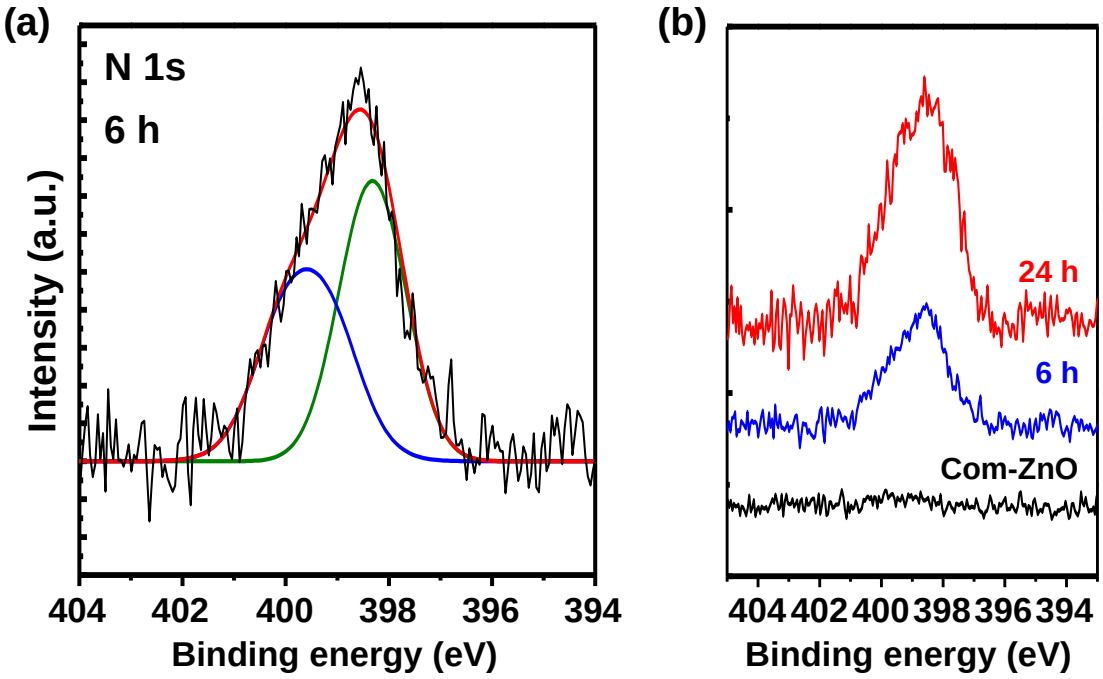

Figure 4-6. (a) XPS spectrum of the N 1*s* region of ZnO rods prepared at 100 °C for 6 h, and (b) XPS spectra of the N 1s region of commercial ZnO and ZnO rods prepared at 100 °C for 6 and 24 h.

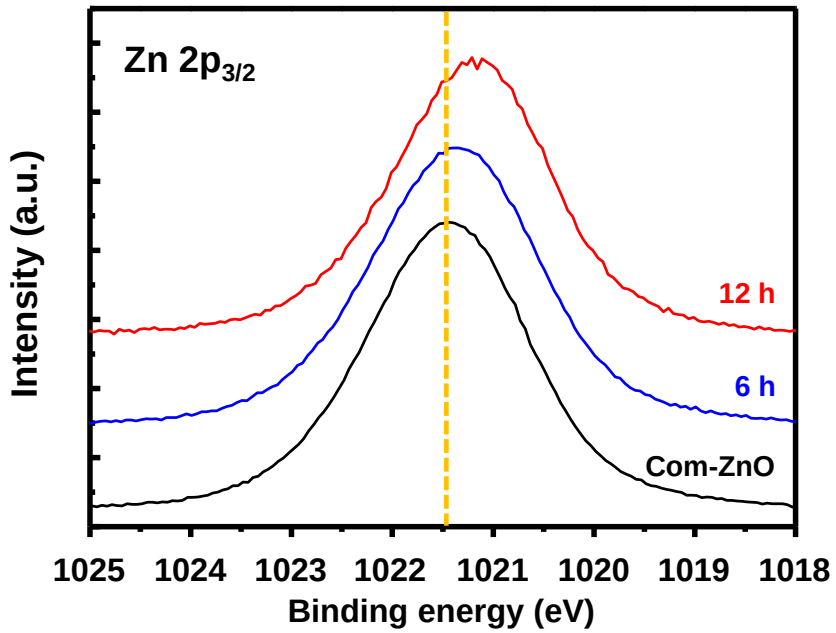

Figure 4-7. XPS spectra of the Zn $2p_{3/2}$ region of commercial ZnO and ZnO rods prepared at 100 °C for 6 and 24 h.

2.4 Summary

Micron-sized N-doped ZnO rods were hydrothermally synthesized from an aqueous ammine-hydroxo zinc complex, and characterized with various physicochemical, structural, spectroscopic and microscopic techniques. The rods were of single crystalline ZnO grown along the c-axis. The absorption edge in the diffuse reflectance UV-vis spectra of the prepared samples shifted toward the visible region, compared with commercial ZnO powder. Raman and XPS spectra indicated that N was incorporated in the ZnO host lattice at O sites. The N concentration could be controlled by varying the reaction time. This procedure did not require specialist equipment, and is applicable for the scale-up fabrication of N-doped ZnO powder. The co-doping of N with other metal ions may further change the properties of ZnO, for example, the conduction properties via band gap engineering. More detailed studies are currently underway.

References

1 C. G. Van de Walle, *Phys. Rev. Lett*., 2000, **85**, 1012−1015.

2 K. T. Ramakrishna, H. Gopalaswamy, P. J. Reddy, *J. Cryst. Growth*, 2000, **210**, 516−520.

3 P. Cao, D. X. Zhao, J. Y. Zhang, D. Z. Shen, Y. M. Lu, B. Yao, B. H. Li, Y. Bai, X. W. Fan, *Appl. Surf. Sci*., 2008, **254**, 2900−2904.

4 J. B. Yi, C. C. Lim, G. Z. Xing, H. M. Fan, L. H. Van, S. L. Huang, K. S. Yang, X. L. Huang, X. B. Qin, B.Y. Wang, T. Wu, L. Wang, H. T. Zhang, X.Y. Gao, T. Liu, A. T. S. Wee, Y. P. Feng, J. Ding, *Phys. Rev. Lett*., 2010, **104**, 137201.

5 X. Chen, Z. L. Wang, *Adv. Mater*., 2011, **23**, 873−877.

6 A. Tsukazaki, A. Ohtomo, T. Onuma, M. Ohtani, T. Makino, M. Sumiya, K. Ohtani, S. F. Chichibu, S. Fuke, Y. Segawa, H. Ohno, H. Koinuma, M. Kawasaki, *Nat. Mater*., 2005, **4**, 42–46.

7 A. Allenic, W. Guo, Y.B. Chen, G.Y. Zhao, X.Q. Pan, *J. Mater. Res*., 2007, **22(8)**, 2339–2344.

8 C. L. Perkins, S.-H. Lee, X. Li, S. E. Asher, T. J. Coutts, *J. Appl. Phys*., 2005, **97**, 034907.

9 M. Mapa, C. S. Gopinath, *Chem. Mater*., 2009, **21**, 351–359.

10 S. T. Meyers, J. T. Anderson, C. M. Hung, J. Thompson, J. F. Wager, D. A. Keszler, *J. Am. Chem. Soc*. 2008, **130**, 17603–17609.

11 G. Yang, Z. Jiang, H. Shi, T. Xiao, Z. Yan, *J. Mater. Chem*., 2010, **20**, 5301–5309.

12 X. Zong, C. Sun, H. Yu, Z. G. Chen, Z. Xing, D. Ye, G. Q. Lu, X. Li, L. Wang, *J. Phys. Chem. C*, 2013, **117**, 4937−4942.

13 J. M. Calleja, M. Cardona, *Phys. Rev. B*, 1977, **16**, 3753–3761.

14 A. Kaschner, U. Haboeck, M. Strassburg, G. Kaczmarczyk, A. Hoffmann, C. Thomsen, A. Zeuner, H. R. Alves, D. M. Hofmann, *Appl. Phys. Lett*., 2002, **80**, 1909–1911.

15 L. L. Kerr, X. Li, M. Canepa, A. J. Sommer, *Thin Solid Films*, 2007, **515**, 5282–5286.

16 B. Chavillon, L. Cario, A. Renaud, F. Tessier, F. C. M. Boujtita, Y. Pellegrin, E. Blart, A. Smeigh, L. Hammarstrom, F. Odobel, S. Jobic, *J. Am. Chem. Soc*., 2012, **134**, 464–470.

17 C. Shifu, Z. Wei, Z. Sujuan, L. Wei, *Chem. Eng. J.*, 2009, **148**, 263–269.

18 X. Yang, A. Wolcott, G. Wang, A. Sobo, R. C. Fitzmorris, F. Qian, J. Z. Zhang, Y. Li, *Nano Lett*., 2009, **9**, 2331−2336.

Chapter-5

Fabrication of Nitrogen-doped ZnO Nanowire Arrays on ZnO Seeded Substrate Using an Ammine-Hydroxo Zinc Complex

Chapter-5 demonstrates the fabrication of Nitrogen-doped ZnO (N-doped ZnO) nanowire arrays by hydrothermal method using zinc ammine complex solution as a precursor. N-doped ZnO nanowire arrays were successfully fabricated using simple two-step process using an aqueous ammine-hydroxo zinc complex precursor without post heat treatment. In the first step, ZnO seed layer was spin-cast several times onto a Si substrate to form a ~100 nm thick film. After ZnO seed layer was coated uniformly on the silicon wafer, hydrothermal ZnO growth was carried out by suspending the wafer upside-down in a Teflon-lined autoclave with an aqueous ammine-hydroxo zinc complex solution. Reaction at 100 °C yielded highly crystalline and vertically oriented ZnO nanowire arrays, whose length and diameter could be controlled by varying the reaction time.

5.1 Introduction

In chapter 4, preparation of N-doped ZnO micro rod powder by hydrothermal method using zinc ammine complex solution as a precursor was demonstrated. In this chapter, hydrothermal fabrication of N-doped ZnO nanowire arrays using zinc ammine complex solution is presented.

In the past decade, ZnO thin films and nanostructures have become promising materials for emerging electronic applications. Doping heteroatoms at Zn or O sites in ZnO can be used to tune the band gap. N is a common heteroatom dopant, due to its compatible size to O and small ionization energy. The introduction of N in crystal lattice of ZnO will result in an intermediate energy level in the bandgap, and reduce the absorption energy. Indeed, previous studies of n-type N-doped ZnO film have shown a significant red shift in light absorption wavelength.[1,2]

However, doping N in the ZnO lattice remains difficult, so developing methods which give high dopant yields and carrier densities is required.

Since the first report of ultraviolet lasing from ZnO nanowires,[3,4] considerable effort has been devoted to the development of synthetic methodologies for one-dimensional ZnO nanostructures. Among the various techniques described in literatures, evaporation and condensation processes are favorable due to their high-quality products and simplicity. However, these gas-phase approaches generally require economically prohibitive high temperatures of 800–900^{o}C.[5,6] Although recent MOCVD schemes that reduced the deposition temperature to 450^{o}C by using organometallic zinc precursors,[7] the commercial potential of gas-phase-grown ZnO nanowires remains constrained by the expensive and/or insulating (for example, Al_2O_3) substrates required for oriented growth, as well as the size and cost of the vapor deposition systems. A low-temperature, versatile and large-scale synthetic process is required before ZnO nanowire arrays find realistic applications in light emission, solar energy conversion and other promising areas.

Solution processes to fabricate ZnO nanowires are attractive because of their low growth temperatures and good potential for scale-up. In this regard, Vayssieres et al. developed a hydrothermal process for producing arrays of ZnO microrods and nanorods on conducting glass substrates at 95^{o}C.[8,9] Recently, a seeded growth process was used to make helical ZnO rods and

columns at a similar temperature.[10]

Here, fabrication of the N-doped ZnO nanowire arrays were demonstrated by hydrothermal treatment of ZnO seeded substrate in an ammine-hydroxo zinc complex.

5.2 Experimental

5.2.1 Preparation of Ammine-hydroxo Zinc Complex

$Zn(NO_3)_2 \cdot 6H_2O$ (>99%, Wako Pure Chemical Industries, Japan), NaOH (>97%, Wako Pure Chemical Industries, Japan) and NH_3 aqueous solution (28%, Wako Pure Chemical Industries, Japan) were used as chemical reagent without further purification. N-doped ZnO rods were hydrothermally synthesized using an ammine-hydroxo zinc complex, which was prepared in Chapter 4. In brief, 10 ml of aqueous 2.5 M NaOH was added dropwise to 15 ml of aqueous 0.5 M $Zn(NO_3)_2 \cdot 6H_2O$ under vigorous stirring. The resulting hydroxide slurry was centrifuged, and the supernatant was removed. Rinsing and separation was carried out three further times to remove Na^+ and NO_3^-. The resulting hydrated precipitate was dissolved in 50 ml of aqueous 6.6 M NH_3 to form a stock solution.

5.2.2 Preparation of ZnO Seed Layer

ZnO seed layers were deposited on 25×35 mm Si(100) substrate by spin-coating the stock precursor solution filtered through a 0.2 μm PTFE syringe filter. All substrates were cleaned by sonication in acetone for 10 min followed by in distilled water for 10 min. The cleaned

substrates were then exposed to atmospheric-pressure glow discharge plasma for 10 min before spin-coating to obtain a hydrophilic surface. Substrate rotation speed and time were 3000 rpm and 30 s, respectively. The film was then immediately cured on a preheated hot plate at 150^{o}C for 5 min. Coating and curing steps were repeated 10 times until reached to the desired thickness.

5.2.3 Fabrication of ZnO Nanowire Arrays

After ZnO seed layers were coated uniformly on the Si substrate, hydrothermal ZnO growth was carried out. The stock solution was diluted with distilled water in three times to form a growth solution. 30 ml of growth solution was transferred in 35 ml Teflon-lined autoclave and the ZnO seeded Si substrate was suspended upside-down in the solution. The reaction was carried out at 100^{o}C for various reaction time. After the hydrothermal reaction, the substrates were rinsed with distilled water immediately. The experimental set up is shown in Fig. 5-1

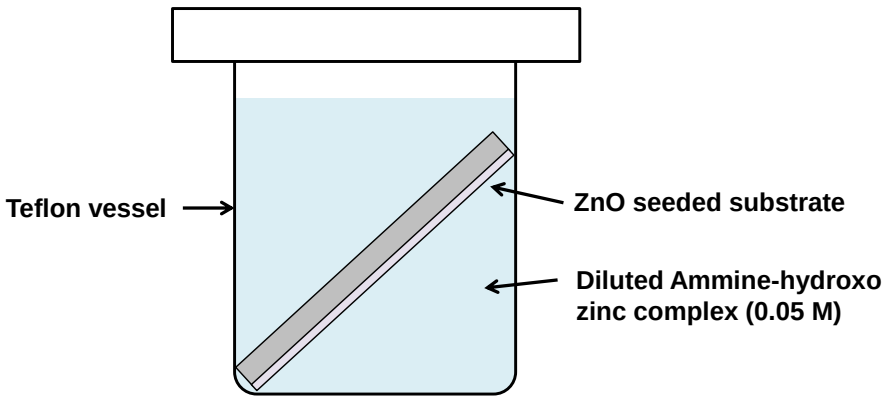

Figure 5-1. Illustration of experimental set up for preparation of ZnO nanowire array.

5.2.4 Characterization

Crystal phases were determined by X-Ray diffraction (XRD), using a RINT2000 diffractometer (Rigaku, Japan) with Cu K_α radiation (λ = 1.542 Å). The observed interplanar d-spacing was corrected with respect to silicon. Sample morphologies were observed by field-emission scanning electron microscopy (SEM) (S4500, Hitachi, Japan). Microstructures were analyzed by transmission electron microscopy (TEM) (H-8100, Hitachi, Japan) at 200 kV. Diffuse reflectance UV-vis spectra were recorded on a spectrophotometer (V-550, JASCO, Japan), with $BaSO_4$ as the reference material. Raman spectra were recorded at room temperature on a Jobin Yvon T64000 spectrometer, with an Ar laser (λ=514.5 nm) excitation source. X-ray photoelectron spectroscopy (XPS) spectra were recorded on a Perkin-Elmer model 5500 MT XPS system, using monochromatic Mg K_α radiation (1253.6 eV) with a pass energy of 58.7 eV. Binding energies were calibrated with respect to the C 1s core level at 284.8 eV. Commercial ZnO powder (>99%, Wako Pure Chemical Industries, Japan) was used for all measurements as a reference.

5.2.5 Photoelectrochemical Characterizations

The photoelectrochemical characteristics were measured in a Zennium electrochemical workstation (ZAHNER) using a standard three compartment cell under Xe light irradiation (500 W mercury lamp). The nanowires were fabricated on FTO substrate for photoelectrochemical

measurement with working electrode area of 4 cm^2. Reference samples were prepared using P25 and commercial ZnO powder by suspending the powder in ethanol (10 mg / 10 ml) which was then dropped onto FTO substrates and subsequent heat treatment at 500^oC for 1 h. A Pt wire and Ag/AgCl electrode were used as counter electrode and reference electrode, respectively. Na_2SO_4 (0.1 M) aqueous solution was used as electrolyte. Schematic illustration of experimental set up is shown in figure 5-2.

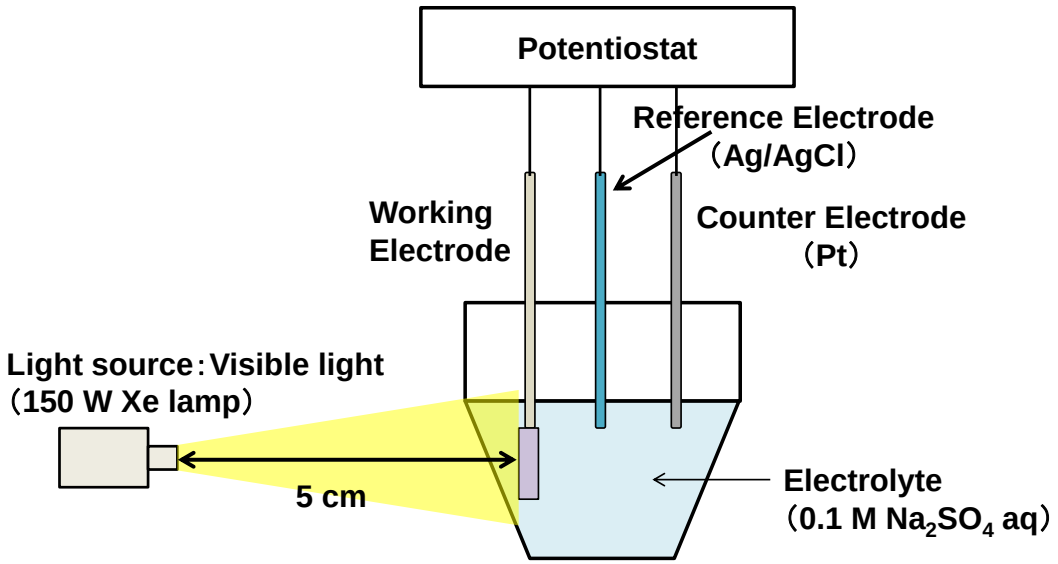

Figure 5-2. Illustration of experimental set up for photoelectrochemical measurement.

5.3 Results and discussion

5.3.1 ZnO Seed Layer

ZnO seed layers were deposited on 25×35 mm Si(100) substrate by spin-coating the stock precursor solution. The XRD pattern of spin-coated ZnO seed layer deposited via 10 coating and curing cycles was shown in Fig. 5-3. The diffraction peaks were in good agreement with that of the hexagonal wurtzite structure of ZnO (JCPDS No. 36-1451). Figure 5-4 shows the corss-sectional and top view SEM images of prepared ZnO seed layer. The thickness of ZnO seed layer deposited via 10 coating and curing cycles was ~100 nm as shown in Fig. 5-4a. The top view SEM image in Figure 5-4b indicated that the prepared ZnO seed layer was consisted of nano sized grains.

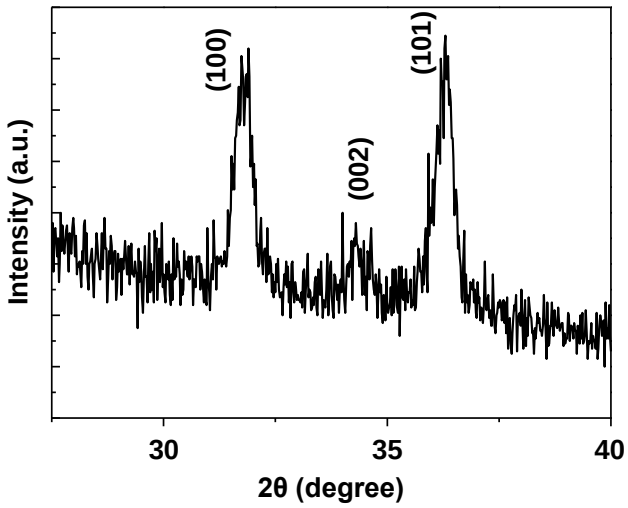

Figure 5-3. XRD pattern of ZnO seed layer deposited by dpin-coating via 10 coating and curing cycles.

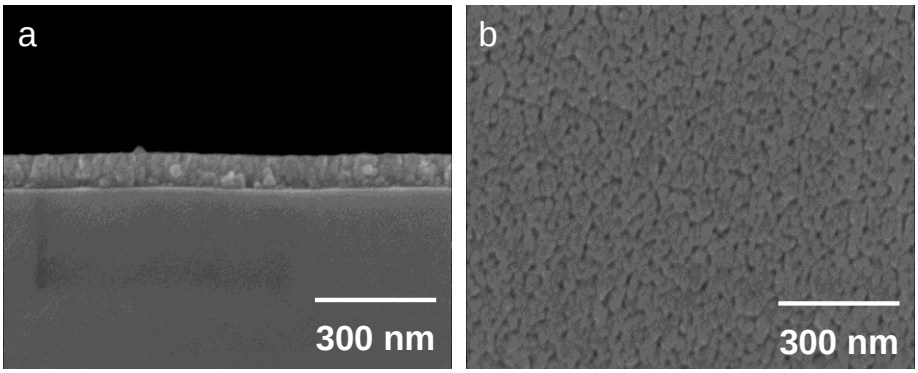

Figure 5-4. Cross-sectional and top view SEM images of ZnO seed layer deposited by dip-coating via 10 coating and curing cycles.

5.3.2 Fabrication of Nitrogen-doped ZnO Nanowire arrays

Figure 5-5 shows the XRD pattern of the sample prepared by hydrothermal treatment for ZnO seed layer using ammine-hydroxo zinc complex solution at 100^{o}C for 12 h. The reflections were identified as wurtzite-type ZnO (JCPDS 36-1451), and no trace of impurity phases such as $Zn(OH)_2$ were found. In particular, the (002) reflection was distinctly intense among the detectable reflections, indicating preferential orientation along the *c*-axis.

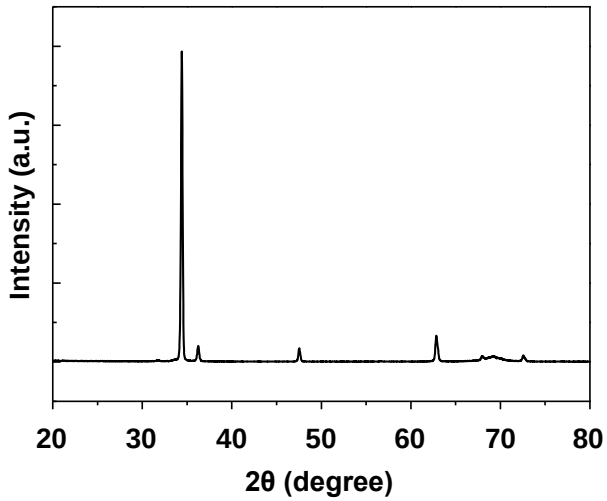

Figure 5-5. XRD pattern of ZnO nanowire array prepared at 100^{o}C for 12 h.

Figure 5-6 shows cross-sectional and top view SEM images of the sample prepared by hydrothermal treatment for ZnO seed layer using ammine-hydroxo zinc complex solution at 100^{o}C for 12 h. As shown in Fig. 5-6a, a high density ZnO nanowire arrays was obtained on the substrate. They were uniform in diameter (125 nm) and in length (11.5 μm). The nanowires tended to grow vertically on the substrate. Preferred orientation along the *c*-axis has often been observed in the literatures.[1-3]

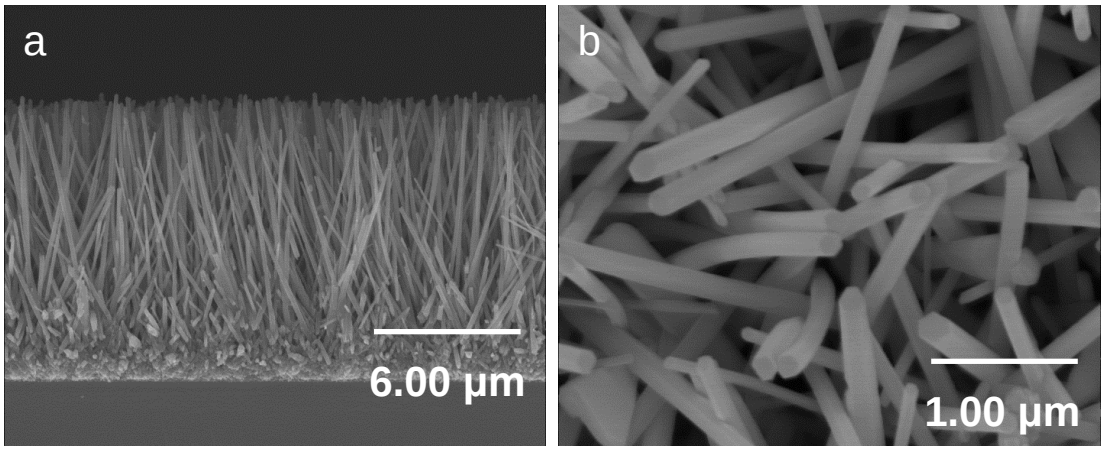

Figure 5-6. Cross-sectional and top view SEM images of ZnO nanowire array prepared at 100^{o}C for 12 h.

Figure 5-7 shows TEM images of ZnO nanowires which was peeled off from the substrate. The periodicity of the lattice fringes along the growth direction of the nanowire was 0.26 nm, corresponding to (002) and FFT analysis suggested that the ZnO nanowires were predominantly single crystals. These results would indicate that the resulting ZnO nanowires are single crystals ZnO grown along the *c*-axis without any intergrowth. Thus, the results of XRD analyses and, SEM and TEM observations revealed that the ZnO nanowire arrays grown by hydrothermal

treatment on ZnO seeded substrate had a preferred orientation along the *c*-axis. By considering the anisotropy and polarity of the crystal structure of ZnO, the growth rates (v) ZnO crystal in different directions were found to be of the order $v[0001] > v[01\bar{1}\bar{1}] > v[01\bar{1}0] > v[01\bar{1}1] > v[000\bar{1}]$, indicating faster growth along the *c*-axis. Here, $v[0001]$ and $v[000\bar{1}]$ denote growth rates on the zinc-terminated (0001) face and the oxygen-terminated $(000\bar{1})$ face, respectively.[11,12]

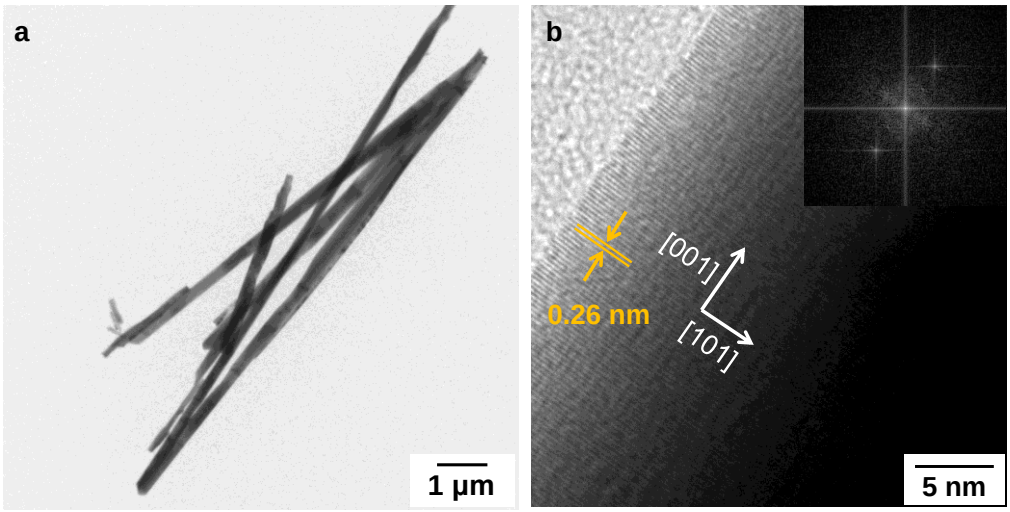

Figure 5-7. (a) TEM images of ZnO nanowire prepared at 100°C for 12 h. (b) HRTEM image and FFT pattern (inset).

Figure 5-8 shows SEM images of ZnO nanowire arrays prepared for various reaction times and the reaction time evolution of the average nanowire length and diameter. The nanowire length increased with hydrothermal reaction time and saturated after 12 h at about 11.5 μm, Although the variation in wire diameter was relatively small (±50 nm), the deviation in diameter became smaller as increasing the reaction time. These results indicate that the Zn ion is almost used in crystal growth after 12 h and the wire diameter become uniform through Ostwald

ripening process.

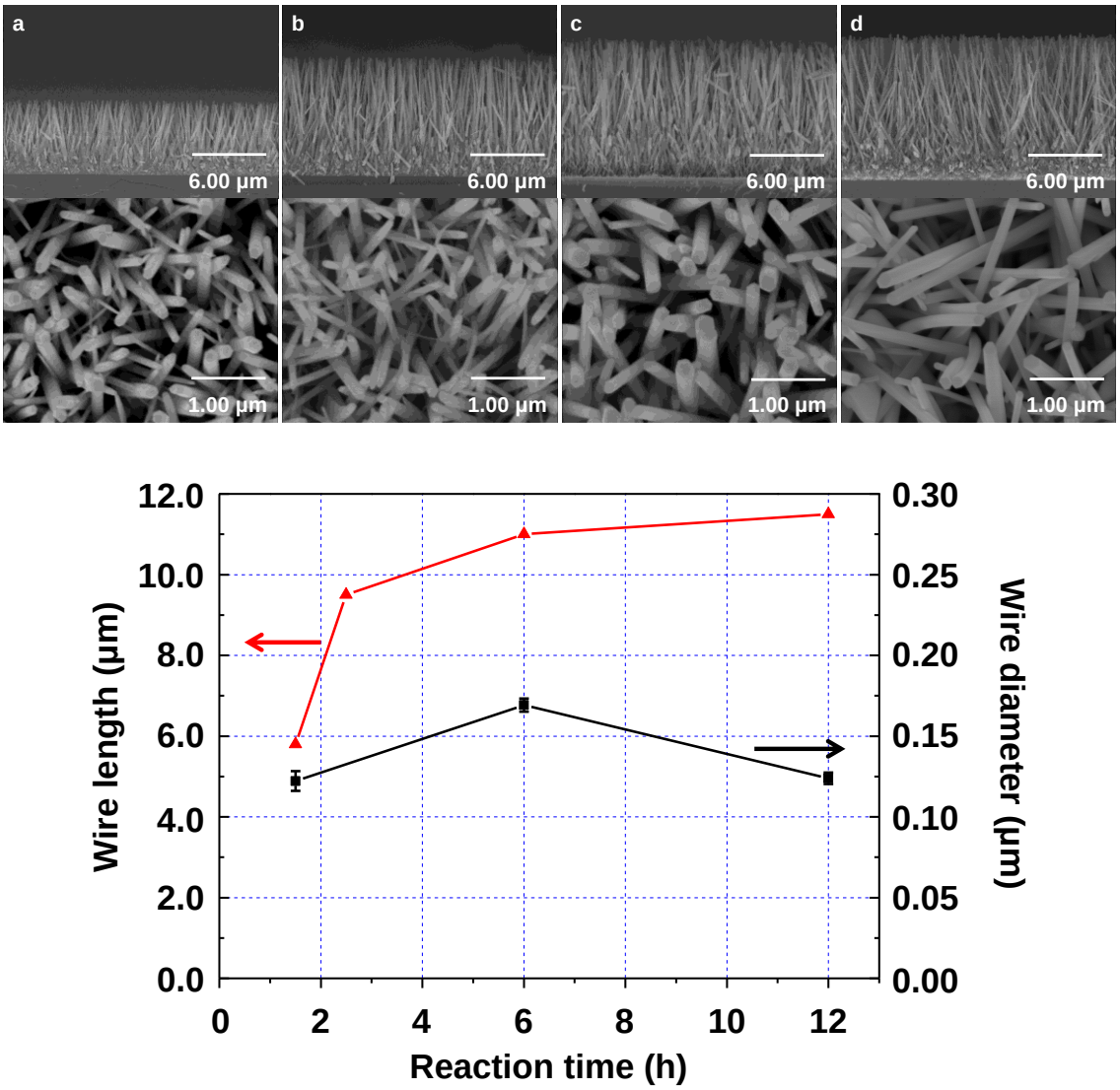

Figure 5-8. SEM images of ZnO nanowire arrays prepared for various reaction times (a) 1.5 h, (b) 2.5 h, (c) 6 h and (d) 12 h and the reaction time evolution of the average nanowire length and diameter.

5.3.3 Characterization of Nitrogen-doped ZnO Nanowire arrays

Diffuse reflectance absorption spectra of commercial ZnO powder and the ZnO nanowire array prepared at 100^{o}C for 6 h are shown in Fig. 5-9. The absorption edge shifted to longer wavelength and occurred at longer wavelength than that of commercial ZnO. This may have reflected the presence of N in the ZnO nanowires, which can shift absorption toward the visible region via band gap narrowing as mentioned in Chapter-4.[13, 14] The red shift in the absorption spectra were consistent with the change in color of the powder samples from white (pure ZnO) to pale-yellow (N-doped ZnO).

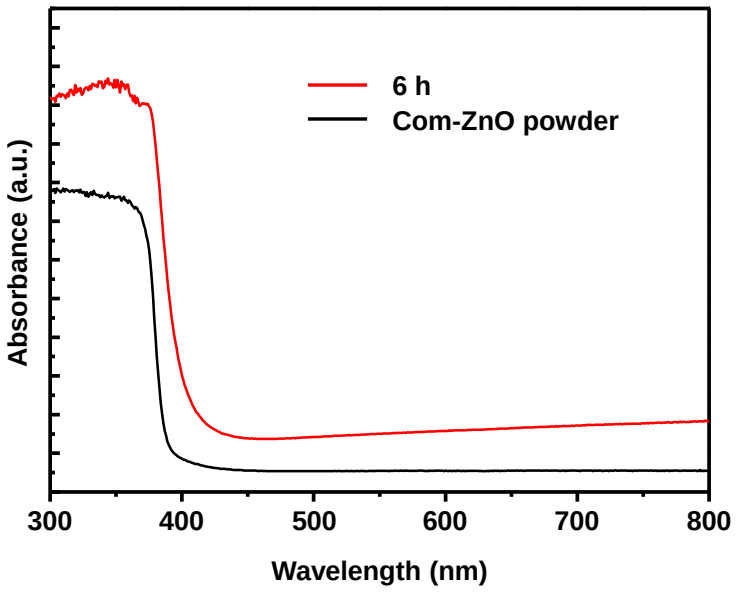

Figure 5-9. Diffuse reflectance absorption spectra of commercial ZnO powder and the ZnO nanowire array prepared at 100^{o}C for 6 h.

Figure 5-10 shows Raman spectra of the ZnO nanowire array prepared at 100 °C for 6 h and commercial ZnO powder as a reference. To aid analyses, all spectra were normalized with

respect to the highest intensity ZnO peak at 437 cm^{-1}. This peak was observed for all samples, and was attributed to vibration of the high frequency E_2 mode, characteristic of the wurtzite phase. Weak peaks at 330 and 380 cm^{-1} arose from the second-order Raman scattering by zone-boundary phonons, E_2 (M),[15] and first-order phonons of A_1 (TO), respectively. A new peak at 582 cm^{-1} for ZnO nanowire array prepared at 100°C for 6 h was not observed for commercial ZnO, and was attributed to the E_2 mode (Zn–N).[16] Other absorption bands classically ascribed to N-related local vibrational modes (*i.e.* near 275, 507 and 635 cm^{-1}) were not observed in the samples as is the case with N-doped ZnO rods demonstrated in Chapter-4.[17-19]

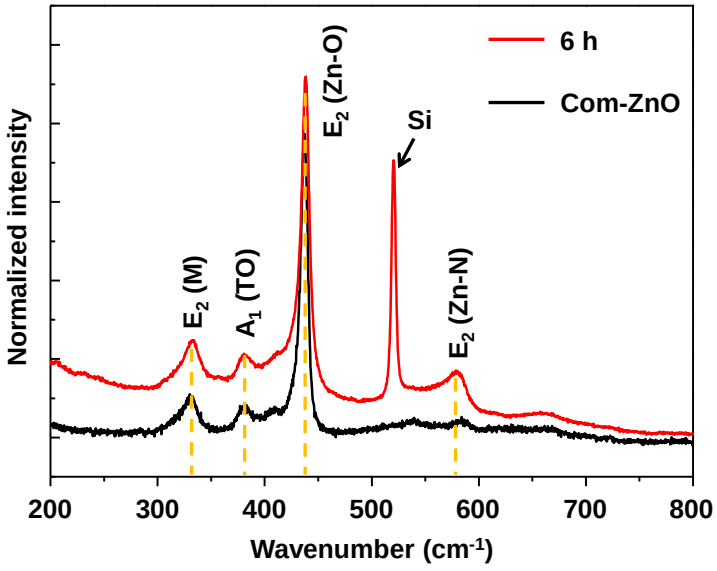

Figure 5-10. Raman spectra of commercial ZnO powder and the ZnO nanowire array prepared at 100°C for 6 h.

XPS spectra for ZnO nanowire array prepared at 100 °C for 6 h is shown in Figs. 5-11. The Zn 2p region revealed two peaks typical for the binding energies of the Zn $2p_{1/2}$ and Zn $2p_{3/2}$

electrons as shown in Fig. 5-11a. The O 1s region in Fig. 5-11b showed two peaks, around 530 eV, attributed to O-Zn bonds[20], and around 531 eV, which is most likely due to the adsorption of OH groups on ZnO nanowire array.[21] The appearance of OH in the XPS spectra of ZnO nanoparticles has been previously reported.[20,21] The core level spectrum of the N 1s region ZnO nanowire array prepared at 100 °C for 6 h exhibited an asymmetric broad peak. This was deconvoluted into two peaks centered at 399.9 and 398.0 eV, as shown in Fig. 5-11c. The peak centered at 398.0 eV was attributed to Zn–N bonds,[20] and that at 399.9 eV to the N 1s binding energy of amines.[20] These results suggested that N was doped at the O sites of crystalline ZnO. UV-vis, Raman and XPS spectra suggested that the N could be incorporated in ZnO and N-doped ZnO nanowire arrays could be fabricated at low temperature (100^{o}C) without any subsequent heat treatment in N_2 or NH_3 atmosphere. Using pure ammine-hydroxo zinc complex solution without any counter ion would enable the N doping to ZnO which is usually difficult by hydrothermal method.

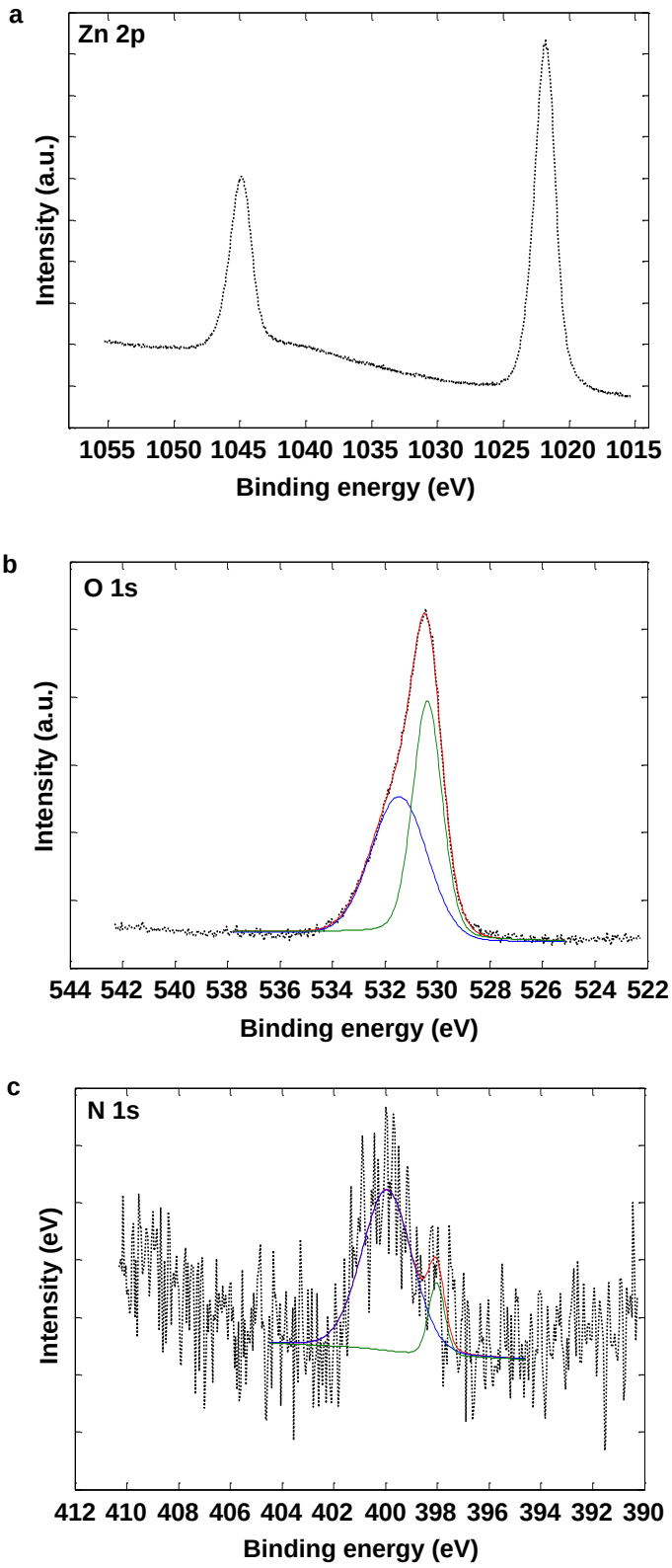

Figure 5-11. XPS spectra of the ZnO nanowire array prepared at 100^{o}C for 6 h (a) Zn 2p, (b) O 1s and (c) N 1s core level spectrum.

5.3.4 Photoelectrochemical Measurement

Figure 5-12 shows a set of linear sweep voltammagrams recorded on N-doped ZnO nanowires in the dark and with illumination of Xe lamp. Dark scan linear sweep voltammagrams from -0.5 to +1.3 V showed almost no current. Upon illumination with a Xe lamp, N-doped ZnO nanowires showed pronounced photocurrent starting at ~ -0.4 V and continues to increase with a photocurrent density of over 30 μA/cm^2 at +1.0 V. Significantly, there is no saturation of photocurrent observed at more positive potential, which indicates efficient charge separation in nanowires upon illumination.

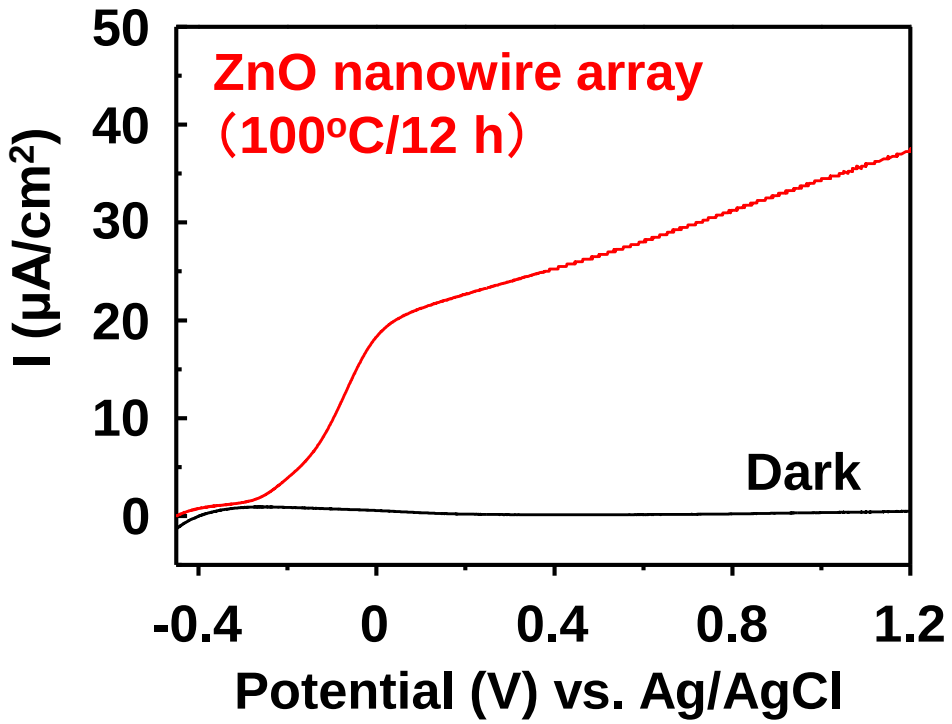

Figure 5-12. Linear sweep voltammagrams at applied potentials from -0.5 to +1.3 V for N-doped ZnO nanowires in the dark (black line) and with illumination (red line).

In addition, amperometric I-t studies were performed to examine the photoresponse of nanowires over time. I-t curve collected from the N-doped ZnO nanowire array prepared at 100oC for 12 h, P25 and commercial ZnO samples with light on/off cycles at +0.5 V are shown in Figure 5-13. The data show a very low dark current of $<10^{-7}$ A/cm^2. Upon illumination with light, it was observed that a spike in photoresponse at all power densities due to the transient effect in power excitation, and the photocurrent then quickly returned to a steady state. Importantly, the photocurrent of N-doped ZnO nanowire array prepared at 100^{o}C for 12 h was over 5 times larger compared with P25 sample and commercial ZnO sample showed very low photocurrent. The advantage afforded by N-doping has been clearly demonstrated regarding enhanced visible absorption and photocurrent generation.

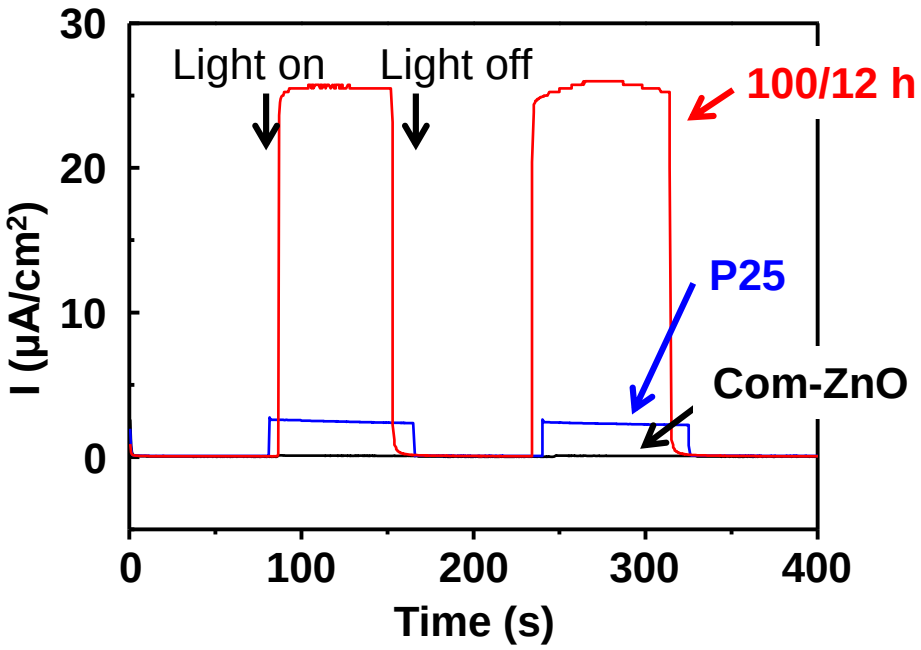

Figure 5-13. Amperometric I-t curves of the N-doped ZnO nanowires prepared at 100^{o}C for 12 h, P25 and commercial ZnO at an applied voltage of +0.5 V with 100 s light on/off cycles.

5.4 Summary

N-doped ZnO nanowire arrays were hydrothermally fabricated from an aqueous ammine-hydroxo zinc complex, and characterized with various physicochemical, structural, spectroscopic and microscopic techniques. The nanowires were of single crystalline ZnO vertically grown along the c-axis to substrate. The length and diameter of ZnO nanowires prepared at 100^{o}C for 12 h was 11.5 μm and 120 nm respectively. The length of nanowire arrays could be controlled by varying the hydrothermal reaction time up to 11.5 μm. The absorption edge in the diffuse reflectance UV-vis spectra of the prepared ZnO nanowire arrays shifted toward the visible region, compared with commercial ZnO powder. Raman and XPS spectra indicated that N was incorporated in the ZnO host lattice at O sites. This procedure did not require specialist equipment, and is applicable for the scale-up fabrication of N-doped ZnO nanowire arrays. This high quality and visible responsible ZnO nanowire arrays would be useful for photoelectrode such as water splitting and dye sensitized solar cells. The photocurrent of N-doped ZnO nanowire array prepared at 100^{o}C for 12 h was over 5 times larger compared with P25 sample. The advantage afforded by N-doping has been clearly demonstrated in terms of enhanced visible absorption and photocurrent generation.

References

1. K. S. Ahn, Y. Yan, S. H. Lee, T. Deutsch, J. Turner, C. E. Tracy, C. L. Perkins, M. M. Al-Jassim, *J. Electrochem. Soc.*, 2007, **154 (9)**, B956–B959.

2. K. S. Ahn, Y. Yan, S. Shet, T. Deutsch, J. Turner, M. Al-Jassim, *Appl. Phys. Lett.*, 2007, **91**, 231909.

3. M. H. Huang, S. Mao, H. Feick, H. Yan, Y. Wu, H. Kind, E. Weber, R. Russo, P. Yang, *Science*, 2001, **292**, 1897.

4. J. Johnson, H. Yan, R. Schaller, L. Haber, R. Saykally, P. Yang, *J. Phys. Chem. B*, 2001, **105**, 11387.

5. P. Yang, H. Yan, S. Mao, R. Russo, J. Johnson, R. Saykally, N. Morris, J. Pham, R. He, H. Choi, *Adv. Funct. Mater.*, 2002, **12**, 323.

6. B. D. Yao, Y. F. Chan, N. Wang, *Appl. Phys. Lett.*, 2002, **81**, 757.

7. W. I. Park, G. Yi,M. Kim, S. L. Pennycook, *Adv. Mater.*, 2002, **14**, 1841.

8. L. Vayssieres, K. Keis, A. Hagfeldt, S. Lindquist, *Chem. Mater.*, 2001, **13**, 4395.

9. L. Vayssieres, *Adv. Mater.*, 2003, **15**, 464.

10. Z. R. Tian, J. A. Voigt, J. Liu, B. Mckenzie, M. J. Mcdermott, *J. Am. Chem. Soc.*, 2002, **124**, 12954.

11. W. J. Li, E. W. Shi, W. Z. Zhong and Z. W. Yin, *J. Cryst. Growth*, 1999, **203**, 186-196.

12. J. H. Kim, E. M. Kim, D. Andeen, D. Thomson, S. P. DenBaars, F. F. Lange, *Adv. Funct. Mater*., 2007, **17**, 463-471.

13. G. Yang, Z. Jiang, H. Shi, T. Xiao, Z. Yan, *J. Mater. Chem*., 2010, **20**, 5301–5309.

14. X. Zong, C. Sun, H. Yu, Z. G. Chen, Z. Xing, D. Ye, G. Q. Lu, X. Li, L. Wang, *J. Phys. Chem. C*, 2013, **117**, 4937−4942.

15. J. M. Calleja, M. Cardona, *Phys. Rev. B*, 1977, **16**, 3753–3761.

16. M. Mapa, C. S. Gopinath, *Chem. Mater*., 2009, **21**, 351–359.

17. A. Kaschner, U. Haboeck, M. Strassburg, G. Kaczmarczyk, A. Hoffmann, C. Thomsen, A. Zeuner, H. R. Alves, D. M. Hofmann, *Appl. Phys. Lett*., 2002, **80**, 1909–1911.

18. L. L. Kerr, X. Li, M. Canepa, A. J. Sommer, *Thin Solid Films*, 2007, **515**, 5282–5286.

19. B. Chavillon, L. Cario, A. Renaud, F. Tessier, F. C. M. Boujtita, Y. Pellegrin, E. Blart, A. Smeigh, L. Hammarstrom, F. Odobel, S. Jobic, *J. Am. Chem. Soc*., 2012, **134**, 464–470.

20. X. Yang, A. Wolcott, G. Wang, A. Sobo, R. C. Fitzmorris, F. Qian, J. Z. Zhang, Y. Li, *Nano Lett.*, 2009, **9**, 2331−2336.

21. Y. Lee, H. T. Y. Shimodaira, K. Teramura, M. Hara, H. Kobayshi, K. Domen, M. Yashima, *J. Phys. Chem. C* 2007, **111**, 1042−1048.

Chapter-6

Conclusion

In the present study, solution process for preparing ZnO micro/nano structures in powder and film form has been advanced. The solvothermal method using ethylene glycol as a solvent realized the direct fabrication of ZnO hollow microspheres without using any templates. On the other hand, the hydrothermal method using ammine-hydroxo zinc complex enabled nitrogen-doping in ZnO crystal and N-doped ZnO nanowire arrays were successfully fabricated using ZnO seeded substrate.

A template-free solvothermal preparation of ZnO hollow microspheres covered with *c* plane was demonstrated to show the unique fabrication process structures. A formation mechanism of the ZnO hollow microspheres was proposed, based on the morphological evolution observed by SEM, TEM and ICP-AES analyses during growth. Solid microspheres initially consisting of ten nm particles were formed, by the agglomeration of primary particles after nucleation. Surface particles on the solid microspheres then grew into hexagonal crystals. When the degree of saturation decreased, the low crystallinity sphere centers preferentially dissolved, and hollow microspheres were formed through Ostwald ripening process. HR-TEM indicated that the microspheres were covered with ZnO *c* planes. These ZnO hollow microspheres may have

applications in photocatalysis, dye sensitized solar cells, photonic crystals and advanced optoelectronic devices. The preparation described within may provide a new strategy for designing generic hollow materials.

C-doping occured when the ZnO hollow microspheres were heat treated by decomposition of residual organic compound in the as-prepared sample. Heat treated samples showed a red shift of absorption edge in the UV-vis spectra. Such a red shift expands the light response range of ZnO hollow microspheres to the visible region. The sample heat treated at 700^{o}C showed the best formation rate of ·OH under visible light irradiation.

The DSSCs were successfully fabricated using ZnO hollow microspheres. The conditions such as the thickness of film and sintering temperature were optimized. The best power conversion efficiency was 0.86 %. The device performance was improved by pre-UV treatment for as-prepared ZnO hollow microspheres to eliminate the residual organic compounds up to 1.05 % of power conversion efficiency. These ZnO hollow microspheres would be useful for DSSCs as scattering layer.

Preparation of nitrogen-doped ZnO microrods by hydrothermal method was demonstrated. Using ammine-hydroxo zinc complex as precursor solution enabled to prepare N-doped ZnO. N-doped ZnO microrods showed significant red shift in the absorption edge compared with pure commercial ZnO powder.

Fabrication of N-doped ZnO nanowire arrays were also demonstrated by hydrothermal treatment for ZnO seeded substrate in ammine-hydroxo zinc complex. The nanowires were of single crystalline ZnO vertically grown along the c-axis to substrate. The length of Nanowire arrays could be controlled by varying the reaction time up to 11.5 μm.

There is still space for improvement of the solution processed ZnO micro/nanostructures such as new applications, quality of products, possibility of doping, obtaining high physical/chemical properties. We believe the possibility of solution process for future applications.

List of pubrications

1. Taiki Ihara, Hajime Wagata, Toshihiro Kogure, Ken-ichi Katsumata, Kiyoshi Okada, and Nobuhiro Matsushita, "Template-free solvothermal preparation of ZnO hollow microspheres covered with *c* planes", *RSC Advances*, **4**, 25148-25154, (2014)

2. Taiki Ihara, Ken-ichi Katsumata, Tomoaki Watanabe, Kiyoshi Okada, and Nobuhiro Matsushita, "Nitrogen-doped ZnO Rods Synthesized from an Ammine-Hydroxo Zinc Complex", *Chemistry Letters, accepted.*

Presentation at International Conference

1. (Poster) Taiki Ihara, Hajime Wagata, Naoki Ohashi, Ken-ichi Katsumata, Kiyoshi Okada, and Nobuhiro Matsushita, "Spherical ZnO nanoparticles synthesized for inkjet patterning", Joint Conference of The 5th International Conference on Science and Technology for Advanced Ceramics (STAC5), Yokohama, Japan, June 2011

2. (Oral) Taiki Ihara, Hajime Wagata, Naoki Ohashi, Yutaka Ito, Kenji Nakane, Ken-ichi Katsumata, Kiyoshi Okada, Nobuhiro Matsushita, "Direct patterning of zinc oxide by Ink-jet deposition suppressing coffee stain effect", The International Meeting of the Pacific Rim Ceramic Societies conference, Cairns, Australia, July 2011

3. (Poster) Taiki Ihara, Hajime Wagata, Naoki Ohashi, Ken-ichi Katsumata, Kiyoshi Okada, Nobuhiro Matsushita. "Direct Fabrication of ZnO patterns at Low Temperature by Inkjet Deposition", 15th International Conference on Thin Films (ICTF-15), Kyoto, Japan, November 2011

4. (Poster) Taiki Ihara, Hajime Wagata, Toshihiro Kogure, Ken-ichi Katsumata, Kiyoshi Okada, Nobuhiro Matsushita, "Template-free synthesis of ZnO micro-hollow spheres by solvothermal process", Materials Research Society (MRS) Spring Meeting (San Francisco, USA), April 2012

5. (Poster) Taiki Ihara, Hajime Wagata, Ken-ichi Katsumata, Kiyoshi Okada, Nobuhiro Matsushita, "N doped ZnO rod synthesized from zinc ammine complex solution", 6th International Conference on Science and Technology of Advanced Ceramics (STAC6) (Yokohama, Japan), June 2012

6. (Poster) Taiki Ihara, Hajime Wagata, Toshihiro Kogure, Ken-ichi Katsumata, Kiyoshi Okada, Nobuhiro Matsushita, "Photocatalytic activity of ZnO micro-hollow spheres prepared by solvothermal approach", 15th International Congress on Catalysis (ICC2012) (Munich, Germany), July 2012

7. (Poster) Taiki Ihara, Hajime Wagata, Toshihiro Kogure, Ken-ichi Katsumata, Kiyoshi Okada, Nobuhiro Matsushita, "Effect of water addition on morphology control of ZnO particles synthesized by solvothermal process", IUMRS-International Conference on Electronic Materials (IUMRS-ICEM 2012) (Yokohama, Japan), September 2012

8. (Poster) Taiki Ihara, Hajime Wagata, Toshihiro Kogure, Ken-ichi Katsumata, Kiyoshi Okada, Nobuhiro Matsushita, "Visible light photocatalytic activity of ZnO micro hollow spheres prepared by solvothermal process", Materials Research Society (MRS) Fall Meeting (Boston, USA), December 2012

9. (Poster) Taiki Ihara, Hajime Wagata, Toshihiro Kogure, Ken-ichi Katsumata, Kiyoshi Okada, Nobuhiro Matsushita, "Template-free ZnO Micro Hollow Spheres Prepared by Solvothermal Process and Hydroxyl Radical Generation under Visible Light", International Conference on Ferrite (ICF11) (Okinawa, Japan), April 2013

10. (Poster) Taiki Ihara, Hajime Wagata, Toshihiro Kogure, Ken-ichi Katsumata, Kiyoshi Okada, Nobuhiro Matsushita, "Carbon doped ZnO micro hollow spheres for visible light responsive photocatalyst", International Conference on Materials for Advanced Technologies 2013 (ICMAT2013) (Singapore), July 2013

11. (Poster) Taiki Ihara, Yi-Bing Cheng, Ken-ichi Katsumata, Kiyoshi Okada, Nobuhiro Matsushita, "Template-free synthesis of ZnO hollow microspheres and their application to dye sensitized solar cells", Materials Research Society (MRS) Spring Meeting (San Francisco, USA), April 2014

12. (Poster) Taiki Ihara, Hajime Wagata, Ken-ichi Katsumata, Kiyoshi Okada, Nobuhiro Matsushita, "Solvothermal Synthesis of ZnO Spherical Particles with Tunable Size", The 15th IUMRS-international Conference in Asia (IUMRS-ICA 2014) (Fukuoka, Japan), August 2014

13. (Poster) Taiki Ihara, Hajime Wagata, Toshihiro Kogure, Ken-ichi Katsumata, Kiyoshi Okada, Nobuhiro Matsushita, "Template-Free Solvothermal Preparation of Carbon doped ZnO Hollow Microspheres", The 15th IUMRS-international Conference in Asia

(IUMRS-ICA 2014) (Fukuoka, Japan), August 2014

14. (Poster) Taiki Ihara, Ken-ichi Katsumata, Tomoaki Watanabe, Kiyoshi Okada, Nobuhiro Matsushita, “N-containing ZnO rods synthesized by hydrothermal method using ammine-hydroxo zinc complex solution”, 6th PCGMR/NCKU Symposium (Tainan, Taiwan), September 2014

15. (Poster) Taiki Ihara, Ken-ichi Katsumata, Tomoaki Watanabe, Kiyoshi Okada, Nobuhiro Matsushita, “N concentration controlled ZnO rods synthesized by hydrothermal method”, E-MRS 2014 Fall Meeting (Warsaw, Poland), September 2014

16. (Poster) Taiki Ihara, Ken-ichi Katsumata, Tomoaki Watanabe, Kiyoshi Okada, Nobuhiro Matsushita, “N-containing ZnO rods with tunable concentration synthesized by hydrothermal method”, Pacific Rim Symposium on Surfaces, Coatings & Interfaces (PacSurf2014) (Hawaii), December 2014

Presentation at Domestic Conference

1. （口頭）Taiki Ihara, Hajime Wagata, Naoki Ohashi, Yutaka Ito, Kenji Nakane, Ken-ichi Katsumata, Kiyoshi Okada and Nobuhiro Matsushita, “Direct patterning of Zinc Oxide by Inkjet deposition”，第２０回日本 MRS 学術シンポジウム、PPA-139、横浜、2010 年 12 月

2. （ポスター）井原大貴、我田元、大橋直樹、伊藤豊、中根堅次、勝又健一、岡田清、松下伸広、“インクジェット析出法による酸化亜鉛のダイレクトパターニング”、4 大学ナノ・マイクロファブリケーションコンソーシアム、川崎、2011 年 3 月

3. （口頭）井原大貴、我田元、大橋直樹、勝又健一、岡田清、松下伸広、“インクジェット析出法による ZnO パターンの作製”、日本セラミックス協会第 24 回秋季シンポジウム、北海道、2011 年 9 月

4. （口頭）井原大貴、我田元、大橋直樹、勝又健一、岡田清、松下伸広、 “Directly fabrication of ZnO patterns on polyimide substrate by inkjet deposition using ammine complex solution”、第 50 回セラミックス基礎科学討論会（東京）、2012 年 1 月

5. （口頭）井原大貴、我田元、勝又健一、岡田清、松下伸広、 “ソルボサーマル法による ZnO 中空粒子の直接合成”、セラミックス協会 2012 年年会（京都）、2012 年 3 月

6. （口頭）井原大貴、我田元、小暮敏弘、勝又健一、岡田清、松下伸広、 “テンプレートフリーZnO 中空粒子の合成と構造解析”、セラミックス協会第 25 回秋季シンポジウム（名古屋）、2012 年 9 月

7. （ポスター）井原大貴、我田元、小暮敏弘、勝又健一、岡田清、松下伸広、 “ソルボサーマル法による ZnO 粒子の形態制御と構造解析”、第 2 回関東支部若手研究発表交流会（東京）、2012 年 11 月

8. （口頭）井原大貴、我田元、小暮敏弘、勝又健一、岡田清、松下伸広、 “テンプレートフリーZnO 中空粒子の合成と熱処理の検討”、セラミックス協会第 26 回秋季シンポジウム（長野）、2013 年 9 月

9. （ポスター）井原大貴、我田元、小暮敏弘、勝又健一、岡田清、松下伸広、 “ソルボサーマル法によるテンプレートフリーZnO 中空粒子の合成と応用”、 第 3 回関東支部若手研究発表交流会（東京）、2013 年 10 月

10. （口頭）井原大貴、我田元、小暮敏博、Yi-Bing Cheng、脇慶子、勝又健一、岡田清、松下伸広、 “ZnO 中空粒子の直接合成と色素増感型太陽電池への応用”、第 32 回固体・表面光化学討論会（東京）、2013 年 12 月

11. （ポスター）井原大貴、我田元、小暮敏弘、勝又健一、岡田清、松下伸広、 “テンプレートフリーソルボサーマル法による ZnO 中空粒子の合成”、 第 4 回関東支部若手研究発表交流会（東京）、2013 年 10 月

12. （口頭）井原大貴、勝又健一、渡邉友亮、岡田清、松下伸広、 “亜鉛アンミン錯体を前駆体とした水熱法による窒素ドープ ZnO ロッドの合成”、セラミックス協会 2015 年年会（岡山）、2015 年 3 月

Honors and Awards

2011 Poster award (Joint Conference of The 5th International Conference on Science and Technology for Advanced Ceramics (STAC5), Yokohama, Japan)

2013 ICMAT 2013 Best Poster Award (at International Conference on Materials for Advanced Technologies 2013 (ICMAT2013), Singapore)

2013 奨励賞（at セラミックス協会第 26 回秋季シンポジウム、長野）

Scholarships

2011 Kato Foundation for promotion of Science Scholarship

Acknowledgement

It is my pleasure to acknowledge the assistance of many who have helped me to bring this work to its final form.

Words fail to express the deep debt of gratitude, I owe to **Prof. Nobuhiro Matsushita and Prof. Kiyoshi Okada**, Materials and Structures Laboratory, Tokyo Institute of Technology, Japan, for their stimulating discussions, critical comments and suggestions, inspiring guidance and constant encouragement during the course of the present investigation.

I thank to Prof. Toshihiro Kogure, The University of Tokyo, for TEM observation and fruitful discussion for analysis. I also thank to Prof. Yi-Bing Cheng, Monash University, Australia, for permitting me to stay at his laboratory as a visiting researcher for 3 months.

I owe to Prof. Hitoshi Kawaji, Prof. Ikuyoshi Tomita, Prof. Junko Nomura and Prof. Takeo Osaka for being my examiners along with Prof. Nobuhiro Matsushita.

My earnest gratitude to Dr. Ken-ichi Katsumata, Dr. Takaaki Taniguchi and Dr. Hajime Wagata, for their timely help, support, interest, valuable discussions and helping me out by doing various mesurements. Dr. Toshihiro Isobe is thanked for XPS measurement. Prof. Tomoaki Watanabe, Meiji University is thanked for permitting me to use some facilities for measurements.

I also express my heartfelt thanks to Mrs. Hiroko Yoshioka and Mrs. Junko Ito of Matsushita

Laboratory, Tokyo Institute of Technology, Japan.

I greately acknowledge to Dr. Mirrabos Hojamberdiev, Dr. Catalin Popa, Dr. Chun Yi Chen, Mr. Shingo Omata, Mr. Yukihiro Komatsubara, Mr. Seitaro Kaneko, Miss Xiau Hou, Miss Rie Takeda, Mr. Yukiaki Ono, Mr. Takuro Kidokoro, Miss Sayaka Nakamura, Mr. Yuki Okayasu, Mr. Ryosuke Motoyoshi, Mr. Kazuya Sakai, Miss Yuriko Fukushima, Miss Sachiko Machida, Mr. Kei Ikeda, Mr. Yuta Okaga, Mr. Keisuke Kojima, Mr. Naoki Sugimoto, Mr. Yukitoshi Takahashi, Mr. Eitarou Tamaru, Mr. Fumihiko Chimoto, Miss Eri Takematsu, Mr. Kazuki Miyamoto, Mr. Tetsuya Yamada, Mr. Tetsuro Watanabe, Mr. Yuta Kubota, Miss Momoko Yamamoto, Mr. Yuto Seino, Mr. Yusuke Tsujimoto, Mr. Ryo Matsudo, Mr. Jiang, Mr Shungo Shimizu Mrs. Hitomi Tokimori, Dr. Yuta Katayanagi and Mr. Satoshi Mori.

My sincere appreciations to all my friends, near and dear ones in the Tokyo Institute of Technology for their kind help throughout my stay in Suzukake-dai.

My sincere acknowledgements to my father Koji Ihara, mother Michiyo Ihara, younger sister Miho Ihara, Miki Ihara, and all other family members for their support throughout.

Finally, I wish to thank all the invisible help rendered by various persons throughout my career.

-Taiki Ihara

Tokyo Institute of Technology, Japan